Escola Politècnica Superior
de Castelldefels
UNIVERSITAT POLITÈCNICA DE CATALUNYA

TREBALL DE FI DE CARRERA

TÍTOL DEL TFC: Design of an experiment of bubble coalescence for the ESA Student Parabolic Flight Campaign

TITULACIÓ: Enginyeria Tècnica Aeronàutica, especialitat Aeronavegació

AUTORS: Oscar Maldonado Díaz
Ramón Manuel Pino Alfonso
Laura Sancho Vidal

DIRECTOR: Ricard González Cinca

DATA: Juliol 2006

Title: Design of an experiment of bubble coalescence for the ESA Student Parabolic Flight Campaign

Authors: Oscar Maldonado Díaz, Ramón Manuel Pino Alfonso and Laura Sancho Vidal

Director: Ricard González Cinca

Date: July 2006

Overview

The current document contains the description of our experiment, called BubCoa, designed to study the dynamics of biphasic flows (liquid and gas). In particular, its main objective is observing the coalescence (collision and bond) between pairs of air bubbles floating in a liquid. This phenomenon presents different behaviours under Earth's gravity field and in a microgravity environment, provided that in the first case buoyancy forces play an important role. Our experiment will be carried out under microgravity conditions. We will get these conditions in the Parabolic Flights of the Student Parabolic Flight Campaign of the European Space Agency (ESA).

Once the objective of the study is defined and the facility to achieve microgravity conditions is selected, our main task lies in designing and building a set up to generate bubbles. It consists on a cavity containing liquid and two microbubble controlled flows introduced through two T shaped injectors placed inside the cavity. Bubbles disperse in the cavity and collide along the way between the cavity inlet and outlet.

In order to run an experiment in a Parabolic Flight, it is desirable to automatize it as much as possible since human response under microgravity conditions become less reliable than in normal gravity conditions. Labview software controls our experiment, which is monitored by temperature and pressure sensors, accelerometers, liquid pump control and data acquisition systems. A high velocity camera records bubbles path where the coalescence takes place.

For the time being, the experiment has been run under normal gravity conditions in the microgravity lab at EPSC. These obtained results will be compared to these got in the Parabolic Flights which will take place next September. It is expected that this experiment will be continued in further work at the EPSC microgravity lab.

Título: Diseño de un experimento de coalescencia de burbujas para la *Student Parabolic Flight Campaign* de la ESA

Autores: Oscar Maldonado Díaz, Ramón Manuel Pino Alfonso y Laura Sancho Vidal

Director: Ricard González-Cinca

Fecha: Julio 2006

Resumen

El presente documento contiene la descripción de nuestro experimento, BubCoa, diseñado para estudiar la dinámica de fluidos bifásicos (líquido y gas). Su principal objetivo es la observación de la coalescencia (colisión y unión) entre pares de burbujas de aire flotando en un líquido. Este fenómeno presenta diferentes comportamientos bajo el campo gravitatorio terrestre y en un entorno de microgravedad, ya que en el primer caso las fuerzas de flotación tienen un papel muy importante. Nuestro experimento se ejecutará bajo condiciones de microgravedad, que se obtendrá mediante los vuelos parabólicos de la *Student Parabolic Flight Campaign* de la Agencia Espacial Europea (ESA).

Una vez definido el objetivo del experimento y elegido el método de obtención de microgravedad, nuestro trabajo principal será el diseño y la construcción del *"set up"*. Este consiste en una cavidad llena de líquido y en su interior se encuentran dos inyectores en forma de T, a través de los cuales se introducen dos flujos de burbujas. Estos flujos se dispersan en la cavidad y colisionan desde el momento que salen de los inyectores hasta su salida de esta. También forman parte del *"set up"* todos los siguientes sistemas: adquisición de datos, actuadores y la estructura.

Cuando se ejecuta un experimento en un vuelo parabólico es recomendable automatizarlo tanto como sea posible ya que la respuesta humana bajo estas condiciones no es la misma que en condiciones de gravedad normal. Por todo esto es conveniente utilizar un software que controle los diferentes sistemas del experimento (sensores de temperatura y presión, acelerómetros, control de bomba de líquido y sistema de adquisición de datos), en nuestro caso se utilizará el LabView. Además una cámara de alta velocidad grabará la trayectoria de las burbujas para observar si se produce la coalescencia.

Hasta el momento se ha realizado con éxito el experimento en el laboratorio de microgravedad de la EPSC, bajo el efecto del campo gravitatorio terrestre. Estos resultados serán útiles para compararlos con los que se obtengan en los vuelos parabólicos, que tendrán lugar el próximo septiembre. Se espera que este experimento tenga una continuidad en diferentes proyectos que se llevarán a cabo en el laboratorio de microgravedad de la EPSC.

Títol: Disseny d'un experiment de coalescència de bombolles per a la *Student Parabolic Flight Campaign* de la ESA

Autors: Oscar Maldonado Díaz, Ramón Manuel Pino Alfonso i Laura Sancho Vidal

Director: Ricard González-Cinca

Data: Juliol 2006

Resum

Aquest document conté la descripció del nostre experiment, BubCoa, dissenyat per a estudiar la dinàmica de fluids bifàsics (líquid i gas). El seu principal objectiu és l'observació de la coalescència (col·lisió i unió) entre parells de bombolles d'aire flotant a un líquid. Aquest fenomen presenta diferents comportaments sota el camp gravitatori terrestre i en un entorn de microgravetat, ja que en el primer cas les forces de flotació tenen un paper molt important. El nostre experiment es durà a terme sota condicions de microgravetat, que s'aconseguiran mitjançant els vols parabòlics de la *Student Parabolic Flight Campaign* de l'Agència Espacial Europea (ESA).

Un cop definit l'objectiu de l'experiment i escollit el mètode d'obtenció de microgravetat, la nostra feina principal serà dissenyar i construir el *"set up".* Aquest consisteix en una cavitat plena de líquid, en el seu interior es troben dos injectors amb forma de T a través dels quals s'introdueixen dos fluxos de bombolles. Aquests fluxos es dispersen per la cavitat i col·lisionen des del moment que surten dels injectors fins que surten de la cavitat. També formen part del "*set up"* tots els següents sistemes: adquisició de dades, actuadors i l'estructura.

Quan s'executa un experiment en un vol parabòlic és recomanble automatitzar-ho tant com sigui possible ja que la resposta humana sota aquestes condicions no és la mateixa que en condicions de gravetat normal. Per tot això, es convenient fer servir un software que controli els diferents sistemes de l'experiment (sensors de temperatura i pressió, acceleròmetres, control de bomba de líquid i sistema d'adquisició de dades), en el nostre cas es farà servir el LabView. A més a més una càmera d'alta velocitat gravarà la trajectòria de les bombolles per observar si es produeix la coalescència.

Fins ara, s'ha executat l'experiment amb èxit al laboratori de microgravetat de l'EPSC, sota l'efecte del camp gravitatori terrestre. Aquests resultats seran útils per comparar-los amb els que s'obtinguin als vols parabòlics, que tindran lloc el proper setembre. S'espera que aquest experiment tingui continuitat en diferents projectes que es duran a terme al laboratori de microgravetat de l'EPSC.

Acknowledgments

We would like to thank Ricard González-Cinca (UPC) for his active participation in the development and management of the project, for providing the needed means to create the experiment and for the invested time in tutoring our TFC and the program of Introduction to Research in Departments of the Technical University of Catalonia started in July 2005.

We would like to acknowledge Oscar Casas Piedrafita (UPC) for his collaboration and participation on the design and development of the acquisition system, its calibration and its operation.

We would like to thank Santiago Arias (UPC) and Francesc Suñol (UB) for their active collaboration and participation on the development and assembly of the experiment and the obtaining of results.

The microgravity laboratory and factory were facilitated by EPSC, as well as its support. We would also like to thank the EPSC Technical Services department for the assembly of the electronic boards needed for our experiment.

Finally, we would want to acknowledge the following members of the IEEC research team: Jaume Casademunt (UB), Jordi Carrera (IEEC), Xavier Ruiz (URV) and Laureano Ramirez-Piscina (UPC), for its support, advice and experience.

El principio de incertidumbre significa que el Universo es más complejo de lo que se suponía, pero no irracional.

INDEX

LIST OF FIGURES AND TABLES

Foreword

This document explains in detail the design, building and operation of the experiment *Bubble Coalescence at different angles of incidence*. But, let's start at the beginning: Who are we? Where do we want to arrive? And, why bubbles and microgravity?

We are a group of students of Aeronautical Engineering at EPSC who have been taking part in the program of Introduction to research in departments of the Technical University of Catalonia in the Department of Applied Physics for the last academic year. Within the framework of this project, we have developed our diploma thesis (TFC) in a parallel way. The project consists on the characterization of bubbles coalescence under microgravity conditions for different angles of incidence and different viscosity values. It contains the following elements: a theoretical introduction of the phenomenology related to coalescence, the set-up design and development to participate in the *2006 Student Parabolic Flight Campaign* of European Space Agency, on board and on land results, their subsequent processing and study, numerical simulations results with FLUENT® software, comparison of data and report's elaboration.

At the beginning of our project, we carried out an initial analysis of the laboratory and the workshop requirements, and we have gradually completed the type of tools and instrumentation available, in order to fulfil emergent necessities.

Unfortunately, our TFC does not include the last part of results in microgravity due to an unexpected delay in the Parabolic Flights Campaign. The European Space Agency has postponed the campaign from the first week of July to the first week of September. Although it is a pity, we will invest all our efforts and illusion as if we had had the chance to perform our experiment under microgravity conditions before delivering this report. The analyzed and processed data will be further included in the TFC by means of an appendix.

Introduction

Our experiment is included in the study of biphasic fluids. Then, the following question arises. Why is it interesting to study biphasic fluids under microgravity conditions in general and, particularly, coalescence? Let's list some of the reasons:

- Bubbles behaviour characterization is important in chemistry, particularly in the development of biphasic reactors where different parameters must be known in order to control and optimize the reactions. Some of these parameters are the contact surface between reagents, the bubbles diameter, the value of the mean rate of coalescence, the flow and the mixture distribution.

- In the case of bioreactors, an optimum injection management and the consequent dissolution of gases in culture of alga or bacteria could give good results for the development of self-supporting systems. This is one of the main research lines in the development of life support systems in Space.

- The absence of gravity allows studying the fluid and bubbles dynamics without buoyancy. This allows to observe a simplified behaviour and to discover phenomena that used to remain hidden by the presence of gravitational forces. Thus, scientific advances in the field of microgravity can contribute to the understanding of classical processes (for example in biomedical and pharmaceutical industry).

- The majority of living beings have single-phase or biphasic flows, and it is important to know the behaviour of them for the development of space missions.

- Many systems containing biphasic flows have shown a better efficiency in terms of mass and energy transport than single-phase flow systems due to the fact that boiling and condensation processes imply a high energy transfer. In addition, the use of a liquid-gas mixture contributes to the decreasing of the total system weight, which is a critical parameter for space exploration systems.

In conclusion, fluid dynamics belongs to an area of physics and engineering that is in some way present in our daily lifes. This factor makes this study technologically and scientifically more interesting.

CHAPTER 1. SOME PHYSICS ABOUT BUBBLES

1.1. Some basic concepts

In order to develop the theory, we will start with a brief introduction to some phenomena and concepts related to the physics of fluids.

1.1.1. Newtonian Fluid

A fluid is a state of the matter which can be continuously deformed under the action of a shear stress while there is no deformation in the absence of this stress. Fluids can be classified depending on the existent relation between the shear stress and the velocity of deformation. In a Newtonian fluid velocity of deformation is proportional to the applied shear stress. The majority of common fluids such as water, air and petrol can be considered Newtonian under normal conditions. On the contrary, the term non Newtonian is referred to those fluids with velocity of deformation not directly proportional to the shear stress.

1.1.2. Surface Tension

Surface tension is the energy per unit of area of the surface of a body. It is a fundamental property of liquids, whose best known sign is the shape of a drop: it is spherical when falling or while floating in a spaceship, but it is semi-spherical when it sticks to a solid, where other contact forces appear. Surface tension is responsible for the resistance that a liquid offers to the penetration of its surface, the rise of liquid inside capillary tubes and the flotation of objects or organisms on the liquid surface.

At a microscopic level, surface tension is related to the fact that forces affecting every molecule are different inside the liquid and on the surface of the liquid. Every molecule in the liquid is subjected to attraction forces that, on average, cancel themselves. This makes these molecules to be at a low energy state. However, at the liquid surface there is a net force on the molecules towards the liquid interior. Rigorously, if there was a gas outside, there would also be a minimum attractive force towards the exterior. This force is negligible due to the big difference of densities between the liquid and the gas.

Molecules on the liquid surface have more energy on average than those placed in the interior due to their smaller number of molecular bonds. The system tends to decrease its total energy, which is achieved by decreasing the number of molecules on the surface. Thus, the area is minimized as much as possible.

The main effect of surface tension minimization is the tendency of the liquid to minimize its surface for a given volume. That is the reason why fluid surfaces adopt a spherical shape, which is the one with lower area/volume rate.

1.1.3. Capillarity

Capillarity is the ability of a thin tube to absorb a liquid against gravity force. It happens when the adhesive intermolecular forces inside the liquid and the solid are stronger than the cohesive ones between liquid molecules. The smaller the diameter of the capillary tube is the larger the capillary pressure and the height reached will be. Capillarity makes the meniscus to have a concave shape when the liquid is in contact with a vertical surface. It also makes porous materials to absorb liquids.

1.1.4. Viscosity

Viscosity is a feature related to the movement of molecules inside the fluid and, more particularly, to the resistance to deformation of the fluid. Molecules of regions with high global velocity can collide with molecules moving at a smaller global velocity. These collisions allow the transfer of momentum from a fluid region to another. Viscosity is related to this momentum transfer and it is a function that depends on the temperature since the stochastic molecular movements are affected by it.

As an example of different viscosities, different Newtonian fluids, glycerine and water, will be deformed at different velocities for the same shear stress applied. Glycerine offers much more resistance to deformation than water; thus, glycerine is much more viscous.

It is commonly used in Fluid Mechanics the ratio of the absolute viscosity μ and density ρ, called kinematic viscosity ν (L^2/t). In the absolute metric system of units, the unit for ν is the stoke (cm^2/s).

1.2. Types of flow

Before describing the different systems for bubble generation in microgravity (section 1.3), it is strongly recommended to analyze some situations that are likely to happen in a pipe containing a biphasic system [1]. In this section we expose briefly each possible situation at 1 g and microgravity. Only bubbly flow, slug flow and annular flow are possible under microgravity [2].

1.2.1. Bubbly flow

1 g:

Bubbles remain in a continuous liquid under these conditions. The relative velocity of the bubbles depends mainly on the density difference between both fluids. As the velocity of liquid increases, bubbles are dispersed into smaller and more widely separated bubbles (Fig.1.1).

Microgravity:

Bubbles are more dispersed than in 1 g, and fill the pipe

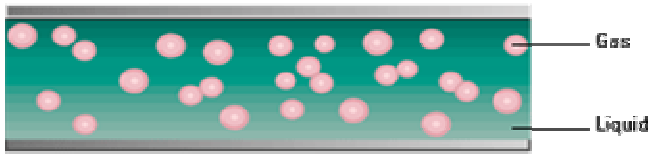

Fig. 1.1 Bubbly flow under 1 g [1]

1.2.2. Slug flow

1 g:

In this situation the lighter fluid is contained in bubbles that are pushed along by the heavier fluid. Bubble size is similar to pipe diameter. Slug flow produces a pressure increase inside the pipe.

Microgravity:

The heaviest phase is uniform and remains trapped between bubbles (Fig.1.2). Under microgravity conditions this effect does not produce a pressure increase.

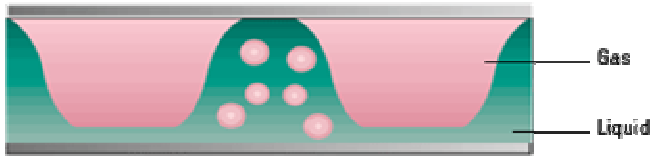

Fig. 1.2 Slug flow under 1 g [1]

1.2.3. Plug flow

In this case (Fig.1.3) there are elongated bubbles in the top of the pipe, and a continuous liquid in the rest. Plug flow is similar to slug flow, but bubbles are generally smaller and move more slowly.

Fig. 1.3 Plug flow [1]

1.2.4. Stratified flow (layered, separated)

In this case fluids are separated into different layers, with lighter fluids flowing above heavier fluids (Fig.1.4).

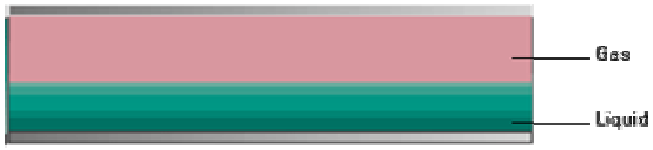

Fig. 1.4 Stratified flow [1]

1.2.5. Annular Flow

1 g:

In this case the lighter fluid is in the centre of the pipe and the heavier fluid is around (Fig.1.5). This situation occurs at high velocities of the lighter fluid.

Microgravity:

This is the most common situation and it can be obtained in a long range of liquid-gas flows. It is used for the transfer of momentum and heat between the gas and the liquid.

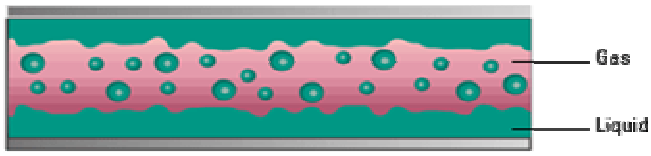

Fig. 1.5 Annular Flow under 1 g [1]

1.3. Bubble Generation in microgravity

The conditions of our experiment (in particular, the relation between the Reynolds numbers of gas and liquid) allow only the appearance of a slug flow.

Furthermore, our interest in Slug flow is the generation of Taylor bubbles [3], which is a sequence of bubbles with known values of diameter and frequency.

In order to generate bubbles the following systems might be used.

1.3.1. Co-flow

Co-flow systems consist on the application of a force in the same direction of a liquid-gas mixture flow in the inner of a pipe to detach the bubble from the pipe (Fig.1.6). The force is usually created by the liquid. Bubble size and frequency of generation can be adjusted by controlling the external liquid velocity.

Fig. 1.6 Co-flow configuration

1.3.2. Cross flow

Cross flow configuration (Fig.1.7) is one of the most used methods for bubble generation. The difference between Co-flow and Cross flow is in the direction of the force. The force in Cross flow is applied perpendicularly to the direction of the mixture. Bubble size and frequency of generation can be adjusted by controlling the velocity of the liquid in the perpendicular direction.

Fig. 1.7 Cross flow configuration

1.3.3. BubGen

The BubGen system [4] is a particular case of the Cross flow configuration that generates a slug flow. The special feature of BubGen is that both phases (liquid and gas) are inserted separately in a T-system whose pipes have a diameter of the same order (Fig.1.8).

Fig. 1.8 BubGen

Some of the advantages of BubGen are:

-In case of small enough pipe diameters, bubble size is nearly equal under normal and microgravity conditions, indicating that the system is gravity insensitive.

-For crossflow configurations in which: $d_g/d_l \approx 1$, where d_g and d_l are the gas and liquid pipe diameters, respectively, bubbles size is much smaller than d_g/d_l at same flow conditions. It happens due to an increase in the effectiveness of the liquid velocity, which does not occur in larger d_l channels.

- Bubble dispersion in microgravity is highly enhanced by the gas-liquid composite injector.

1.4. Basic laws of coalescence

In this section the phenomena of coalescence between bubbles is described from a physical point of view.

Coalescence lies in the collision of two or more bubbles, which are inside a fluid, and in the bond between them to form a single one. The sequence would be the following:

-Collision between two or more bubbles. It is a reversible process.

-Contact surface's flattening and drainage of the film of liquid which separates the bubbles. It is an irreversible process.

-Film break giving rise to coalescence. It is an irreversible process as well. It takes place at smaller time scales than the previous ones, so it can be considered instantaneous. Moreover, the film break does not take place when it reaches a specific threshold value in the liquid thickness but it depends on lot of factors such as impurities. Nevertheless, it is known that the film break for a certain size of bubbles takes place when the thickness is about hundreds of Å and tens of Å in smaller ones.

More details about these phenomena are given as follows.

1.4.1. Coalescence

Two processes should take place before coalescence: collision and bubbles bonding. During the first one, the path of the bubbles collide; during the second one, the bubbles remain in contact just separated by a film of liquid which has a thickness much smaller than the initial radius of the bubbles.

Once the bubbles are together, it is possible that the film placed between bubbles break and they unite and form a bigger one. This phenomenon is known as coalescence.

As a result, a bubble with a volume equal to the sum of the volumes of the initial bubbles $(V=V_1+V_2)$ is generated. This phenomenon happens in a short period of time (approximately miliseconds). The new bubble adopts spherical shape due to the action of surface tension which makes the surface grow without modifying the volume.

Coalescence causes important changes on the properties of both colliding bubbles because they press to the film in between. When this pressure is bigger than the film's pressure, it starts to reduce until its breakage. The gas contained inside the two bubbles mix up and a single volume is formed. This breakage hole grows and the gas forms an inertia revolution ellipsoid.

However, surface tension tries to keep the spherical shape. It produces the generation of capillarity waves along the ellipsoid surface and its harmonic

oscillation. The frequency of this state is determined by the *capillarity wave's equation*. In spherical coordinates it is a linear combination of spherical harmonics.

Some energy of these waves is transmitted to the liquid as heat. Finally, the new bubble adopts a spherical shape.

1.4.2. Contact surface flattening and drainage of the film

In this section a model that describes the evolution process of the film which separates the bubbles is presented [5] (Fig.1.9). The main objective is finding out an equation that describes its evolution in time, in microgravity conditions. We will start with the following assumptions:

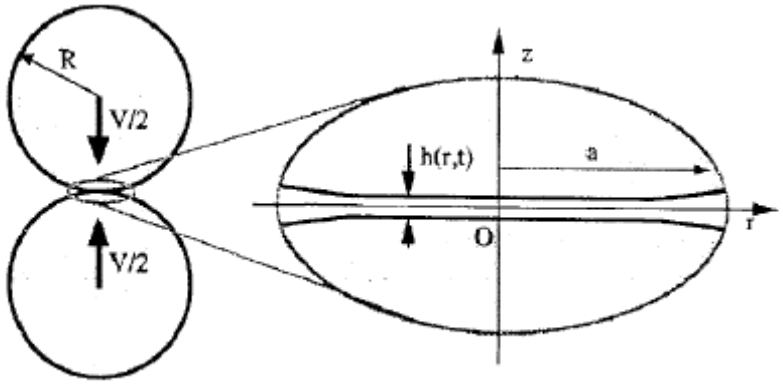

Fig. 1.9 Schematics of contact surface flattening. [6]

-The fluid is Newtonian.
-Density *ρ* and viscosity *μ* have constant values.
-The model has cylindrical symmetry. The cylinder axis is defined by the centres of the bubbles.
-Gravity is negligible.
-This theory is valid when film thickness (*h*) is smaller than bubbles radius (*h(r,t)<<R*).

When using cylindrical coordinates, Navier-Stokes equations can be written as follows:

$$\rho_c\left(\frac{\partial v_r}{\partial t}+v_r\frac{\partial v_r}{\partial r}+v_z\frac{\partial v_r}{\partial z}\right)=-\frac{\partial P}{\partial r}+\mu_c\left[\frac{\partial}{\partial r}\left(\frac{1}{r}\frac{\partial}{\partial r}\left(rv_r\right)\right)+\frac{\partial^2 v_r}{\partial z^2}\right] \qquad \textbf{(1.1)}$$

$$\rho_c\left(\frac{\partial v_z}{\partial t}+v_r\frac{\partial v_z}{\partial r}+v_z\frac{\partial v_z}{\partial z}\right)=-\frac{\partial P}{\partial z}+\mu_c\left[\frac{\partial}{\partial r}\left(r\frac{\partial v_z}{\partial r}\right)+\frac{\partial^2 v_z}{\partial z^2}\right] \quad \textbf{(1.2)}$$

where v is velocity, P is pressure, and ρ_c and μ_c, density and viscosity, respectively, of continuous phase.

The continuity equation for incompressible fluids is:

$$\frac{1}{r}\frac{\partial}{\partial r}(rv_r)+\frac{\partial v_z}{\partial z}=0 \quad \textbf{(1.3)}$$

We will consider the following hypotheses:

-The velocity value at Z axis can be considered 0, because the liquid film has a thickness $h(r,t)$ which varies very slowly in time. A v_z different to 0 would imply big variations, which is not common.

On the contrary, variation of z velocity component is not 0 because v_z of the air near the interface can be higher than the v_z of the liquid in the film, since it moves more freely.

$$v_z(z=0)\approx 0 \qquad \frac{\partial v_z}{\partial z}\neq 0 \quad \textbf{(1.4)}$$

-We must imagine two points: the initial point of contact between two colliding bubbles and a point near to this one. When bubbles become closer, the contact takes place at a disk shaped surface. The initial point doesn't move and the other one does move in radial direction. The velocity at which these two points separate can be considered constant in time.

$$\frac{\partial v_r}{\partial t}=0 \quad \textbf{(1.5)}$$

-Eq.1.6 is inertia expression. The radius is much smaller than the film height. On the other hand, radial velocity of the fluid varies very little for different values of r. So, this expression becomes a constant divided by a term that tends to infinite, which equals 0.

$$\frac{v_r\partial v_r}{\partial r}\approx 0 \quad \textbf{(1.6)}$$

As *h(r,t)<<R*, we can suppose that the water flow between bubbles is laminar, with a direction parallel to the interface. It means that $\partial v_r / \partial z$ is a function only depending on *z*. The left-hand side of Eq. 1.1 and 1.2 can be omitted because it is considerably smaller than the right-hand side. Thus, Eq. 1.1, Eq. 1.2 and Eq. 1.3 can be written as:

$$\frac{\partial P}{\partial r} = \mu_c \frac{\partial^2 v_r}{\partial z^2} \tag{1.7}$$

$$\frac{\partial P}{\partial z} = 0 \tag{1.8}$$

$$\frac{1}{r}\frac{\partial}{\partial r}(r v_r) + \frac{\partial v_z}{\partial z} = 0 \tag{1.9}$$

The system has the following boundary conditions:

$v_r = 0$ at the surface *(z=0.5h)*
$v_z = 0.5\frac{\partial h}{\partial t}$ at the surface
$\frac{\partial h}{\partial t} + v_r \frac{\partial h}{\partial r} = v_z$ known as kinematical boundary condition
$\frac{\partial v}{\partial z} = 0$ at *z=0*, due to mass conservation
$v_z = 0$ for symmetry

Integrating Eq. 1.7 twice, we obtain:

$$v_r = \frac{1}{2\mu_c}\frac{\partial P}{\partial r} z^2 + C_1 z + C_2 \tag{1.10}$$

Integration constants can be computed by using the boundary conditions. Then, the equation turns into:

$$v_r = \frac{1}{2\mu_c}\frac{\partial P}{\partial r}\left(z^2 - \left(\frac{h}{2}\right)^2 \right) \tag{1.11}$$

which represents a parabolic velocity originated by the pressure gradient.

The integration of Eq. 1.9 along the upper half of the film (just the upper one because, as we said before, the problem is symmetric) leads to:

$$\int_0^{h/2}\frac{1}{r}\frac{\partial}{\partial r}(rv_r)dz=\int_0^{h/2}\frac{1}{r}\frac{\partial}{\partial r}(\frac{r}{2\mu_c}\frac{\partial P}{\partial r}(z^2-(h/2)^2)dz=-\int_0^{h/2}\frac{\partial v_z}{\partial z}dz \qquad \textbf{(1.12)}$$

It is necessary to use Leibnitz Theorem[1] to solve the central integral since *h* depends on *r*.

By integrating the left side of Eq. 1.12 from 0 to *h/2*, we obtain:

$$\frac{1}{r}\int_0^{h/2}\frac{\partial}{\partial r}\left(\frac{r}{2\mu}\frac{\partial P}{\partial r}\left(z^2-\left(\frac{h}{2}\right)^2\right)\right)dz=$$

$$\frac{1}{r}\frac{\partial}{\partial r}\int_0^{h/2}\left(\frac{r}{2\mu_c}\frac{\partial P}{\partial r}\left(z^2-\left(\frac{h}{2}\right)^2\right)\right)dz-\frac{r}{2\mu_c}\frac{\partial P}{\partial r}\left[\left(\left(\frac{h}{2}\right)^2-\left(\frac{h}{2}\right)^2\right)\frac{\partial h}{\partial r}-\left(0-\left(\frac{h}{2}\right)^2\right)\frac{\partial P}{\partial r}\right] \qquad \textbf{(1.14)}$$

Computing the integral of the first term on the right-hand side of Eq. 1.14, leads to:

$$\frac{1}{r}\frac{\partial}{\partial r}\int_0^{h/2}\left(\frac{r}{2\mu_c}\frac{\partial P}{\partial r}\left(z^2-(h/2)^2\right)\right)dz=$$

$$\frac{1}{2\mu_c}\frac{\partial}{\partial r}\left[r\frac{\partial P}{\partial r}\left((1/3)z^3-(h/2)^2z\right)\right]\Bigg|_0^{h/2}=\frac{1}{24\mu_c r}\frac{\partial}{\partial r}\left(rh^3\frac{\partial P}{\partial r}\right) \qquad \textbf{(1.15)}$$

And the right-hand side of Eq. 1.12 results:

[1] Leibnitz Theorem :

$$\frac{d}{dt}\int_{a_1(t)}^{a_2(t)}f(x,t)dx=\int_{a_1(t)}^{a_2(t)}\frac{\partial f}{\partial t}dx+\left(f(a_2,t)\frac{da_2}{dt}-f(a_1,t)\frac{da_1}{dt}\right) \qquad \textbf{(1.13)}$$

In this particular case a_1 (t)=0, a_2 (t)= h/2. We replace dt by ∂r and dx by dz. The function is:

$$f=\frac{r}{2\mu_c}\frac{\partial P}{\partial r}\left(z^2-(h/2)^2\right) \qquad \textbf{(1.18)}$$

$$\int_0^{h/2} \frac{\partial v_z}{\partial z} dz = v_z\Big|_0^{h/2} = (1/2)\frac{\partial h}{\partial t} - 0 = (1/2)\frac{\partial h}{\partial t} \qquad \textbf{(1.16)}$$

The Eq. 1.17 of evolution in time of the film thickness is computed by combining the previous equations:

$$\frac{\partial h}{\partial t} = \frac{1}{12\mu_c r}\frac{\partial}{\partial r}\left(rh^3\frac{\partial P}{\partial r}\right) \qquad \textbf{(1.17)}$$

1.4.3. Boundary condition *vr≠0* at surface *z=h/2*

In this section the first boundary condition given in the previous section is changed, and v_r is considered to be non zero at the surface equal to *h/2*. Once more, the objective is to get the equation that rules the evolution in time of the film thickness.

If Eq. 1.17 is integrated again, but with the new boundary conditions:

$$v_r = \frac{1}{2\mu_c}\frac{\partial P}{\partial r}\left(z^2 - (h/2)^2\right) + U_o \qquad \textbf{(1.19)}$$

Following the same steps as in the previous section:

$$\int_0^{h/2}\frac{1}{r}\frac{\partial}{\partial r}\left(\frac{r}{2\mu_c}\frac{\partial P}{\partial r}\left(z^2-(h/2)^2\right)\right)dz + \int_0^{h/2}\frac{1}{r}\frac{\partial}{\partial r}(rU_0)dz = -\int_0^{h/2}\frac{\partial v_z}{\partial z}dz \qquad \textbf{(1.20)}$$

The second term in Eq. 1.20 is solved with Leibnitz Theorem again, since *h* depends on *r.*

$$\int_0^{h/2}\frac{1}{r}\frac{\partial}{\partial r}(rU_0)dz = \frac{1}{r}\frac{\partial}{\partial r}\int_0^{h/2} rU_0 dz - \left[rU_0\frac{\partial h}{\partial r} - 0\right] \qquad \textbf{(1.21)}$$

According to the approximation of lubrication theorem $\frac{\partial h}{\partial r} \approx 0$, the previous equation becomes:

$$\int_0^{h/2} \frac{1}{r}\frac{\partial}{\partial r}(rU_0)dz = \frac{1}{r}\frac{\partial}{\partial r}(rU_0 z)\Big|_0^{h/2} = \frac{1}{2r}\frac{\partial}{\partial r}(rU_0 h) \qquad \textbf{(1.22)}$$

Finally, the equation that rules the evolution in time of the film's thickness is obtained by combining Eq. 1.3, Eq. 1.16, Eq. 1.20 and Eq. 1.22:

$$\frac{\partial h}{\partial t} = -\frac{1}{r}\frac{\partial}{\partial}(rU_0 h) + \frac{1}{12\mu_c r}\frac{\partial}{\partial r}\left(rh^3\frac{\partial P}{\partial r}\right) \qquad \textbf{(1.23)}$$

1.4.4. Film breakage

Film breakage is a much less known and studied phenomenon than the contact surface flattening. It is a stochastic process because it depends on the noise and the resulting variation of some magnitudes.

The film is not broken at *h=0*, but when it has a limit value that depends on several variables and the impurities of the liquid in which bubbles are immersed. The values of h for which the film breaks depends on the values of *We* number (Weber) and *Mo* number (Morton), which define the behaviour of the bubbles [6]. The film is broken when its thickness is about hundred of Á. It can be considered an instantaneous process.

Weber number defines the bond of bubbles:

$$We = \frac{\rho v^2 R_B}{\sigma} \qquad \textbf{(1.24)}$$

where ρ, v, R_B and σ are the liquid density, the relative approach velocity of bubbles, their radius and the surface tension, respectively. If We is too high, coalescence cannot take place due to the fact that the film between bubbles will not drain. Chesters & Hofman [7] established the following criterion:

Coalescence is possible only when *We≤0.5*. Otherwise, the film will not break and coalescence will not take place.

The Morton number determines the behaviour of the bubbles once they are together. Coalescence will take place If $Mo>0.4\cdot10^{-9}$. Morton expression is the following.

$$Mo = \frac{g\mu^4}{\rho\sigma^3} \quad \textbf{(1.25)}$$

being g and μ the acceleration due to gravity and the liquid dynamic viscosity, respectively.

CHAPTER 2. Methods to obtain microgravity

This chapter shows the different microgravity facilities that researchers have at their disposal in order to execute experiments under microgravity conditions. An explanation of the main features, advantages and disadvantages of each facility is given. We will specially focus on parabolic flights because it is the facility where our experiment will be run.

Fig. 2.1 shows the levels of gravity that every kind of platform reaches, and its general time of exposure.

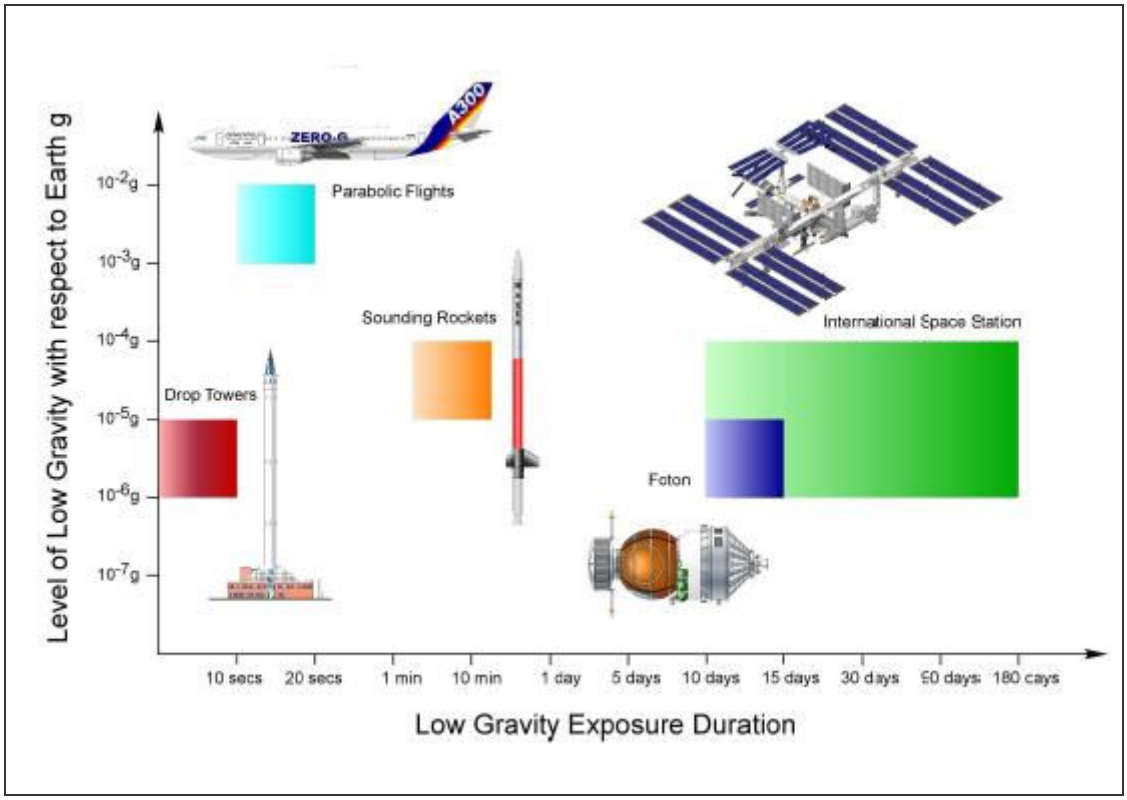

Fig. 2.1 Levels of gravity and low gravity time of exposure [7]

In table 2.1 it is shown the different fields of research which take place in the five available platforms in ESA.

Table 2.1 Research at ESA facilities [7]

	Parabolic Flights	*Drop Towers*	*Sounding Rockets*	*Foton*	*Iss*
Fundamental Physics : Complex plasmas & dust particle physics	✓	✓	✓	✓	✓
Fundamental Physics : Cold atoms and quantum fluids	?	✓	✓	✓	✓
Fluid and Combustion Physics: Structure and dynamics of fluids & multiphase systems	✓	✓	✓	✓	✓
Fluid and Combustion Physics Combustion	✓	✓	✓	?	✓
Materials Sciences: Thermo physical properties	✓	✓	✓	✓	✓
Materials Sciences: New materials, products and processes	✓	✓	✓	✓	✓
Biology: Biotechnology	✓	✗	✓	✓	✓
Biology: Plant physiology	✓	✗	✓	✓	✓
Biology: Cell and development biology	✓	✓	✓	✓	✓
Physiology: Integrated physiology	✓	✗	✗	✗	✓
Physiology: Muscle and bone physiology	✓	✗	✗	✗	✓
Physiology: Neuroscience	✓	✗	✗	✗	✓
Astro/exobiology: Planetary Exploration: Origin, evolution and distribution of life	✓	✗	✗	✓	✓
Astro/exobiology: Planetary Exploration: Preparation of human planetary exploration	✓	✗	✗	✓	✓

In Fig. 2.2 it is represented the average time of launch and integration of each platform.

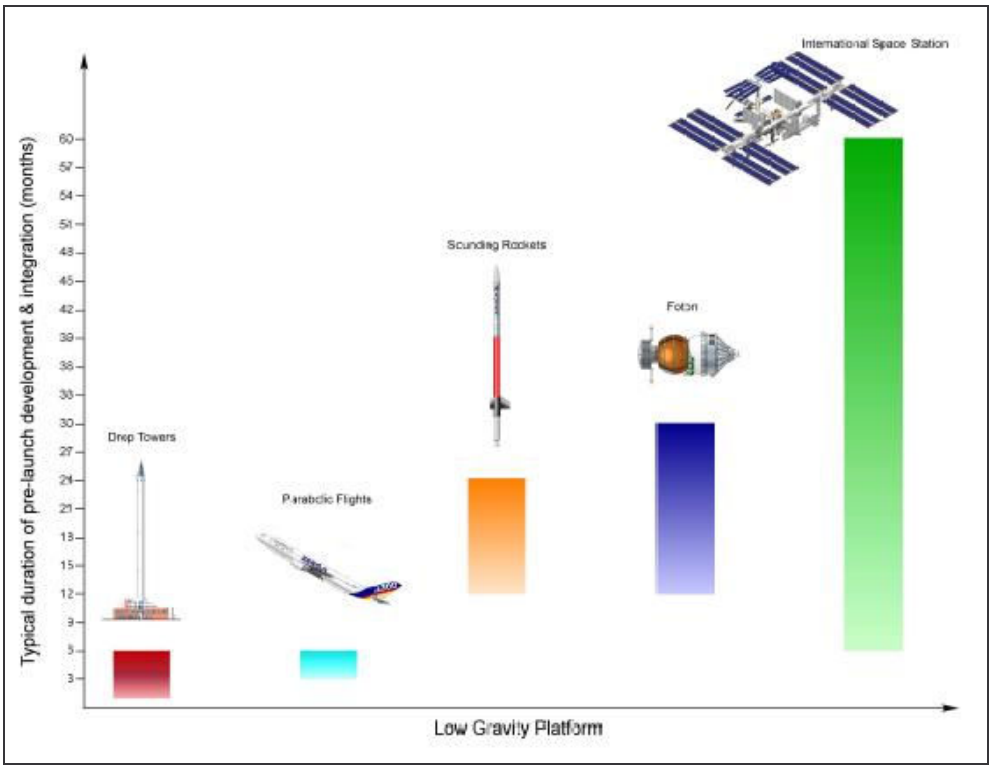

Fig. 2.2 Launch and integration time [7]

2.1. Parabolic flights

Parabolic flights (PF) are carried out by specially configured aircrafts that manoeuvre a series of parabolas to reach microgravity. ESA airplane for parabolic flights is Airbus A300, whose technical characteristics will be detailed afterwards. During each parabola, the aircraft experiments different levels of gravity: 1 g, 1.5-1.8 g and 0 g.

PF offer the opportunity to run research experiments under microgravity conditions and are commonly used among new researchers. One of their main advantages is the fact that people can flight inside the airplane; it means not only that researchers may directly act on the experiment during the flight but also that humans can be the subject of the study. Moreover, it is one of the most economical microgravity research facilities. However, the microgravity time lasts less than in the rest of methods.

PF are highly indicated for experiments with human subjects, new researches in the field, students and for users who want to get preliminary data or to test equipment before a long duration mission proposal.

Experiments from a big spectrum of research fields are executed in parabolic flights: fundamental physics, fluid and combustion physics, material science, biology, technology and physiology.

2.1.1. Characteristics of the A300

The Airbus A300 used by ESA is the largest parabolic flight aircraft in the world. NASA has traditionally used the KC-135.

The A300 has been used since 1997. The French company Novespace manages the flights, based at the Bordeaux-Mérignac airport. Novespace has several alternative airfields in case of bad weather conditions.

The main characteristics of the A300 are detailed in ANNEX A

2.1.2. PF manoeuvres

Airbus A300 usually executes a series of 31 parabolas (the first one is for testing).

As it can be seen in Fig. 2.3, a whole parabola lasts 3 minutes and parabolas are performed in 6 series, separated by breaks of 4, 5 or 8 minutes. During this time, researchers can check their set-up and results.

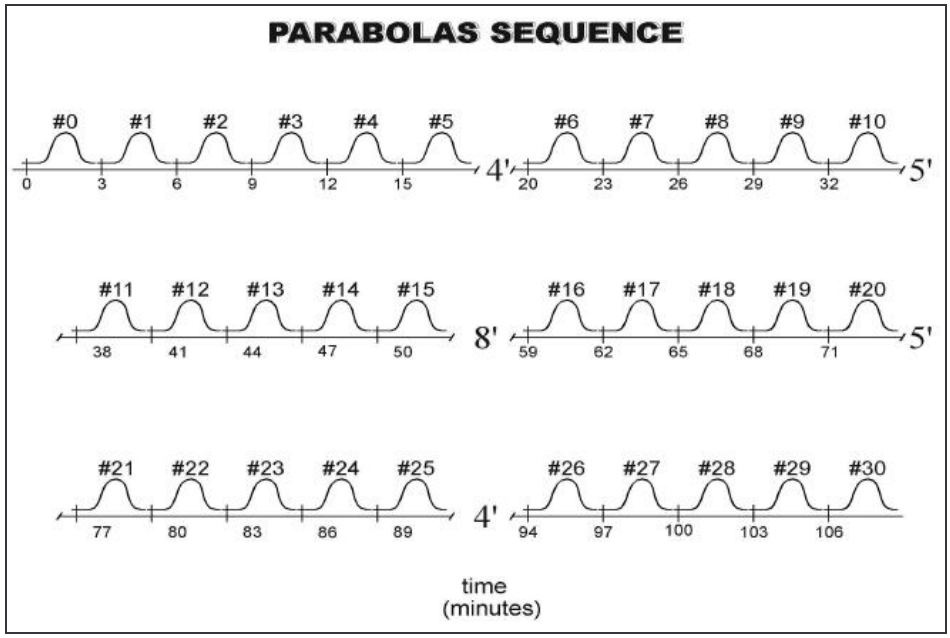

Fig. 2.3 Parabolas sequence [7]

Fig. 2.4 shows the performance of the aircraft while executing a single parabola, and the different phases regarding to the microgravity levels achieved.

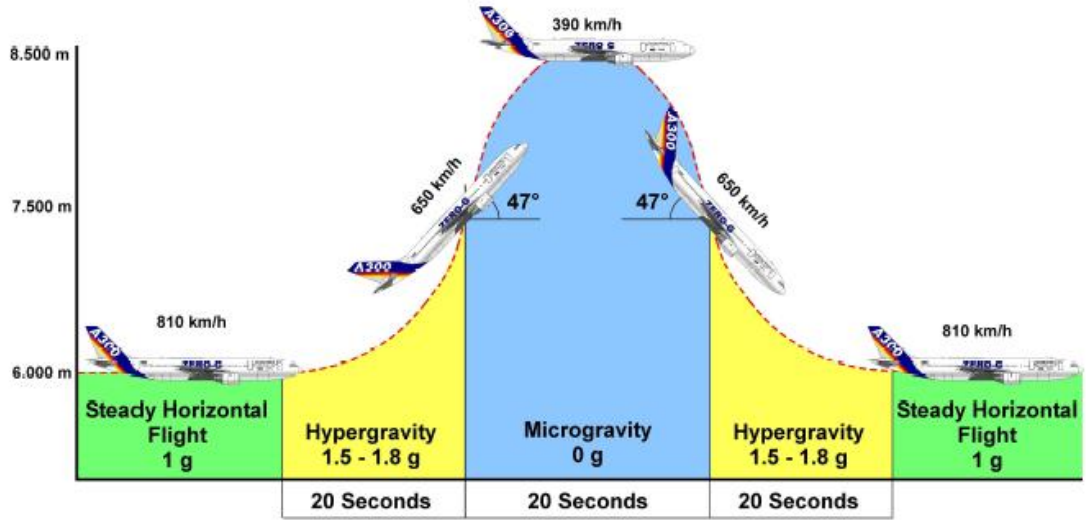

Fig. 2.4 Single parabola sequence [7]

Firstly, the aircraft flights horizontally at an altitude of 6000 m with an air speed of 810 km/h. During this first phase, the airplane is under normal gravity conditions. Then, the nose of the aircraft is pulled up and it starts climbing; at this phase, which lasts about 20 seconds, levels of hypergravity are achieved (between 1.5 and 1.8 g). When the airplane is at an altitude of 7500 m with an angle of 47º with respect to the horizontal and an air speed of 650 km/h, the thrust is decreased and the A300 achieves a parabolic path with a level of 0 g. The peak of this parabola is at 8500 m of altitude, where the airplane flights at a speed about 390 km/h. The microgravity phase lasts 20 seconds as well. When the airplane is again at 7500 m, it pulls out and achieves hypergravity one more time. When the altitude has reduced to 6000 m, it describes a steady horizontal path as it did at the beginning.

The cabin speakers announce regarding times, angles, pull-up, injection and pull out so that passengers are informed at any time.

2.1.3. Aircraft environment and acceleration levels

Although the cabin pressure is around 0.79 atm, the equipments must be tested for lower levels of pressure in case of loss of cabin pressure.

During the flight the cabin temperature remains between 18º and 25º. Neon lights illuminate the testing area. In our case, this system is not enough to illuminate our experiment so we use LED array board.

Parabolic Flights achieve 20 seconds of microgravity in each parabola. The residual gravity level varies between $-5 \cdot 10^{-2}$ g and $5 \cdot 10^{-2}$ g along Z axis (Fig.2.5), and between -10^{-2} g and 10^{-2} g along X and Y axis.

Fig. 2.5 A300 axis [7]

2.2. Drop towers

This is the most accurate simulation of microgravity that can be achieved without leaving Earth's atmosphere.

This facility allows autonomous experiments to be under free-fall conditions during a maximum period of time. Some times, the experiments remain in a vacuum chamber.

Despite the short time of microgravity, the levels achieved in drop towers are around 10^{-5} g, which provides high quality data.

2.2.1. ZARM Drop Tower

Zarm drop tower is a 146 m high tower located in Bremen, Germany. Microgravity conditions can be obtained three times per day by means of two methods: free-fall and catapult. The residual acceleration values achieved are lower than 10^{-5} g. In free fall, experiments are dropped from the top of the tower, getting microgravity conditions for 4.74 seconds. Experiments catapulted upwards from 11 m below the tower obtain 9.48 seconds of microgravity. The system it can propel a 300-500 kg capsule in 0.28 seconds with a speed of 48 m/s.

The capsule (Fig.2.6) has a diameter of 800 mm and 1.6 m or 2.4 m in length, depending on the required space.

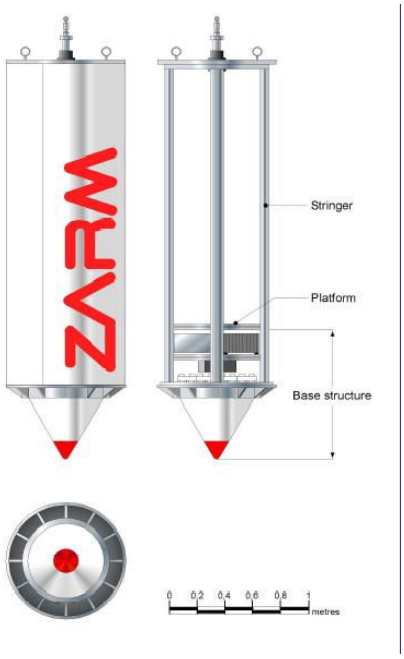

Fig. 2.6 Zarm capsule [7]

Once the experiment is assembled into the capsule, a winch takes the capsule up to the maximum internal height (120 m) in the free-fall system. The interior of the tower is evacuated every time that an experiment is executed. There is an 8 m deceleration unit under grown level which is filled with polystyrene to stop the capsule (Fig.2.7).

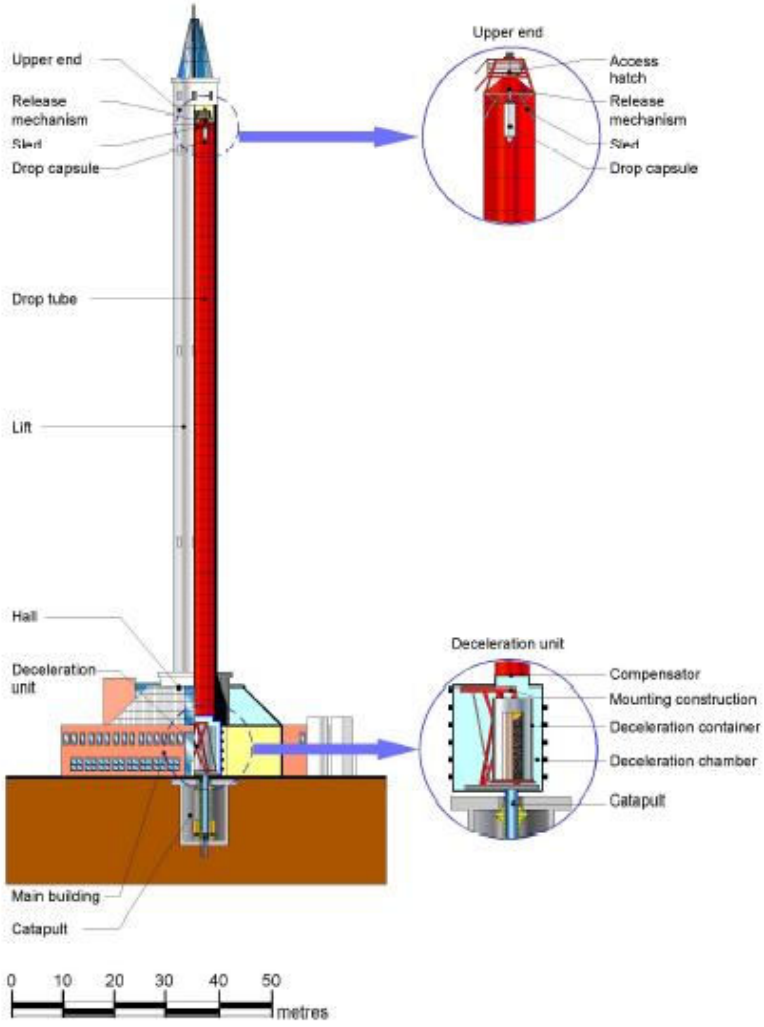

Fig. 2.7 Upper end and deceleration unit in detail [7]

2.3. Sounding rockets

At their beginning, around fifties, Sounding Rockets were used to take meteorological measurements for the study of the atmosphere. The European Space Agency started to use sounding rockets for microgravity research in 1982. Between 3 and 13 minutes of microgravity are achieved, with a residual value equal or less than 10^{-4} g. Sounding Rockets are a good way to get an experiment ready for the ISS.

Table 2.2 gives information about the sounding rockets Mini Texus, Texus, Maser and Maxus.

Table 2.2 Sounding Rockets used by ESA [7]

Project	*Managed by*	*μg time (min)*	*Number of experiment modules*	*Paylod Diameter (cm)*	*Scientific payload length (m)*	*Scientific payload mass (kg)*	*Spin rate (Hz)*
MiniTexus	*EADS-ST Bremen*	*3-4*	*1-2*	*43.8*	*1*	*100*	*5*
Texus	*EADS-ST Bremen*	*6*	*4*	*43.8*	*3.4*	*260*	*3-4*
Maser	*SSC*	*6*	*4*	*43.8*	*3.4*	*260*	*3-4*
Maxus	*EADS-ST Bremen*	*12-5*	*5*	*64.0*	*3.8*	*480*	*≤0.5*

Sounding Rockets are launched from Esrange (Sweden), at 200 km above the Artic Circle. Rockets impact area is placed in the north of Esrange, in the Swedish tundra region. There are three different areas: A, B and C, with a surface of 5600 km^2. Engines impact at area A; the payload and second and third phases are assigned to areas B and C.

Fig. 2.8 shows the altitudes achieved by ESA Sounding Rockets compared with Space Shuttle and ISS.

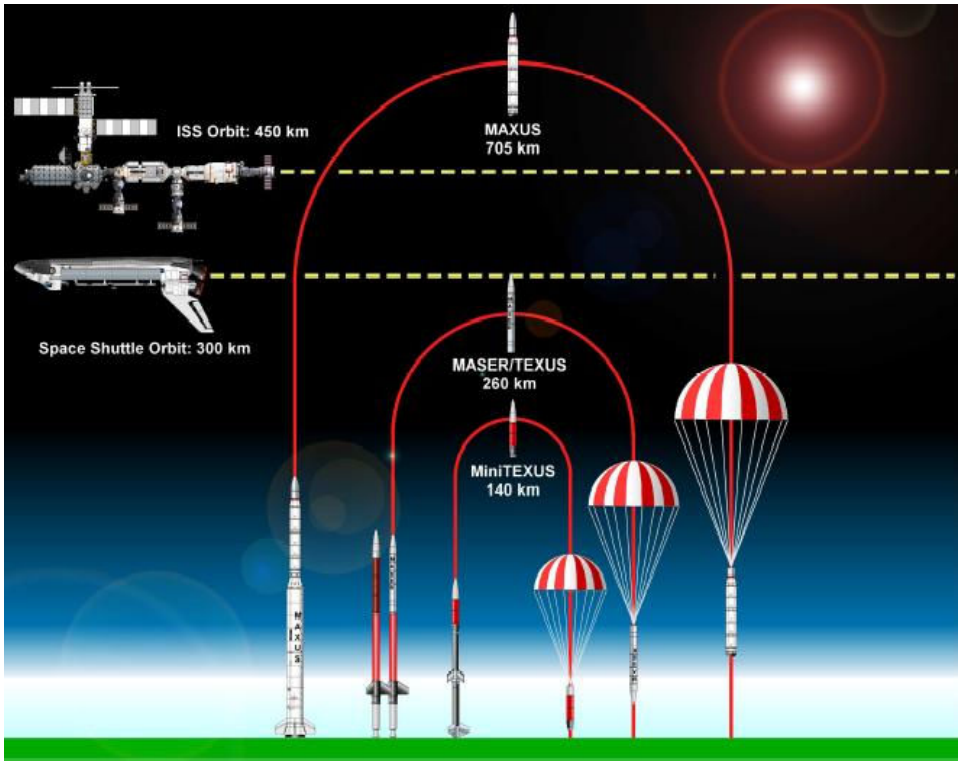

Fig. 2.8 Altitudes achieved by Sounding Rockets [7]

2.4. Foton capsules

The unmanned Foton capsules (Fig.2.9) stems from the Soviet military aircraft Vostok in the sixties and from the military reconnaissance satellites. The first capsule (called Cosmos 1645) was launched in 1985 and in 1988 the name was changed to Foton. ESA joined the Foton programme in 1991.These capsules are launched into near-circle, low-earth orbit by a Soyuz-U. The level of microgravity obtained is 10^{-5} g for a two weeks period.

This facility is ideal for experiments that have already been executed under short time microgravity conditions because it offers the possibility of analyzing them for a longer period of time.

A Foton capsule is 6.2 m long and weights 6500 kg. It may carry a 650 kg payload having three main modules: service module, battery module and re-entry module.

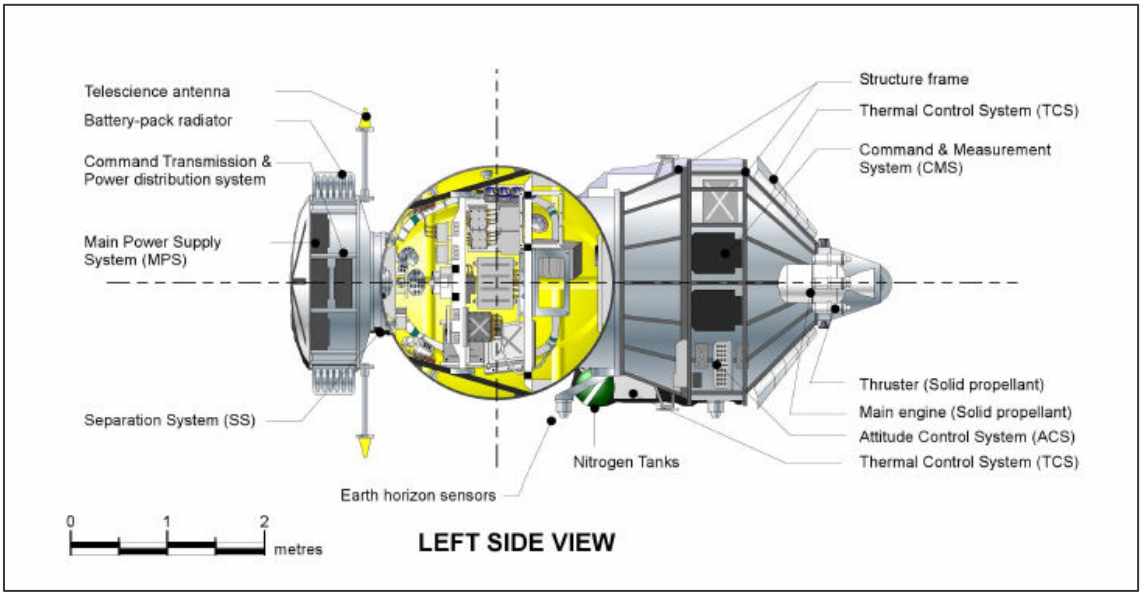

Fig. 2.9 Foton Capsule [7]

2.5. ISS

Nearly all the Space Agencies (NASA, JAXA, ESA, Russian Space Station, Canada and AEB) of the world take part in the International Space Station (Fig.2.10) which is expected to be completed in 2010.
This facility can achieve 10^{-6} g for a period of time that lasts from 1 to 6 months. It is considered the last phase of an experiment designed to be tested under microgravity conditions.

The inclination of the ISS orbit is 51.63º and it is located at an altitude that varies between 330 and 400 km. It moves at 27000 km/h with an orbit above

earth of 91 minutes. Once its assembly is finished, it will weight 450 tones and its dimensions will be 108x79x43 m. Its maximum power out will be 108 kW, with and average of 30 kW available to payload operations.

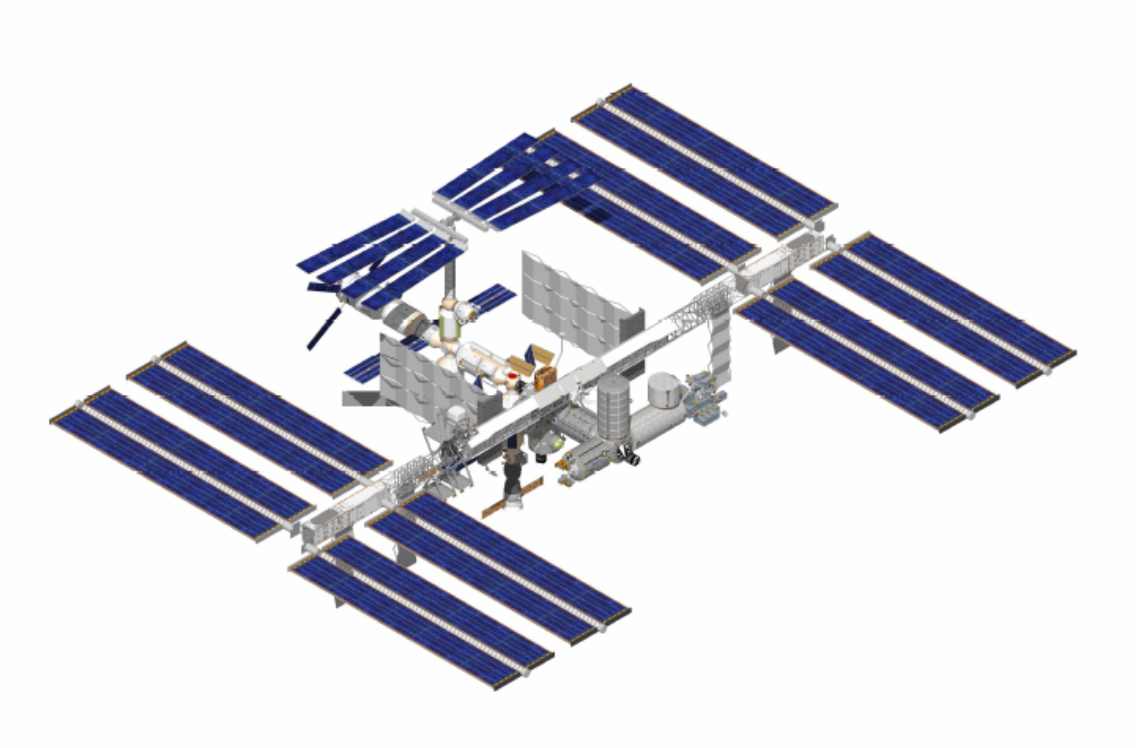

Fig. 2.10 International Space Station [7]

2.6. Student parabolic flight campaign

This project of ESA is a chance for students from Europe and Canada to perform their experiments under microgravity conditions and to experiment weightlessness by themselves.

ESA organizes a Student Parabolic Flight Campaign (SPFC) per year. Only 30 teams are selected among all the applications. The selection is a long process done by ESA experts, according to different criteria: interest, safety, technical aspects and outreach activities planned by the team. The winner experiments fly twice accompanied by two students each time.

The requirements to apply to participate in this campaign are the following:

-To be a 4 members team of university students from one of the 17 ESA member states.
-To propose an interesting experiment to be performed under microgravity conditions.
-To have an endorsing teacher.

-To be between 18 and 27 years old at the time of the campaign application deadline.
-Not to have taken part in a SPFC before.

2.6.1. Experimental Form

Once the team has decided to apply for the SPFC, the next step is registering at a website exclusively created for the campaign [8]. Then students can download the Experimental Form file to fill in. ESA experts will decide which experiments will take part in the campaign by analysing this form whose main contents are:

- Experiment objectives
- Experiment description
- Technical description of the experiment set-up
- Products used
- Installation of the experiment in the aircraft
- Power consumption
- Mechanical resistance
- In flight procedures
- Dangerous material analyses
- Outreach programme

The last section, outreach programme, includes the activities that each team carries out in order to promote their experiment and the campaign. In our case, we have carried out the following ones:

- Creation of a webpage where all the objectives of the experiment are described. It also includes the activities that we do in the Microgravity Laboratory at EPSC in Castelldefels (Barcelona). There is a large number of links to diverse websites that deal with topics related to microgravity, [9].

- Contact with a journalist who will prepare a TV programme in a public Spanish TV channel (TVE1) in which we will explain the project and our experience in the ESA parabolic flights.

- During our stay in France, we will do a *blog* explaining our experiences.

- We will also try to manage publishing a scientific review.

In the Experimental Form nearly all the details of the experiments are asked. Time given to prepare the Experimental Form is about three months. Once it is ready, students may upload it and wait for ESA experts preselection. It takes place around one month later, when a file with the shortlisted teams is published.

Selected teams have to fill in some new sections of the Experimental Form and handing it in again into two weeks time. Then it is time to wait again for the selection of the final winner teams.

The contact person of ESA for the campaign is Ms.Elisabeth Celton, who deals with the management of the teams, the deadlines, the organization of the workshop and the stays in Holland and Bordeaux.

2.6.2. Workshop

Winner teams must carry out several tasks once the selection decision is taken. Firstly, the Experimental Form must be updated again. Secondly, a medical exam to get the Certificate JAR FCL3 Class 2, which (the one required to obtain the private pilot license) must be passed. Thirdly, students must attend a workshop in Holland.

The workshop takes place at ESA installations in Noordwijk called ESTEC. The activities developed during three days are the following ones:

- Teams have to give a short presentation about their experiments to the other teams.

- Teams are interviewed by ESA and Novespace experts in order to ensure the experiment safety and to give technical advices to the students.

- Visit to ESTEC facilities.

The interviewing process is very interesting and useful. Experts show students their points of view about the experiment and give practical suggestions on how to build it and solutions to the problems they may meet. During our stay Ms.Marie-Laure Chauffour was the expert in charge of our experiment.

The interviews alternate with lectures on the ways to achieve microgravity conditions, ESA missions and the team's presentations.

2.6.3. Novespace visit and Parabolic Flight in Bordeaux

The lab where the experiment is being prepared will be visited by Novespace experts in order to check its state before going to Bordeaux. We expect them to arrive by early July, when some tests will have been done.

The experiment must be completely ready at the end of August, when the teams will travel to Bordeaux. Many tasks will be performed there after the flight: loading the experiment, attaching it to the rails of the A300, passing some safety tests, etc. The schedule of these activities is detailed in table 2.3.

Table 2.3 Campaign schedule

Task	Dates	State
Send Experimental Form to ESA	January	Complete
Experiment selection	March	Complete
Workshop at ESTEC	April	Complete
Send Experiment Form to NOVESPACE	31/03/06	Complete, but being updated constantly
Send Medical forms to NOVESPACE: Certificate JAR FCL3 Class 2	02/06/06	Complete
Safety review	06/07/06	Work in progress
NOVESPACE visits the laboratory of EPSC/experiment visit by NOVESPACE	?	Getting ready
Journalist selection	November	Complete
Campaign at Bordeaux	From 30/08/06-07/09/06	
Arrival to NOVESPACE	30/08/08	Work in progress
Experiment loading	30/08/08	Work in progress
Experiment loading and preparation in the A300	31/08/06	Work in progress
Experiment in flight configuration	01/09/06	Work in progress
Safety visit, flight suits delivering and safety briefing	02/09/06	Work in progress
Flights	03-04/09/06	Work in progress
Experiment unloading	04/09/06	Work in progress

CHAPTER 3. EXPERIMENT

3.1. Objective of the experiment

The main objective of this experiment is the study of biphasic flows (gas-liquid) in the absence of gravity. In particular, we are interested in determining the behaviour and the dynamics of bubbles in these conditions.

Some members of our lab conducted a series of 12 drops in the ZARM Drop Tower in 2003 to test a novel concept of a micro-channel injection system of bubble generation. This BUBGEN technology [4] will be used in our experiment too. Jets of bubbles of very uniform size, and a diameter of the order of the injection capillary were obtained, and interesting collective dynamics of the bubble were observed.

The buoyancy force dominates the dynamics of bubbles under normal gravity. That is the reason why this phenomenon has a different behaviour in microgravity conditions. The microgravity environment achieved in the parabolic flights is necessary to determine how bubble detachment and dispersion occur in the absence of buoyancy forces.

Bubble dynamics is a very complicated process, due to the nonlinear and long range nature of hydrodynamic interactions. The interactions are induced by the local relative velocity between the bubble and the surrounding fluid. In the presence of gravity, buoyancy is the determining factor of this relative velocity, and hence the dynamics of the group of bubbles. On the contrary, in the absence of gravity, bubble movement is essentially passive, and the hydrodynamic interactions are mainly determined by inertial forces and shears in the liquid. The lack of information on the effects of these interactions, mainly due to the experimental difficulty in efficiently generating large numbers of small and uniform bubbles, has left unsolved some interesting questions on bubble dynamics of technological importance, such as collisions and coalescence events, dispersion efficiency and homogeneity, and clustering of bubbles.

The management of two-phase fluxes is a key step in many technological and scientific applications. Its control would mean increasing the efficiency of heat and mass transport technologies and also improving significantly space systems designs by the replacement of conventional single-phase flow with two-phase flow systems. The replacement of devices currently operated with one phase flows (gas or liquid) by biphasic flow systems is one factor that would favour an important technological advance. The need to characterize this kind of systems is of great scientific importance.

The scientific knowledge gained from the proposed experiment could particularly help to the development of a technology capable of generating gas bubbles in low-gravity environments to support Environmental Control and Life Support Systems (ECLSS). It may allow the improvement of the current expectations of mass transport, power generation systems, bioreactors for

biological and medical research or capillary pump loop technologies among others.

The techniques that enable full control of bubble formation and accurate dispersion in low gravity environments will permit the design of more efficient space systems.

There are many concepts which depend on processes that are performed inefficiently by porous membranes in low gravity (i.e. bioreactors). Our experiment could help to achieve some improvements in features and possibilities, as well as to get energetic advantages by the technology developed in this research (i.e. loop heat pipe management).

The scientific approach of this research project is the following:

The main objective of this experiment is studying the behaviour of biphasic flows in non-gravity; in particular, bubble dynamics and coalescence [10] [11]. It pays special attention to the influence of variations in viscosity and impact angle. Nowadays, there isn't a clear theory of coalescence in microgravity and there are many interesting points to be explored.

We can't predict any result because there are no clear bases of this phenomenon. We just expect that viscosity and impact angle will have an effect on coalescence.

Many physical properties will be studied, such as:

- Velocity distribution in the cavity.
- Collisions suffered by bubbles, relative velocity effect, impact parameter effect and characteristic time of coalescence.
- Effect of liquid viscosity on global dynamics and on coalescence.
- Distribution of bubbles positions in the jet.
- Bubble size study and its frequency of generation.
- Clustering of bubbles.

The results of this research will be obtained from experiments performed in real microgravity conditions. We will compare them with the results get at ground.

Once the experiment is performed, we will perform a statistical study of the data obtained, as well as compare them to theoretical models [12][13][14]. Conclusions on the validity of these models are expected.

Another implicit objective in this project is increasing the quality and quantity of the current experimental results.

3.2. Operation of the experiment and systems

Our experiment is designed to study biphasic flow dynamics and its behaviour in low gravity conditions. In particular, the effect that a variation in the incidence angle between bubbles or a variation in the viscosity of the liquid in which they are immersed has in coalescence. The main goal is to obtain a systematic description of the behaviour in a selected range of parameters.

The experiment is planned to be run in two flights:

-In the first flight, the behaviour of biphasic flows (water and air) is studied. Two injectors are placed, face to face with a changeable incidence angle (explained afterwards).

-In the second flight, the same method of incidence angle is used. The difference lies in the different viscosity of the liquid (silicone oil instead of water).

The basic set up consists on a cavity full of liquid. Two flows of controlled bubbles are introduced through the injectors. The bubbles disperse in the cavity and collide along the way between the cavity inlet and outlet (sketch shown in Fig. 3.1). A high velocity camera records the whole experiment in the bubble path where coalescence is likely to occur.

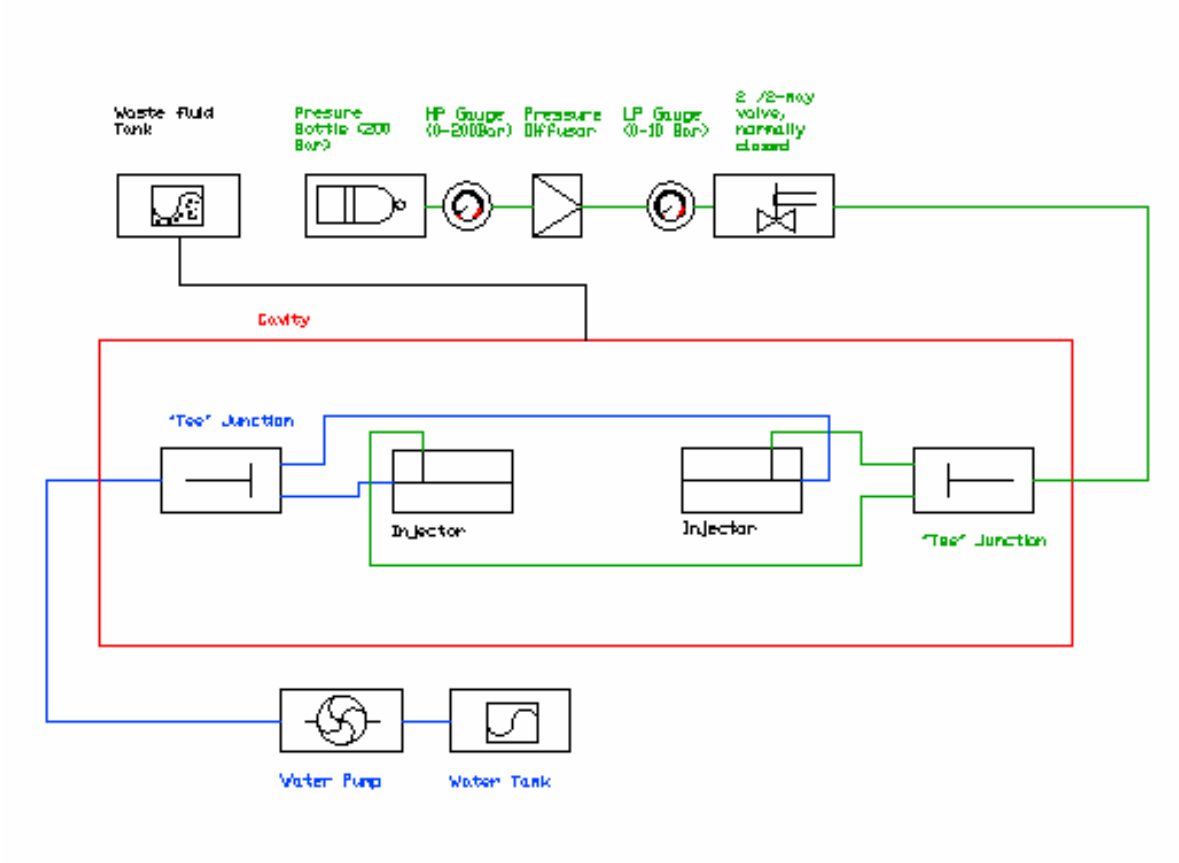

Fig. 3.1 Diagram of the operation

The generation of bubbles in the presence of gravity is generally controlled by the balance between buoyancy forces and capillary forces. In the absence of gravity, additional mechanisms must be employed in order to achieve bubble formation and detachment. In our experiment, we use two injectors (Fig.3.2) based on the pre-generation of a slug flow in a capillary which operates in a regime dominated by inertial and capillary forces. The operation of the injectors is based on the generation of air and water flow (controlled by a regulator, some sensors and a liquid pump) through two different channels. These channels are t-shaped connected and their diameter of 1 mm will limit the bubble size. This technique to generate bubbles (BUBGEN technology)[4] shows certain advantages, such as insensitivity to gravity, easy control of bubble generation and the constant bubble size. The characterization of the injector can be performed in experiments with normal gravity because its performance is independent from the gravity level.

Two bubble injectors will be placed one in front of the other one. This position corresponds to an impact angle of 0º helping the coalescence control. The injectors are fixed to a mobile shaft which is motor operated. The impact angle can be varied by changing the angle of the shafts from 60º to 0º. During each parabola different impact angles from 60º to 0º will be selected, with a decreasing value of 2º approximately. This procedure has been chosen in order to maintain the centre of the cavity without bubbles.

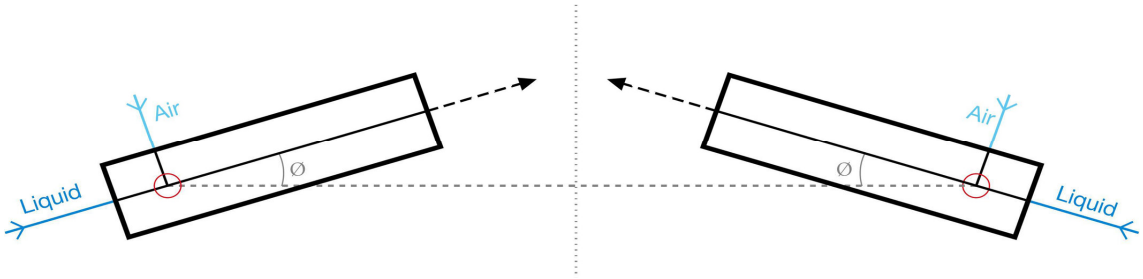

Fig. 3.2 Detail of the shafts

Labview software controls the experiment which is easily monitored by temperature and pressure sensors, water pump control and data acquisition systems.

The experiment contains three main systems:

- Automation and control with Labview. This software manages all the sensors, water and air flow and motors movement.

- Image capture. It contains the camera, server, software and illumination.

- Connections of the equipment. It includes the water and air tubes and the liquid evacuation system and feeding.

3.3. Experiment Design

3.3.1. Cavity

In order to develop the experiment we needed a container where the coalescence took place. It had to be transparent and totally watertight. Methacrylate fulfils all these requirements and it is a common material easy to find.

Waterproofness is a complex requirement because there will be some tubes that will enter the cavity. So, every particular situation must be analyzed.

For selecting the cavity size, a compromise between the following possibilities must be achieved:

- An easy to transport and small cavity on which temperature and pressure changes are more easily noticed.

- A big cavity without space problems for placing the injectors, the sensors and all the mechanisms. Bubbles not removed under microgravity wouldn't difficult the coalescence recording.

After analyzing the experiment requirements, we decided building a 200x360x360 mm cavity because of the following reasons:

- Illumination and motors cause fewer changes on the liquid conditions inside the cavity.

- There are no space problems.

The experiment running lasts about three hours, so a huge number of bubbles is generated. It will be impossible to eliminate many of them, so they would disturb the recording in a small cavity.

3.3.2. Injectors and shafts

Making a 100 mm length and 1 mm diameter hole in a methacrylate block is technically impossible so we had to look for another solution. We have built the injectors by mechanizing a half T pipe in a face in two different blocks of methacrylate and then we have joined them. In addition we have added some holes in order to fix the injectors to the shafts. The injector assembled and disassembled is shown in Fig. 3.3

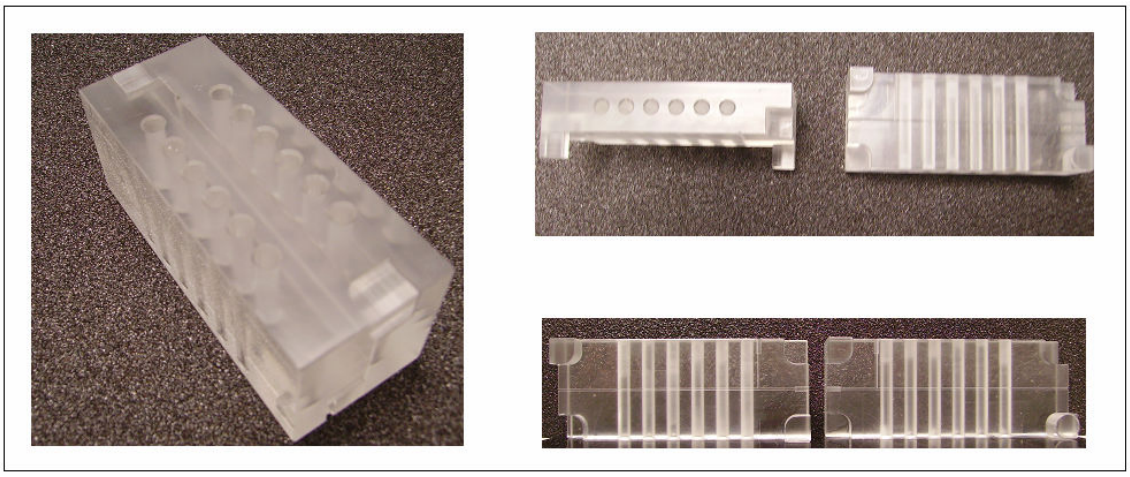

Fig. 3.3 Injector

The solution to vary the incidence angle is leaning both injectors over two anodized aluminium shafts which are moved by stepper motors. In order to install these shafts in the cavity, two cylindrical stands with a ball-and-socket joint and a retainer will be anchored at two opposite faces of the cavity.

The ball-and-socket joint is necessary to make the movement of the shaft easier. The retainer is the element that will provide waterproofness.

Shafts have been mechanized in aluminium since they should be resistant and lightweight. They are the moving part of the cavity. They have been anodized because they have to be in contact with different liquids.

The anodized process consists of obtaining oxide layers thicker and with better protection characteristics than the natural ones. These are obtained through electrolytic and chemical processes (by using a sulphuric environment). It is a good way to protect the aluminium from atmospheric agents.

Shafts are built over ball-and-socket joint in order to avoid unnecessary frictions and facilitate the rotation. The shaft is fitted in two ball-and-socket joints instead of using bearings because if they were used, an undesired misalignment in the shafts may occur since the system works at low velocity (rotation angle lower than 60º) and, consequently, the bearings can wear out.

3.3.3. Waterproofness

As it has been mentioned in previous sections, there are some elements that pierce and enter the cavity. It contains liquid so it is compulsory to avoid water leak through the entrance holes of these elements. To carry out this process, every case must be analyzed separately:

Shafts: To protect the experiment from water leak, retainers and waterproof o-ring joints have been used.

Tube entrance holes: These holes have been sealed with silicone, because it allows flexibility to changes for future experiments.

Temperature Sensor: It incorporates a cable bulkhead and has been sealed with silicone in order to avoid leaks.

The selected materials to ensure waterproofness are:

Retainers: It is an element that guarantees waterproofness in a rotating axis. They are placed between the shafts and the cylindrical stands. Our choice was double lipped retainers with ring springs (Fig 3.4).

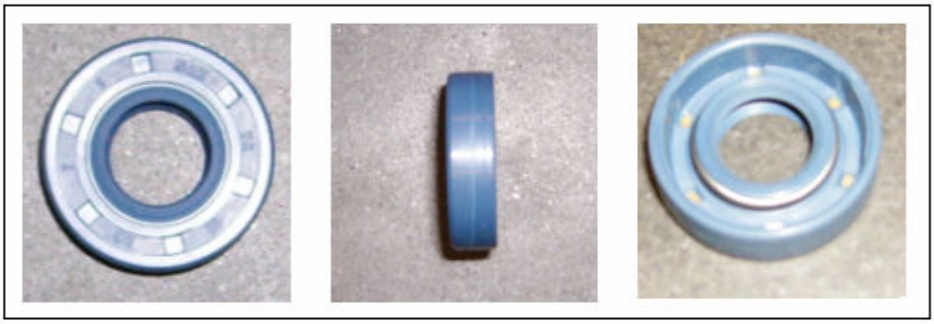

Fig. 3.4 Retainer

Waterproofness joints: They are made of a 2 mm thick rubber sheet. They are placed between the cylindrical stand and the cavity, and offer waterproofness in an area where silicone cannot be used since it needs a solid support.

Fig. 3.5 shows the cross section schematic and the different parts of the waterproofness system assembled.

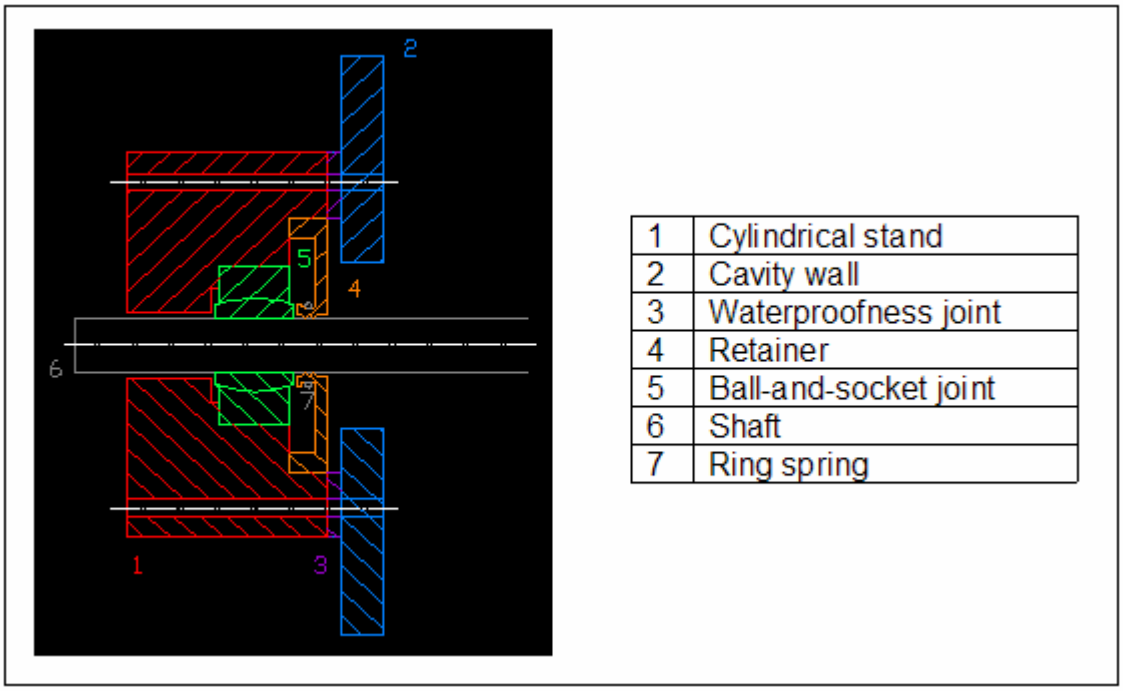

1	Cylindrical stand
2	Cavity wall
3	Waterproofness joint
4	Retainer
5	Ball-and-socket joint
6	Shaft
7	Ring spring

Fig. 3.5 Waterproofness system

3.3.4. Motors

A stepper motor is required in order to accurately control the shaft movement. A union element between the shaft and the motor such as an Oldham connector is required. Moreover it is necessary to have a motor subjection system in order to ensure the alignment with the shaft.

The McLennan 23HSX stepper motor model has been chosen. It has a torque of 1.63 Nm, which is enough to rotate the shaft of the injectors. This model allows working in single-polar or bipolar mode. We will work in single-polar model because of its simplicity, despite it causes a loss in motor's efficiency.

The stepper motor is connected to the shafts by using an iron disc. It fits the shape of the motor and allows the fixation to the screwed sticks. Threads will remain under the surface of the disc so holes must have two levels, one with a diameter of 3 mm for the sticks and another for the threads. The diameter of the second one must be wide enough (10 mm) to introduce the spanner. All the parts are shown in Fig. 3.6.

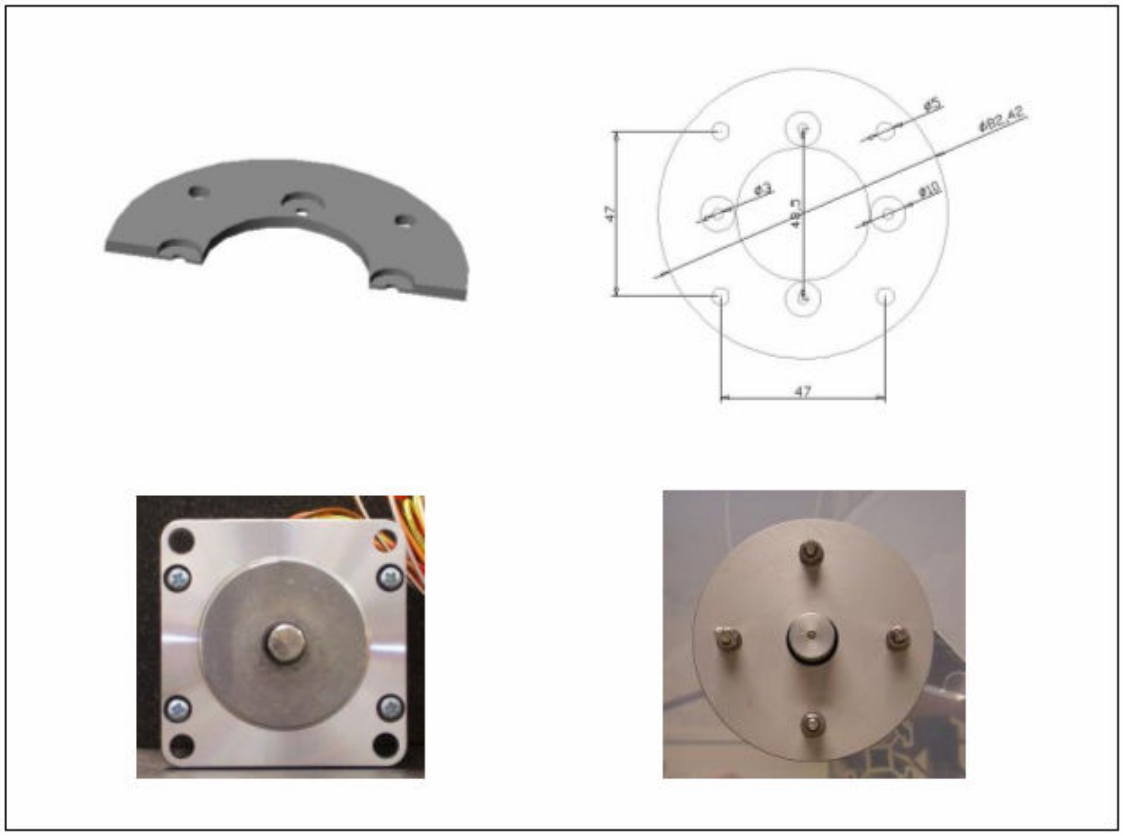

Fig. 3.6 Motor Fixation

An union element which transmits the force and maintains the motors and the shafts aligned is needed. We have chosen an Oldham transmission system (Fig.3.7) in order to provide motion to the shafts, that is, to connect motors with shafts.

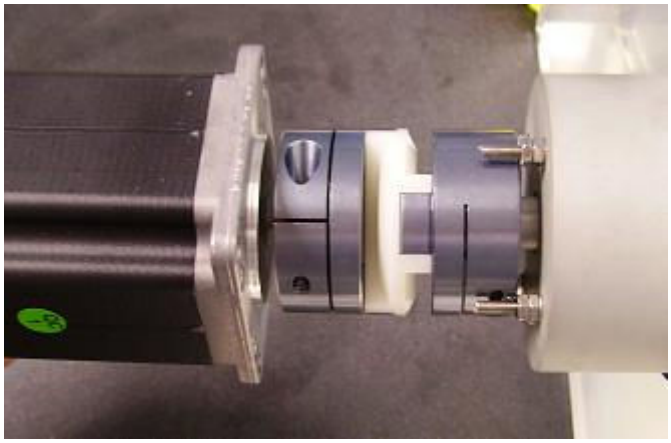

Fig. 3.7 Oldham transmission system

3.3.5. Liquid pumping and tank system

A liquid pump is necessary to inject the liquid. As we don't want to introduce perturbations in the injected liquid it is necessary a pump that ensures a constant flow. This requirement is guaranteed by gear pumps. The selected gear pump is Ismatec MCP-Z Standard which allows generating a vast variety of flows and PC remote control by Labview. The pump needs to have an input of remote control in order to monitor it by PC.

The two liquid containers needed (one for the liquid entering the cavity and another for the mixture that leaves the cavity) will be a type of saline solution bags. They will make up for the pressure and avoid possible problems under microgravity conditions.

Tube size is another important point of the pumping system to take into account. The diameter of injectors is 1 mm and the one of the pump outlet is 1/16". In order to solve this difference of diameter a series of size converters are required. They must offer a sure fixation and without leak.

Tubes selected are made of Teflon. This material offers good resistance to internal pressure and flexibility facilitates the liquid flow and allows using the GyroLok® system [16]. GyroLok® system (Fig. 3.8) consists of a rear ferrule that pushes a front ferrule. It enters the body and its cone angle decreases as shown in Fig. 3.9. Thus, the tube which is enveloped by all these pieces remains held and fitted. This system has the ability to mix components of different manufacturers and tubes configurations.

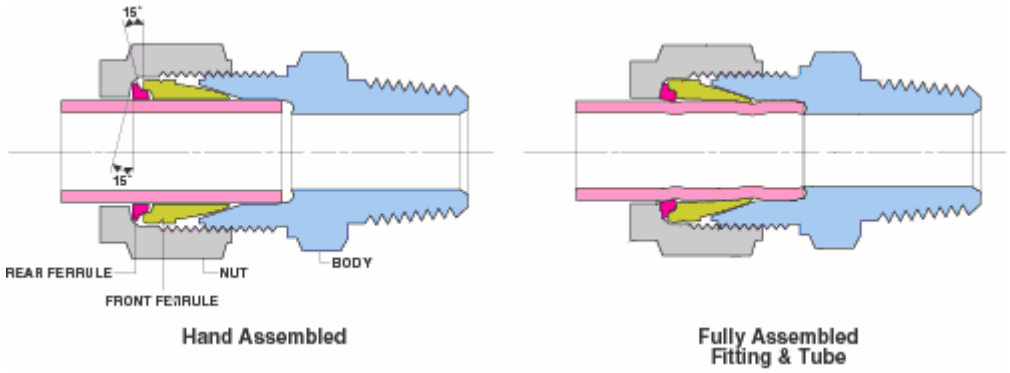

Fig. 3.8 GyroLok system [15]

Fig. 3.9 GyroLok Parts [16]

3.3.6. Air injection system

Two different components may be used for air injection: a pressure air bottle or a compressor. The experiment needs laboratory synthetic air so that the minimum amount of particles enters the injector and affects the experiment environment. Air injection must be PC controlled, because in some phases of the experiment the air flow will be stopped.

An air pressure bottle has been selected because of the following reasons:

- An air compressor would introduce vibrations in the experiment.
- A pressure air bottle provides synthetic air, particle free. Using a compressor would imply having filters to remove the particles of the air coming from the exterior.
- The air pressure bottle provides a more regular air flow than the compressor.

To achieve air flow remote control, an integrated electronic valve is placed at the outlet of the gauge. The air flow can be stopped by the PC (see more details in section 3.4).

3.4. Data acquisition and control system

Let's review what we have and what we want. We have an enormous amount of bubbles, with an approximate diameter of 1 mm, and others that will have a bigger size once coalescence have taken place. We need to capture some parameters on real time in order to monitor the cavity: high velocity video recording, temperature, pressure and acceleration. Other characteristics such as fluids viscosity and density will be obtained in the lab.

Parameters like density, viscosity, pressure or temperature are important in order to compare experimental results with theoretical models, since they appear in many equations and models. As it is an experiment in microgravity, it is really useful to register the gravity level achieved at every moment. Moreover, it is an important safety measure to know the pressure in the more sensitive to leaks areas (the cavity).

Relative velocity of bubbles can be obtained from the images taken. We also need to control the water pump, the shafts inclination and the valve which opens and closes the air flow. In table 3.1 the specifications of our system are indicated:

Table 3.1 System specifications

Magnitude	Minimum	Maximum
Pressure in cavity	0 atm	3 atm
Temperature in cavity	0 ºC	30 ºC
Acceleration	-2 g	2 g

The board with an integrated ATMEL® ATmega8 microcontroller will be programmed to manage sensors data capture, control subroutines of the stepper motors, the electronic valve and the communication ports. Fig. 3.10 shows the device schematics.

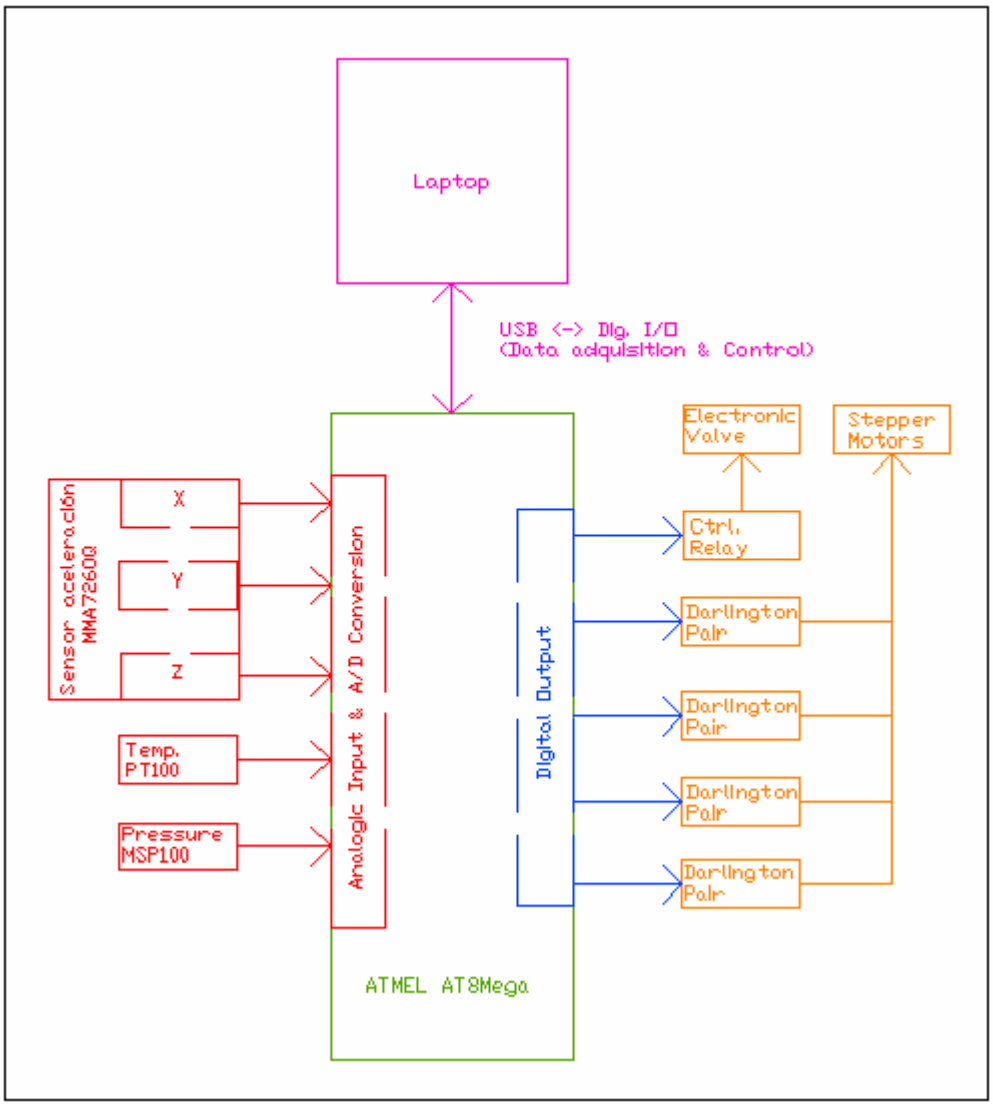

Fig. 3.10 Device schematics

3.4.1. Sensors conditioning and selection

Temperature sensor

We have chosen a PROBE PT100 (Fig.3.11) instead of another technology like NTC, PTC or Thermocouples because of its accuracy, sensitivity and linearity. As it will be underwater, it's composed by a watertight stainless steel probe that contains the thin platinum film temperature transducer.

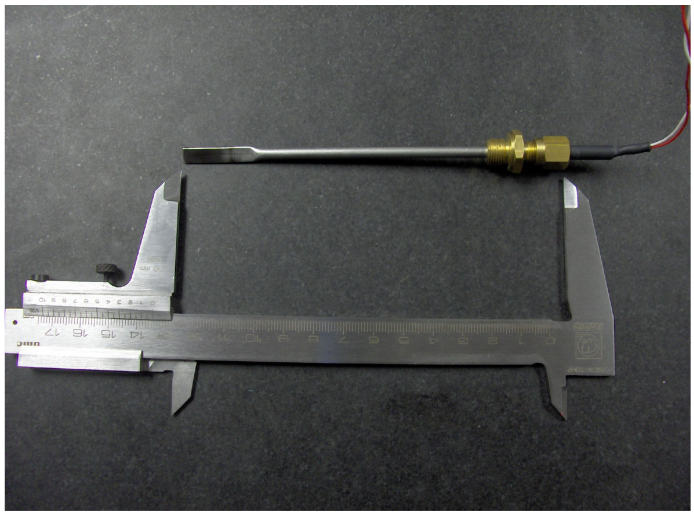

Fig. 3.11 Probe PT100

The detection area is 25 mm length and is placed at the extreme of the probe. Its technical specifications are shown in Table 3.2.

Table 3.2 Probe PT100 features [17]

Detector material	Platinum film
Resistance at 0 ºC	100 ±0,1 Ω
Sensitivity (α)	0.00385 Ω/ºC
Tolerance	BS 1904 Class B (DIN 43760)
Operating temperature	From -50 ºC to +250 ºC

Eq. 3.1 characterizes the PT100 resistance behaviour.

$$R_P = R_0\left(1+\alpha\left(T-T_0\right)\right) \qquad \textbf{(3.1)}$$

Table 3.3 shows the results of the tests done with a HART 9102S climatic camera and a PREMA 5017 7½ digit multimeter in order to characterize the sensor.

Table 3.3 Test table

T (ºC)	R (Ω)
0	*100.5*
10	*103.9*
30	*111.5*
50	*118.9*

In order to set up the temperature sensor we will use a Wheatstone bridge. Temperature caption is based in the measurement of the electric potential difference between V_a and V_b. Fig. 3.1 shows the schematics.

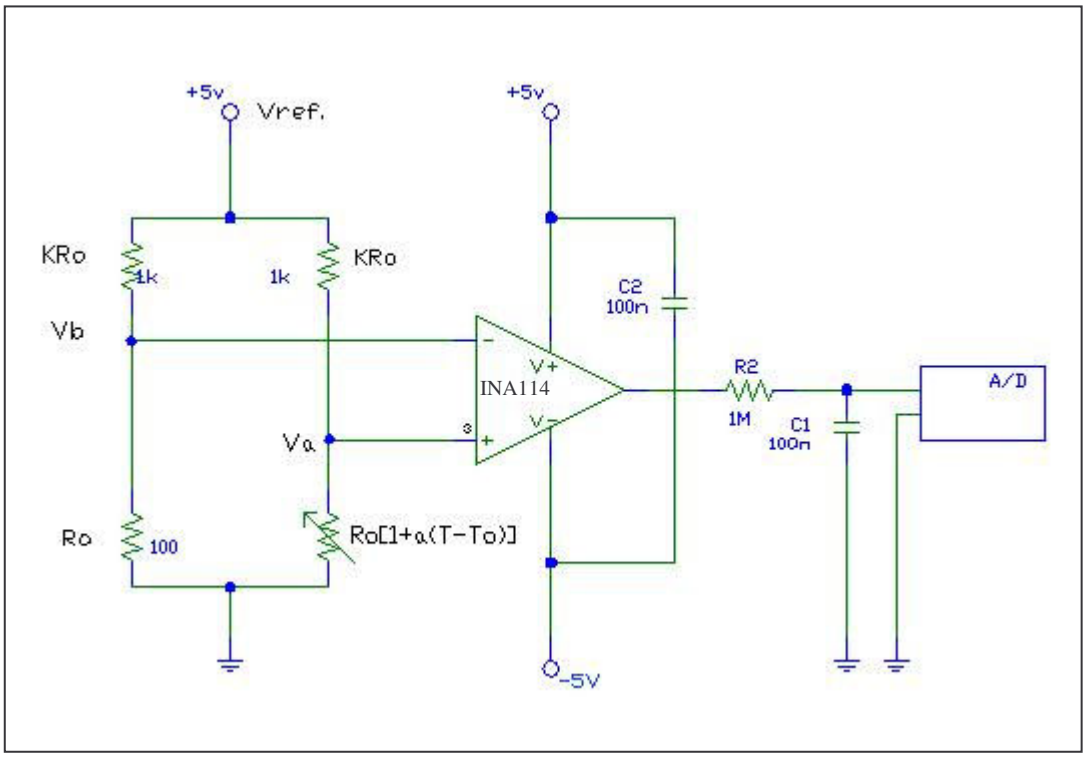

Fig. 3.12 Temperature sensor conditioning

Let's explain how circuit in Fig. 3.12 works. We will start with the Wheatstone bridge. Eq. 3.1, Eq. 3.2 and Eq. 3.3 rule the bridge. They are just the development of Ohm's Law:

$$V_a = V_{ref.} \frac{R_0(1+\alpha\Delta T)}{R_0(1+\alpha\Delta T)+KR_0} \qquad \textbf{(3.2)}$$

$$V_b = V_{ref.} \frac{R_0}{R_0 + KR_0} \quad \textbf{(3.3)}$$

Temperature is obtained measuring the electrical difference of potential between V_a and V_b, as shown in Eq. 3.4. V_{ref} value must be very stable and must be known. Let's analyze its behaviour.

$$V_d = V_a - V_b \quad \textbf{(3.4)}$$

The expression of V_d is simplified with the following mathematical development of the equality:

$$V_d = V_{ref} \left[\frac{R_0(1+\alpha\Delta T)}{R_0(1+\alpha\Delta T)+KR_0} - \frac{R_0}{R_0+KR_0} \right] \quad \textbf{(3.5)}$$

$$V_d = V_{ref} \left[\frac{1+\alpha\Delta T}{1+\alpha\Delta T+K} - \frac{1}{1+K} \right] \quad \textbf{(3.6)}$$

$$V_d = V_{ref} \frac{(1+\alpha\Delta T)(1+K)-(1+K+\alpha\Delta T)}{(1+K+\alpha\Delta T)(1+K)} \quad \textbf{(3.7)}$$

$$V_d = V_{ref} \frac{1+\alpha\Delta T+K+K\alpha\Delta T-1-K-\alpha\Delta T}{(1+K+\alpha\Delta T)(1+K)} \quad \textbf{(3.8)}$$

As the term *(1+K)* of the denominator is much greater than the term $\alpha\Delta T$, Eq. 3.8 becomes Eq. 3.9. V_d variation can be considered as a linear parameter.

$$\alpha\Delta T << (1+K) \quad \Rightarrow \quad V_d \approx V_{ref} \frac{K\alpha\Delta T}{(1+K)^2} \quad \textbf{(3.9)}$$

The linearity increases when K parameter gets higher in Eq. 3.1 and Eq. 3.2, but sensitivity decreases.

Bridge resistances must be made of metallic film since this kind of resistances are less sensitive to temperature changes.

The next step to follow is configuring the amplifier gain. In our case, we use an INA114 precision instrumentation amplifier, from Texas Instruments. Fig. 3.13 shows its pin configuration.

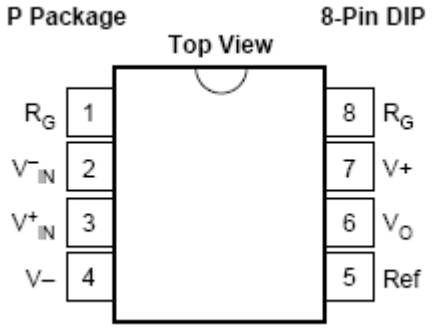

Fig. 3.13 INA114P pin configuration [18]

The gain is selected through a resistance R_G, placed between the pin numbers one and eight. By solving Eq. 3.10 any gain between 1 and 10.000 can be tuned.

$$G = 1 + \frac{50\ \text{k}\Omega}{R_G} \tag{3.10}$$

In order to find the required specific gain, we must establish the operational range of our sensor. It has to be capable of determining temperatures between 0 ºC and 30 ºC. Let's apply Eq. 3.9.

$$V_{d_{30°C}} = 5 \times \frac{10 \times 0.00385 \times (30 - 0)}{(1+10)^2} = 0.048\ \text{V} \tag{3.11}$$

$$V_{d_{0°C}} = 5 \times \frac{10 \times 0.00385 \times (0 - 0)}{(1+10)^2} = 0\ \text{V} \tag{3.12}$$

Then, we must choose a DC offset and a gain, in order to optimize the analogical to digital conversion. The following system must be solved.

$$\left(V_{d_{0°C}} + V_{offset}\right)G = 0\ \text{V} \tag{3.13}$$

$$\left(V_{d_{30°C}} + V_{offset}\right)G = 5\ \text{V} \tag{3.14}$$

Once the system is solved, it is known that the offset and the gain values are 0 V and 104.76, respectively. We will approximate the last value to 100. The required resistance can be obtained from Eq. 3.10 or from the charts given by the manufacturer. In our case, resistance has a value of 505.1 Ω. The commercial resistance which closely approaches this value is 511 Ω, with a tolerance of 1 %.

The instrumentation amplifier must have a high value of CMRR (Common Mode Rejection Ratio). INA114 has a CMRR value of 120 dB for a gain of 100 and at a frequency below 100 Hz.

The next step is configuring the RC low pass filter at the outlet of the amplifier. We will take one measurement of temperature per second (1 Hz). Thus, filter's frequency cutoff (the point where the signal starts to be attenuated 3 dB) will have an approximate value of 3 Hz. Eq. 3.15 shows the ratio:

$$f_c = \frac{1}{2\pi RC} \qquad \textbf{(3.15)}$$

In our case, the values of the resistance and the capacitor are 1 MΩ and 100 nF, respectively. It is also necessary to place decoupling capacitors in the active elements supplies, i.e. in the instrumentation amplifier (see C2 in Fig. 3.13).

In addition, the digital resolution of the acquisition system can be computed by means of Eq. 3.16.

$$resol. = \frac{F.S.}{2^n} \qquad \textbf{(3.16)}$$

Where *F.S.* is the full scale (30 ºC - 0 ºC) and n is the bits number of the AD converter (10). Thus, the maximum digital resolution of our system is 0.03 ºC.

It is possible that impedances of wires in PT 100 PROBE sensor vary with temperature. Then, it is needed to minimize the length of the wire in order to avoid these variations.

Pressure sensor

As temperature, pressure is one of the most important parameters to monitor.

We have chosen an integrated MSI MSP100-100P sensor (Fig.3.14) because its pressure operational range is suitable for our requirements, the frequency response is high and the sensor is compact and waterproof.

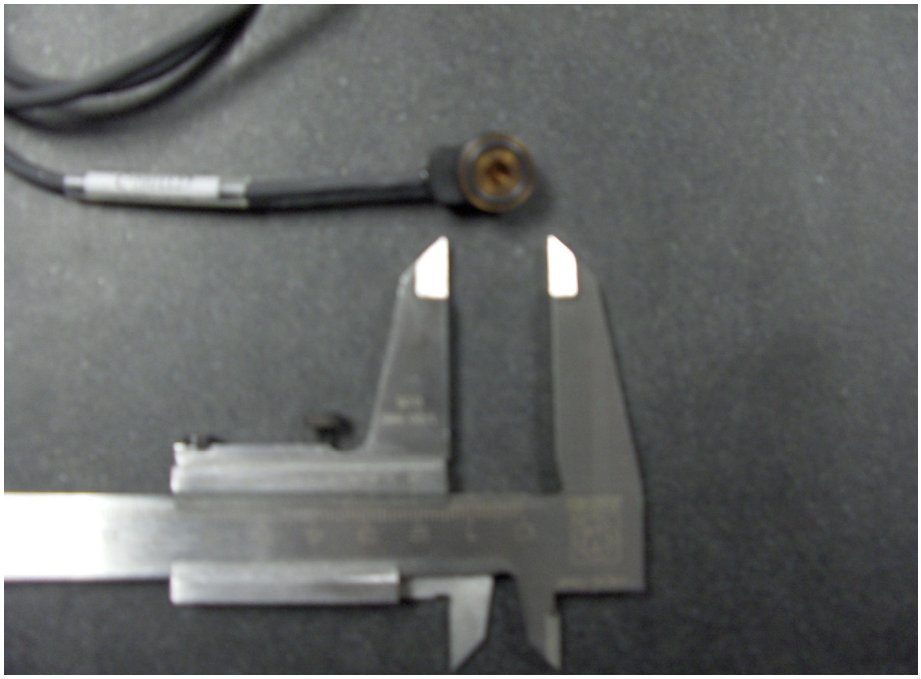

Fig. 3.14 MSP 100-100P

MSP100 presents an important advantage compared to the temperature sensor: the signal conditioning circuit is integrated in the sensor and it offers a linear output from 0 mV to 100 mV between 0 psi and 100 psi (that is a range between 0 atm and 6.8 atm). Its sensibility value is 0.068 atm/mV.

A suitable gain for pressure range (0 atm – 3 atm) must be selected. In the Eq. 3.17 and Eq. 3.18 we will compute the gain and the offset.

$$\left(V_{d_{0atm}} + V_{offset}\right)G = 0 \text{ V} \quad \textbf{(3.17)}$$

$$\left(V_{d_{3atm}} + V_{offset}\right)G = 5 \text{ V} \quad \textbf{(3.18)}$$

The values found for the gain and the offset after solving the system of equations are, respectively, 113 and 0 V. The gain must be configured in a INA114 as explained before, that is, solving the Eq. 3.10 in order to find the value of R_G. The resistance needed is 446.4 Ω.

The digital resolution of the acquisition system can be computed by means of Eq. 3.16, where *F.S.* is the full scale (3 atm – 0 atm) and n is the bits number of the AD converter (10). Thus, the digital resolution of our system is 0.003 atm. Fig. 3.15 shows the system schematics.

Eq. 3.15 is used in order to allocate the filter's values (*R2* and *C2*). A resistance of 1 MΩ and a capacitor of 1 nF are needed frequency cutoff of 160 Hz. It is also necessary to place decoupling capacitors in the active elements supplies

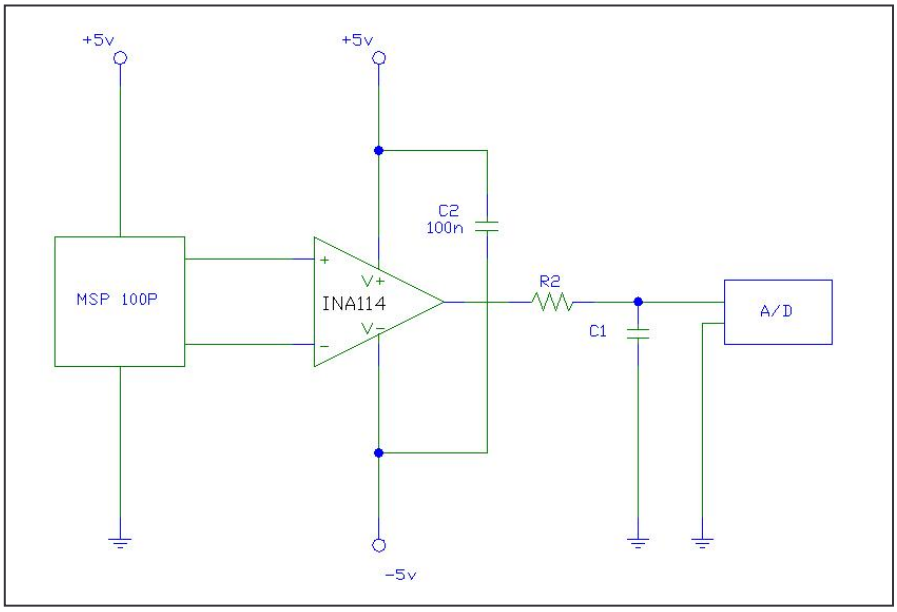

Fig. 3.15 MSP-100P circuit schematics

Accelerometers

Considering that our experiment is designed to be run under microgravity, it is very useful to have an acceleration data register which is synchronized with the other sensors and the data acquisition system. In Fig. 3.16 an image of the selected acceleration sensor is shown.

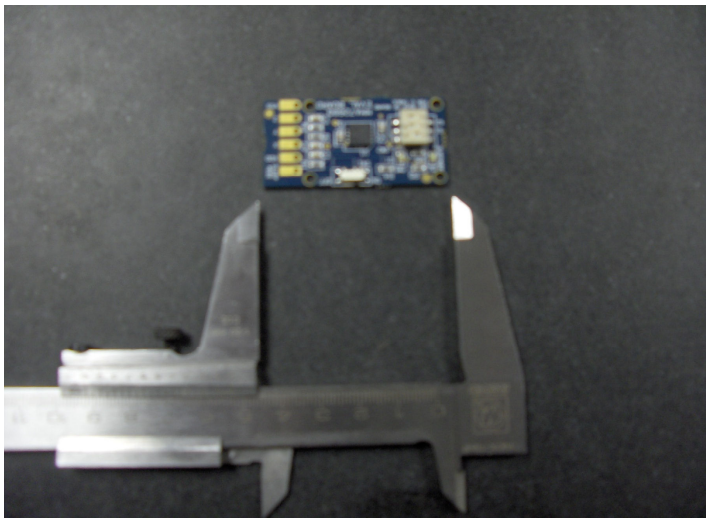

Fig. 3.16 FreeScale MMA7260Q

We have selected the MMA7260Q, an integrated Sensor of FreeScale. It offers acceleration data on the three axes with a resolution of 10^{-2} g. As the rest point is at 1.65 V and the sensitivity is 600 mV/g, we can connect the accelerometer directly to the board. Thus, there is no need of an extra signal conditioning except in the filter area. This accelerometer allows a dynamic variation in the full scale, which is an useful feature. It can be configured at ±1.5 g, ±2 g, ±4 g and ±6 g.

Eq. 3.15 is used in order to allocate the filter's values (*R2* and *C2*). A resistance of 1 MΩ and a capacitor of 1 nF is needed. The cutoff frequency is 160 Hz.

Table 3.4 shows the output of the accelerometer board. These data are used for sensor output characterization, referred to positions given in Fig. 3.17.

Table. 3.4 Outputs depending on the board heading.

Position	**V_{dd}**	**V_X**	**V_Y**	**V_Z**
A	*3.3*	*1.574*	*1.65*	*2.42*
B	*3.3*	*2.398*	*1.673*	*1.614*
C	*3.3*	*1.54*	*0.843*	*1.611*

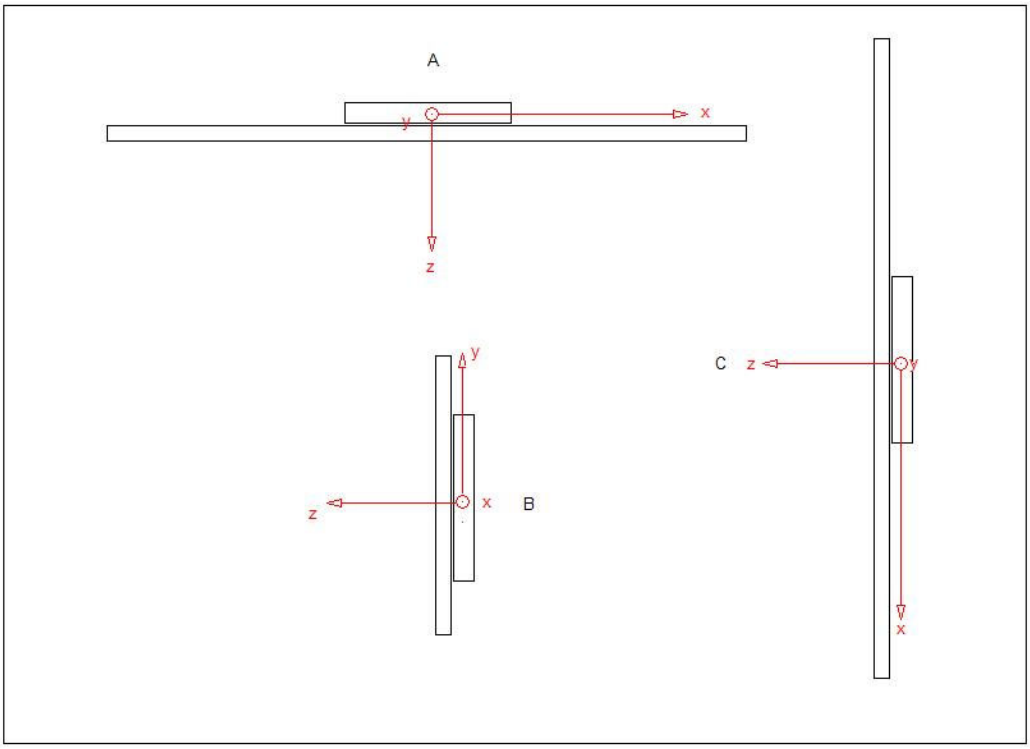

Fig. 3.17 Board heading

The accelerometer board output signal will be between 0 V and 3 V and the full scale will be between -2 g and 2 g. As our 10 bit converser works between 0 and 5 V we will only be using 612 of 1024 levels of quantification (204 per Volt). Our digital resolution will be 0.0065 g.

3.4.2. Actuators

Stepper motors

Stepper motors are a very important part of the control system since they control the inclination of the shafts and it requires precision. We have selected the HSX 23 hybrid model with high efficiency. Its retention torque is 1.52 Nm. It contains 4 windings. Rotation is done in steps of 0.9º or 1.8º by applying energy in the coils following a proper sequence. Fig. 3.18 shows the selected models.

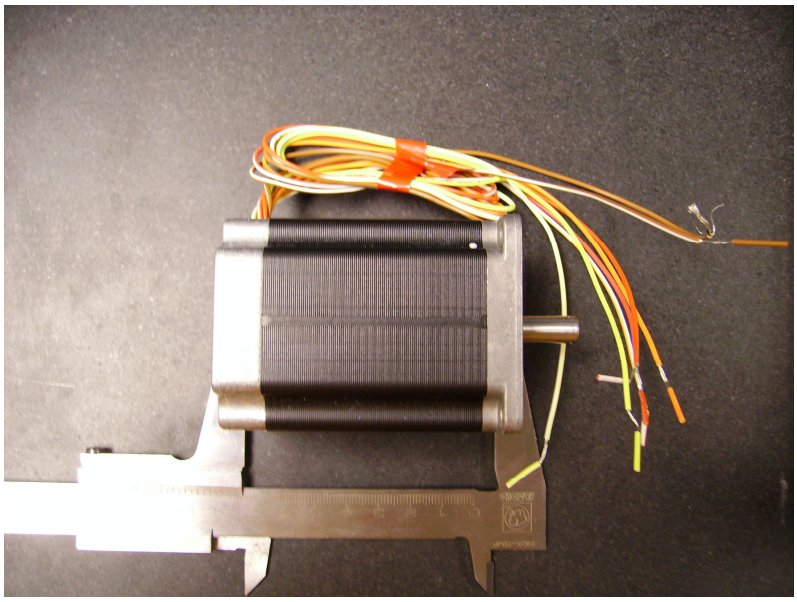

Fig. 3.18 HSX 23 Stepper Motors [19]

HSX 23 hybrid can be run in single-polar or bipolar mode. In our case, it will work in single-polar mode since its performance is simpler. Nevertheless, its efficiency is lower in single-polar mode but in our case it is not relevant because we will work at low revolutions and the torque needed is quite low.

Fig. 3.19 shows the coils distribution, the connections colours code and the electric parameters of the motor.

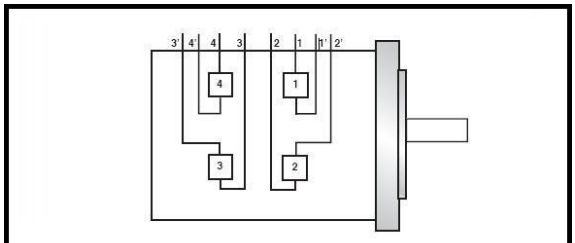

Lead colours

1	1'	2'	2	3	3'	4'	4
Brown	Brown/ White	Orange/ White	Orange	Red	Red/ White	Yellow/ White	Yellow

Size 23 stepper motor specification

Maximum Holding Torque	Maximum phase current		
	Uni-polar	Bi-polar	
		Coils in series	Coils in parallel
0.47 Nm	1.0 Amp	0.7 Amp	1.4 Amp
0.98 Nm	3.0 Amps	2.1 Amps	4.2 Amps
1.63 Nm	3.0 Amps	2.1 Amps	4.2 Amps

Fig. 3.19 Motor configuration [19]

As this motor works with a higher current than the board, it will be necessary to insert a power phase between the control board and the motors since it supplies just a few mA. In order to amplify the intensity we will use BD645 Darlington pair. Its parameter of current amplification (β) is 1000, and its maximum outlet intensity is 5 A. 1 kΩ resistances will be wired in series at the outputs of the control board in order to achieve enough base current to work in cut-saturation mode. Fig. 3.20 shows the connection diagram of the stepper motor.

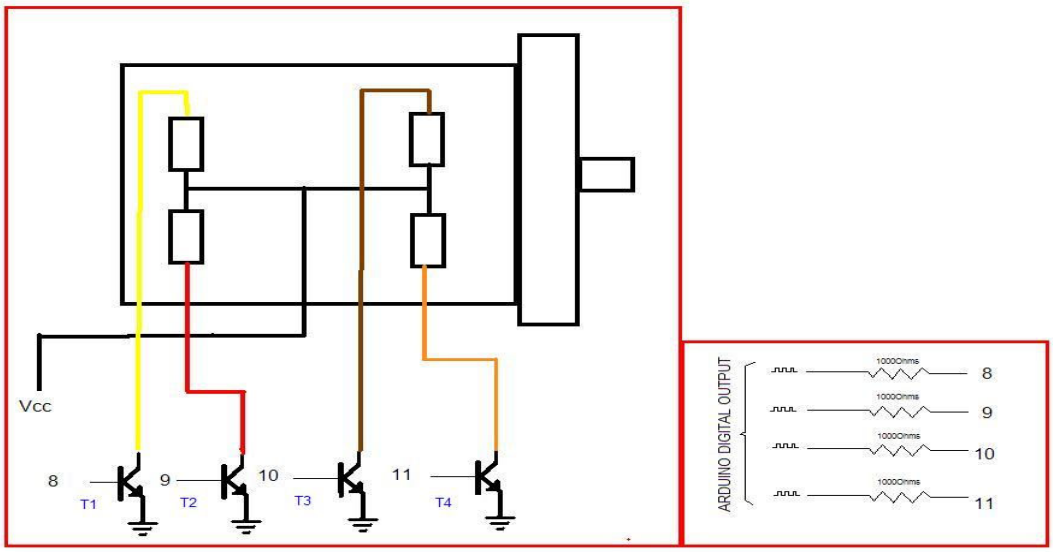

Fig. 3.20 Motor assembly schematics [20]

Once we know how to build a motor we must use a routine that makes it rotate properly. Table 3.5 shows a routine that allows the motor conditioning in single-polar half step mode.

Table 3.5 Motor Conditioning [20]

	Step	T1	T2	T3	T4	
Counter clockwise ↑	1	**1**	0	**1**	0	↓ Clockwise
	2	**1**	0	0	0	
	3	**1**	0	0	**1**	
	4	0	0	0	**1**	
	5	0	**1**	0	**1**	
	6	0	**1**	0	0	
	7	0	**1**	**1**	0	
	8	0	0	**1**	0	

Now we can manage axis rotation by a control routine programmed on the Arduino board.

Electronic valve

In order to control the air injection we will use an electronic valve from Bükert (Fig. 3.21). It works at 220 V, so we will control it by means of a relay connected to an Arduino board.

Fig. 3.21 Electronic valve [21]

The valve allows the air flow pass when it is connected to the power supply. Thus, if the current is cut off, the air flow will be blocked. Fig. 3.22 shows the electronic valve schematics.

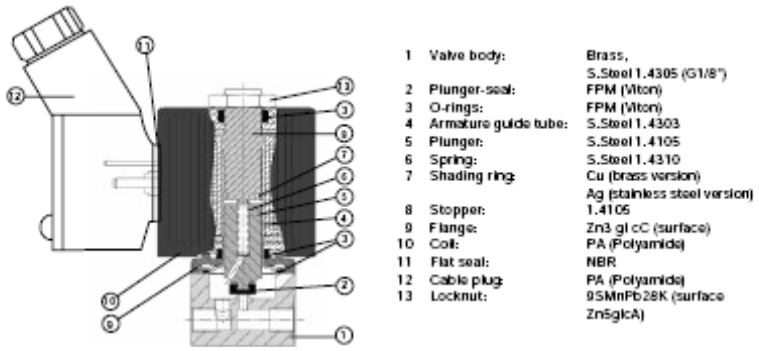

Fig. 3.22 Electronic valve schematics [20]

3.4.3. PCB integration of the data acquisition elements and actuators

Two boards have been designed in order to facilitate the operation of the elements explained before. Fig. 3.23 shows the schematics of P-CAD software which integrates the sensors of temperature and pressure and the acceloremeters whilst Fig. 3.24 shows the motors control circuit.

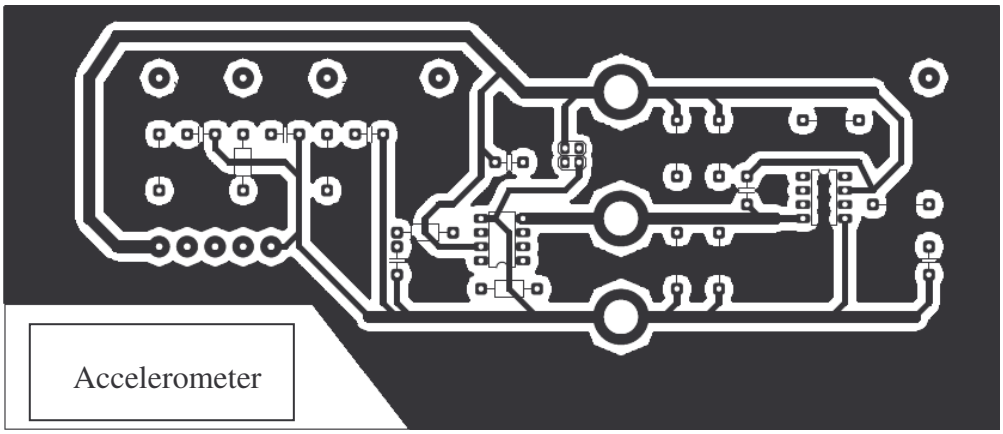

(a)

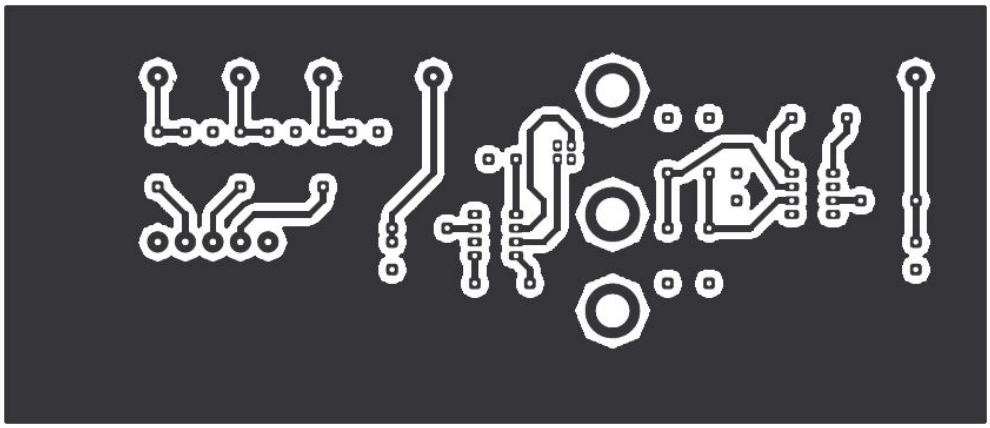

(b)

Fig. 3.23 Sensor PCB design: top face (a), bottom face (b)

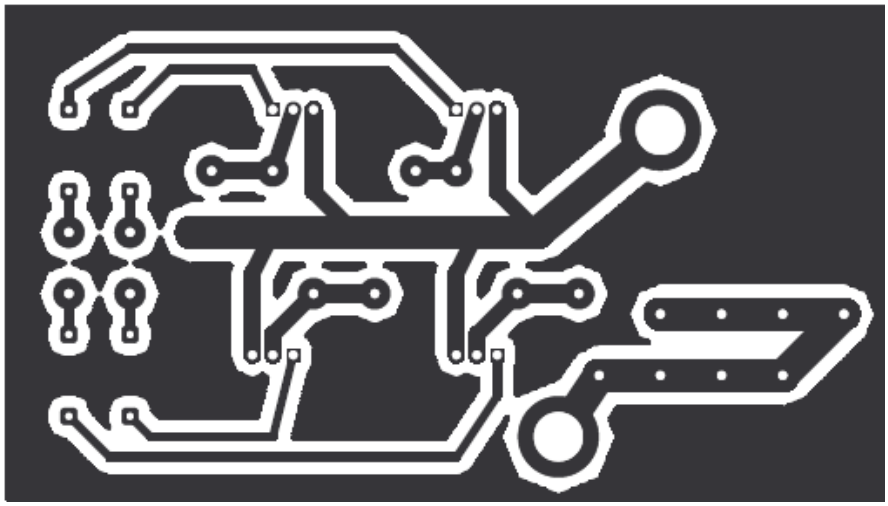

Fig. 3.24 Stepper motor PCB design.

3.4.4. Control software

The programme which controls the board must include the software necessary to manage its hardware. At the same time, it must also be coordinated with Labview software, by an USB connection. These are the elements that will take part in this operation:

- Temperature sensor
- Pressure sensor
- Accelerometer
- Stepper motors
- Electronic valve

Sensors will measure with a fixed refresh frequency. Motors and the electronic valve will be controlled from the PC.

Arduino board has six analogical inputs. Three of them will be used for acceleration, one for pressure and another one for temperature measurement. In addition, five of the fourteen available digital inputs will be used; four of them will control the motors, and another one will control the electronic valve. Fig 3.25 shows the board.

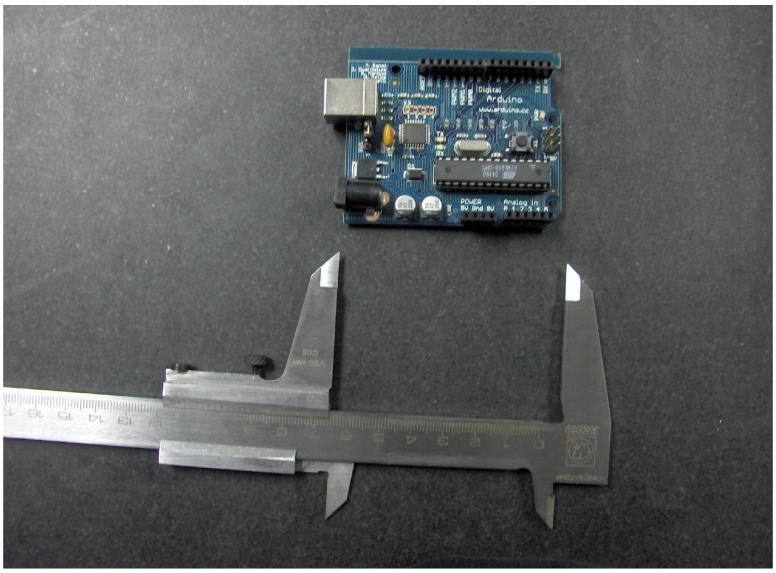

Fig. 3.25 Arduino Board

In order to control Arduino board it's necessary to introduce a programme with the instructions it must follow. Programming these instructions is very similar to programming on C language. Nevertheless, it has special features linked to the board. It is not expected to directly operate the board while running the experiment, but it will be operated through LabView®. This software allows creating a graphic interface easy to use. It controls and monitors the whole experiment. It also manages the PC ports, which is an essential process to control Arduino board and obtain the information. Labview will store the obtained data in order to analyse it after running the experiment.

3.5. Image capture system

In order to study the behaviour of bubbles it is necessary to examine their movements in detail. These movements occur at so high velocities that a normal video camera cannot detect them. Then, high velocity cameras are needed.

There are different kinds of high velocity cameras. The features that characterize each camera are listed next:

- Colour: Colour/Monochrome.
- Sensor: CCD/CMOS.
- Connection type.
- Data storage.
- Crash resistance.

Selecting a camera is a complex process and all the characteristics must be analyzed in detail in order to choose a camera that satisfies one's necessities.

Small details in the selection process can mean some thousands of euros in the final price.

Our camera had to fulfil the following parameters:

-Resolution: 500x500 pixels
-Velocity: 500 fps

Once we knew what we needed, we determined what we did not specifically need: a colour camera, a camera that could reach a higher velocity than 500 fps, neither more resistance than 2 g (the maximum level of gravity achieved by the A300 during the parabolic flights). So a conventional camera was enough for our necessities, because they are certified for 5 g. The last steps were choosing the kind of sensor we were going to use, the connection type and the data storage system.

3.5.1. Optical sensors

There are two types of sensors in the market for the construction of digital cameras: CCD and CMOS.

CCD Sensors

Its abbreviation stands for Charge-Coupled Device, which means device of interconnected electric charges.

When a photograph is taken, the CCD sensor receives the light that passes trough the lens of the camera. Each one of the tiny pixels that compose the CCD sensor turns the light into electrons. The number of electrons, generally known as pixels accumulated charge, is measured and turned into a digital value.

CMOS Sensors

CMOS stands for Complementary Metal Oxide Semiconductor. It is a semiconductor device composed by two field-effect transistors made of metal oxide (MOSFET). One of them is type N (NMOS) and the other one is type P (PMOS) and both are integrated in a unique chip of silicon. As CCD, CMOS turns light into electrons but, in this case, each pixel makes the conversion.

Differences between CMOS and CCD

Fig. 3.26 compares CMOS and CCD sensors.

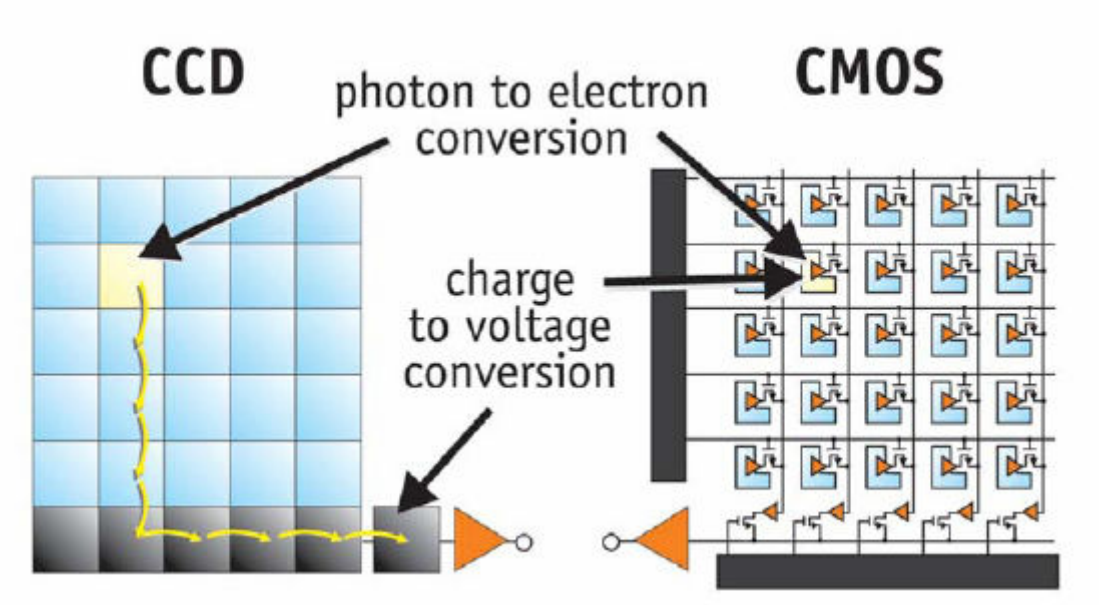

Fig. 3.26 Operation difference between CCD and CMOS [22]

Firstly, there was a big difference of price and quality between them. Recently, they have achieved a balance and it makes no sense to say which one is better but it makes sense saying that one is better than the other for specific purposes. Table 3.6 shows the pros and cons of each sensor.

Table 3.6 CCD vs CMOS [23]:

Features	CCD	CMOS	Comments
Scan/Sweeping Velocity	N	G	CMOS has not register H
Sensitivity	N	B	CMOS has low conversion factor
Sign/Noise ratio	G	B	CMOS due to Fixed Pattern Noise
Dark current	G	B	CMOS 10 times higher than CCD
Smear	N	G	Excellent for high velocity cameras CMOS
Dynamic range	G	B	Due to photodiodes
Random access to pixels	B	G	CMOS allows capturing random pixels
Multiple ROI	B	G	CMOS can work with multiple interest regions
Fill Factor	G	N	CCD can achieve 100%
Miniaturization	G	N	CMOS just a small percentage of the area is occupied by photodiode

G: Good N: Normal B: Bad

We chose a camera with a CMOS sensor, which offers the following advantages:

-Higher velocity with the same price of a CCD
-Adjustable resolution.
-Possibility of making masks.
-The noise introduced by this sensor is characteristic and easy to eliminate.

3.5.2. Storage system

There are several options of storage systems available in the market. Cameras with internal capacity and others needing a computer for data storage are the most common. The camera that we have chosen needs a computer for data storage.

One of the main reasons why this system was selected was its economy. It was also important the fact that we were not limited by the space. Buying a server and a camera can seem more expensive than buying just the camera, but it is a mistake. In fact, if you compare two similar models, you realize that the one with internal memory is three times more expensive than the total cost of the camera and the server.

Frame Grabber is the device that makes the capture of images at high velocity possible. In the past, these devices had incorporated processors because computers could not work at high velocities. Now, with the 64 bits PCI buses the velocity of transfer and the real time visualization have increased, without needing a processor in the Frame Grabber.

The connection between the server and the camera is done by the standard CameraLink. This system is the one used between the frame grabber and the digital camera and one of its main advantages is the fact of allowing the high velocity data transference. It uses the Channel Link TM protocol and allows a velocity up to 7,1 Gbps.

3.5.3. Illumination

When using a high velocity capture system high luminosity is required since the camera time exposure is very short. We decided to use high luminosity LEDs, which are a source of cold light, and thus, the water temperature is not changed.

In order to get uniform illumination a diffuser is placed in front of the s board.

The illumination system is designed over a PCB with 280 LEDs (Fig. 3.27).

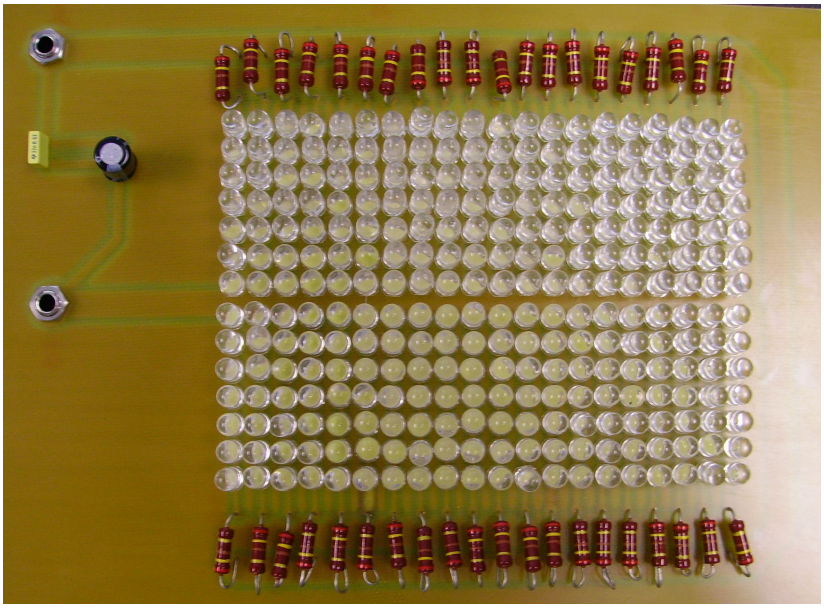

Fig. 3.27 LED board

3.5.4. Camera support

After performing the first laboratory tests a new necessity appeared. We needed some kind of support in order to fix the camera. It must provide stability, two axis mobility and robustness.

As systems in the market do not satisfy our requirements, we have designed a support with Bosch-Rexroth profiles, like the ones used in the rack. They will be fixed to a wood plate to give a stable base. Fig. 3.28 Shows the frame.

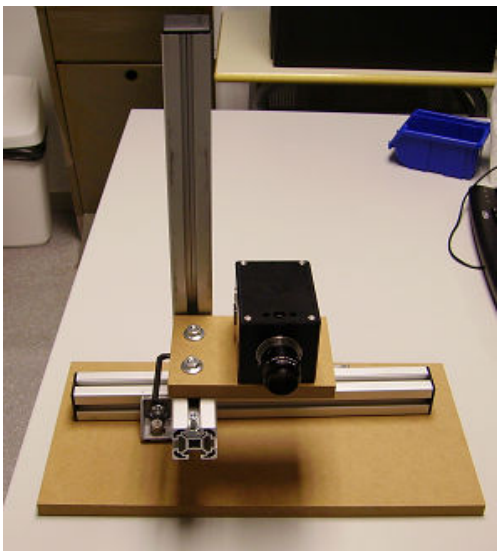

Fig. 3.28 Camera support

3.5.5. Selected system

The selected image capture system is composed by the following equipment:

-Camera: Photon Focus MV-1024
Sensor: 2/3” CMOS Global Shutter
Resolution: 1024x1024
Pixel Size: 10,6 x 10,6 microns
Velocity at maximum resolution: 150 fps

-Server: Intel Xeon 2,8 GHz
4 Gb RAM
ATI X300 256 Mb
230 Gb Hard disc

-Frame Grabber: X64CL-DUAL CORECO IMAGING

-Illumination: System of high luminosity LEDs.

3.6. Experiment installation in the A300 ZERO-G

In order to load the experiment in the aircraft, it is necessary to build a rack which has to accomplish the Novespace norms. The main characteristics of the rack selected are:

1- Y Axis length.
2- X Axis length.
3- Power Supply.
4- Materials.
5- Double sealing.

3.6.1. Y axis length

The allowed dimensions for Y axis are 503 mm and 1006 mm. We have chosen the longer one because we need a large space for a 360x220x360 mm methacrylate cavity, a pressure air bottle, a server, a laptop, etc. Fig. 3.29 shows the space availability and its distribution in the Airbus A300.

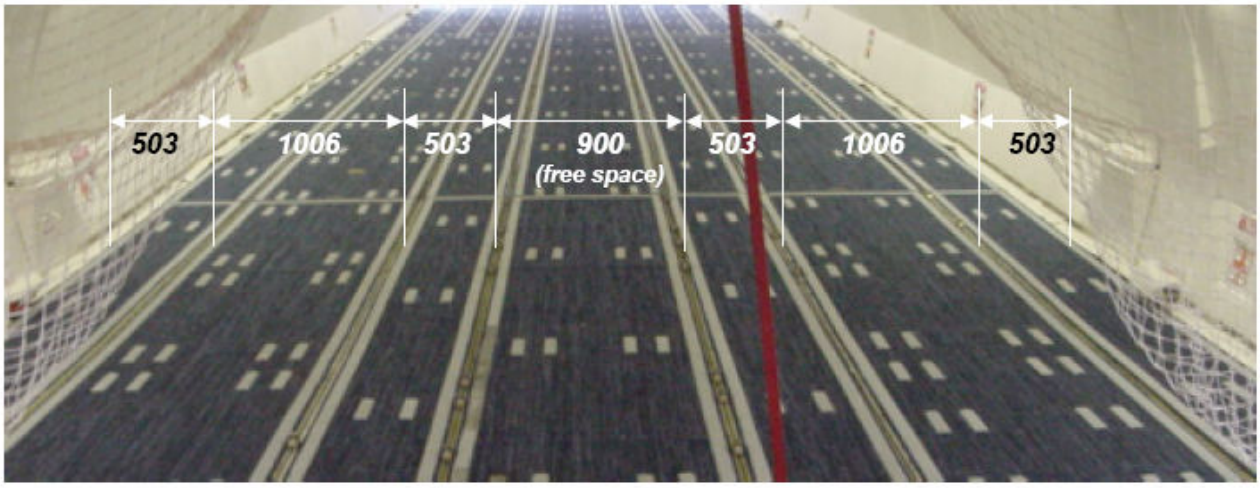

Fig. 3.29 Aircraft space distribution [24]

3.6.2. X axis length

In order to fix the experiment to the plane, it has rails with holes of M10, separated by a distance of 2.54 cm. Fig. 3.30 shows the conditions to fix the experiment to the plane:

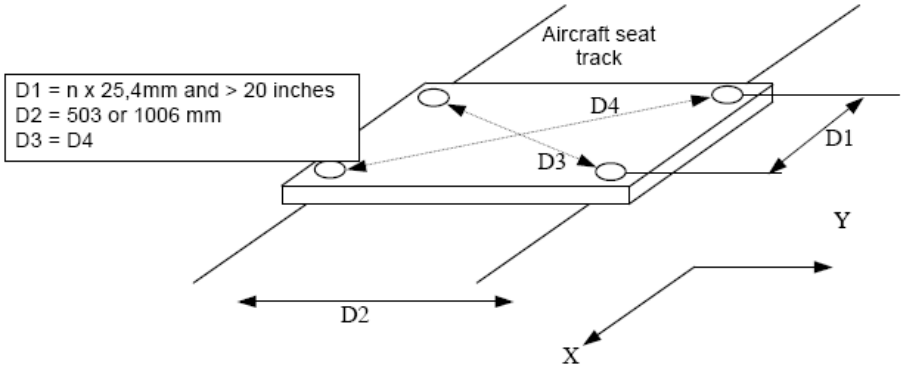

Fig. 3.30 Conditions to fix the experiment to the plane [24]

We use a 1036x 1270 x10 mm aluminium plate (Fig.3.31). The length of 1036 mm allows fixing the plate ensuring the required separation of 1006 mm. The length of 1270 mm allows a rack with the needed space for the set-up without wasting unnecessary space. According to the conditions of Fig. 3.30 it can be noticed that there will be a separation of 50.8 cm between fixations and 25.4 cm of border (12.7 cm per corner). Finally, the plate has a thickness of 10 mm, which is a condition of Novespace for experiments with a weight higher than 50 Kg.

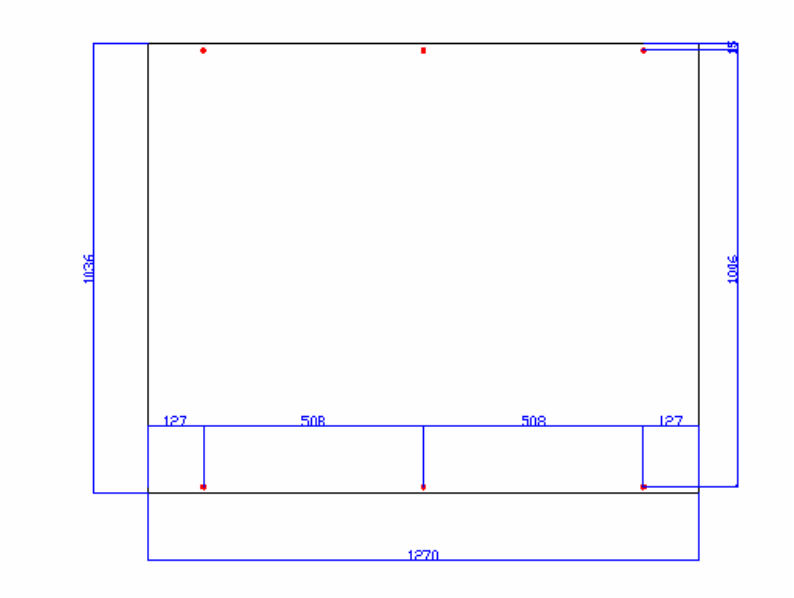

Fig. 3.31 Dimensions of the aluminium plate

3.6.3. Power supply

There are two sorts of power supply on board: 220 V or 28 DC. In order to meet our needs of electricity supply, we will use our own DC supply apart from the offered 220 V.

3.6.4. Materials

Following the advice of Novespace, we have decided to use Rexroth Bosch profiles to build the rack, which have the following advantages:

- Material and structure certifications are not required.
- Technical support is given for the design and construction of the rack.
- Vast selection of materials and parts.
- Quick building and assembling.

After studying the previous points and considering the different possibilities the design shown in Fig. 3.32 has been selected. Fig. 3.33 shows the distribution of the equipments in the first and second floor of the rack.

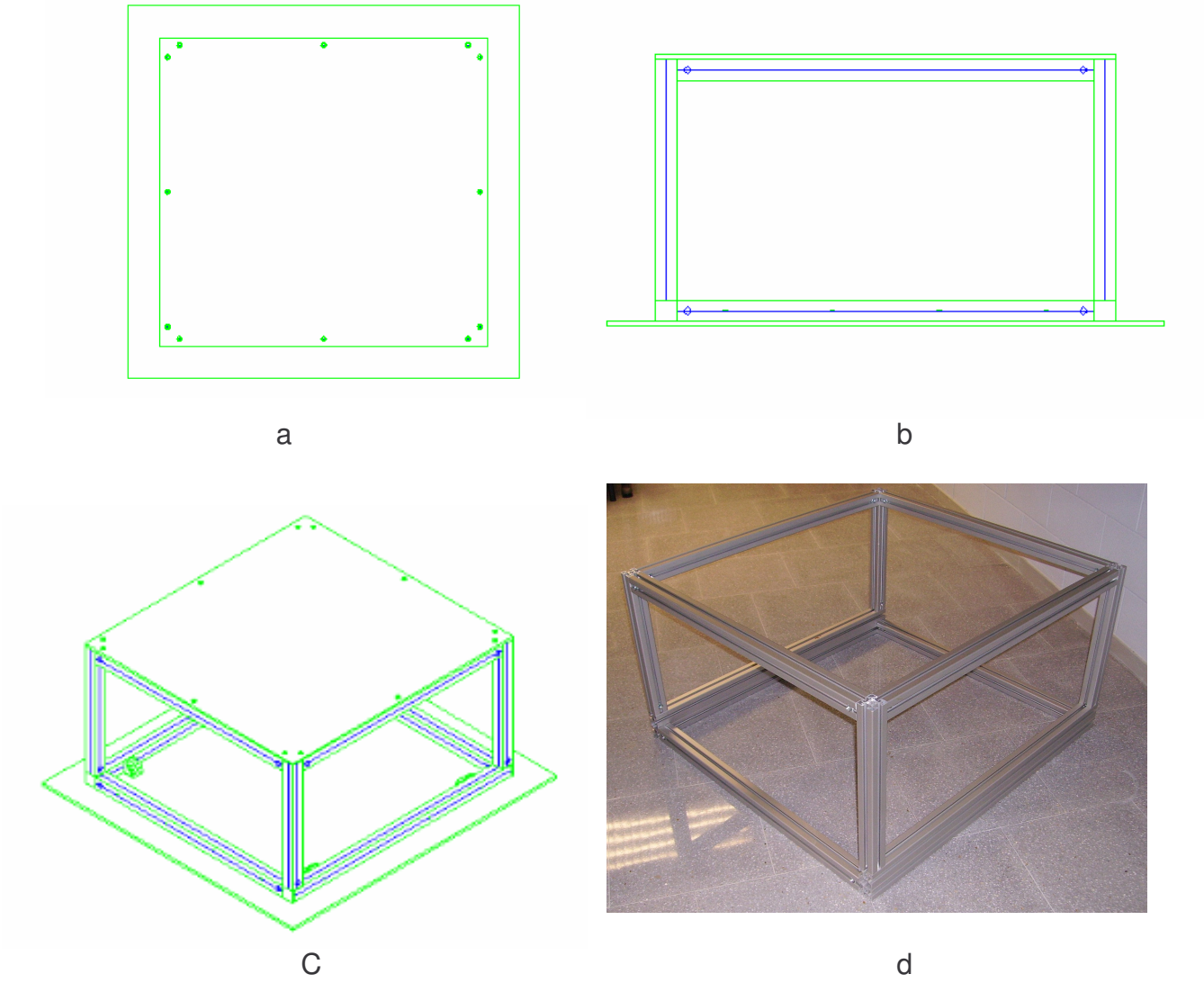

Fig. 3.32 Rack: Upper (a), lateral (b), 3D views (c) and Rack photo (d)

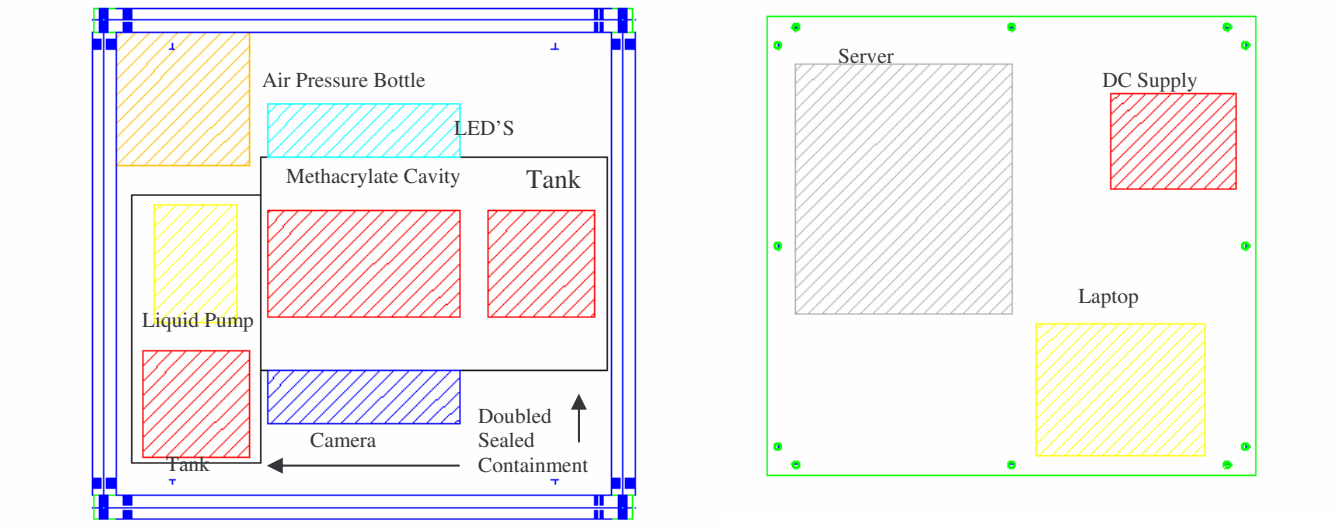

Fig. 3.33 First and Second floor distribution

One of the Novespace requirements is to deliver the calculation about the safety factor (Annex D). To compute it, it is necessary to know the weight and dimensions of the rack.

3.6.5. Double sealing

The volume of liquid in the experiment is higher than ½ litre, which implies the necessity of building a double sealing. Novespace norms are very strict on this point, due to the risk of liquid spilling in the aircraft.

Aside from the double sealing, in order to guarantee the maximum insulation, the tubes containing liquid must have an extra tube which covers them.

Once the double sealing is built, some security tests will be repeated at Novespace facilities. They consist on filling the external tank with water and rotating it around the three axis.

CHAPTER 4. EXPERIMENTAL AND SIMULATION DATA

4.1. Experimental results

First tests have been performed at the Microgravity Laboratory by using all the systems explained in previous sections. Three interesting processes have been observed.

4.1.1. Detachment of the bubbles at the T

Pictures on Fig. 4.1 show the operation of the BubGen system. Air and water are being injected through the vertical and horizontal pipe, respectively. Their diameter has a value of 1 mm. According to the results obtained previously [4], gravity does not affect the process.

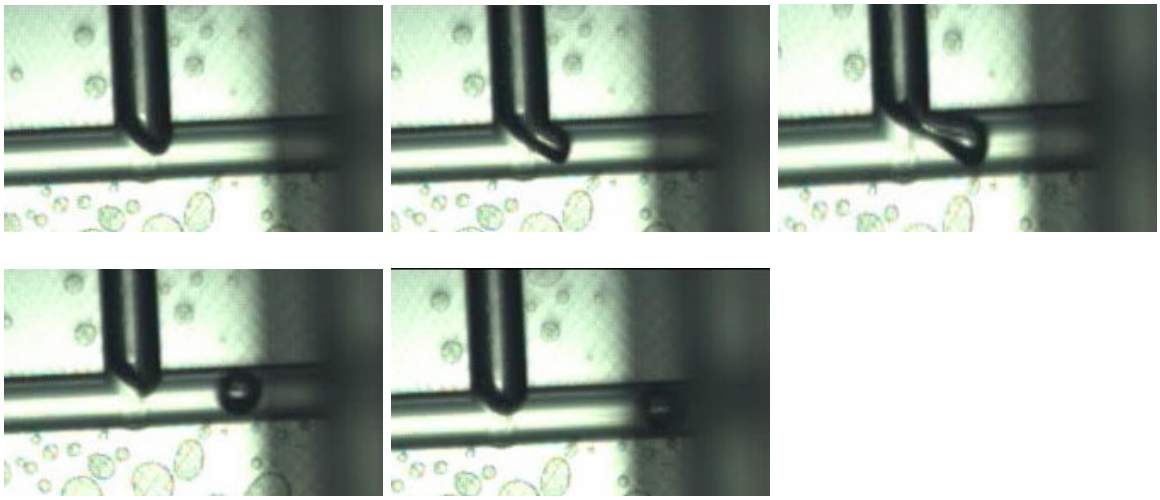

Fig. 4.1 Bubble detachment

4.1.2. Slug Flow

Figures bellow show the effect of a variation in the air to water flow ratio. In Fig. 4.2, Fig. 4.3, Fig. 4.4 this ratio decreases progressively. While it decreases, bubble size decreases until a critical value (nearly spherical). At this point, the bubbles frequency starts to decrease.

Fig. 4.2 High air to water ratio slug flow

Fig. 4.3 Medium air to water ratio slug flow

Fig. 4.4 Low air to water ratio slug flow

4.1.3. Coalescence

Fig. 4.5 shows coalescence of 3 mm diameter bubbles in six frames. Oscillation process explained in chapter 1 can be shown at the three pictures of the lower file.

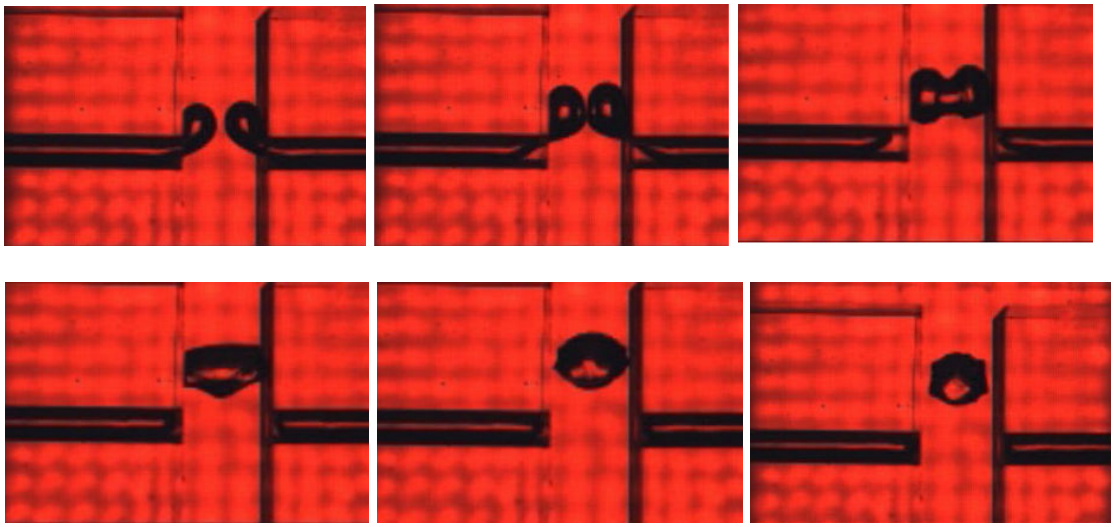

Fig. 4.5 Bubble Coalescence

4.2. CFD simulations

A numerical simulation of the experiment with the CFD tool FLUENT® has been carried out in order to have an approximation to the fluid dynamics in the system. We haven't been able to obtain a clear slug flow in FLUENT®. However, this would be an interesting issue for another TFC.

Firstly the geometry must be generated; then the mesh is configured and initial and boundary conditions are defined. Finally, data is obtained by running the simulation.

These are the steps followed to generate the geometry with Gambit:

1. Generate the basic body of the experiment: the cavity.
2. Generate two injectors.
3. Place one injector in front of the other. External faces (outlets) have to be in contact with two vertical and opposite faces.
4. Use *SPLIT* command for the cavity and the extremes of the injectors.
5. Create an outlet pipe at the upper face.
6. Use *SPLIT* command in the outlet pipe and the cavity.

Fig. 4.6 shows the geometry of the experiment once all the previous steps are done.

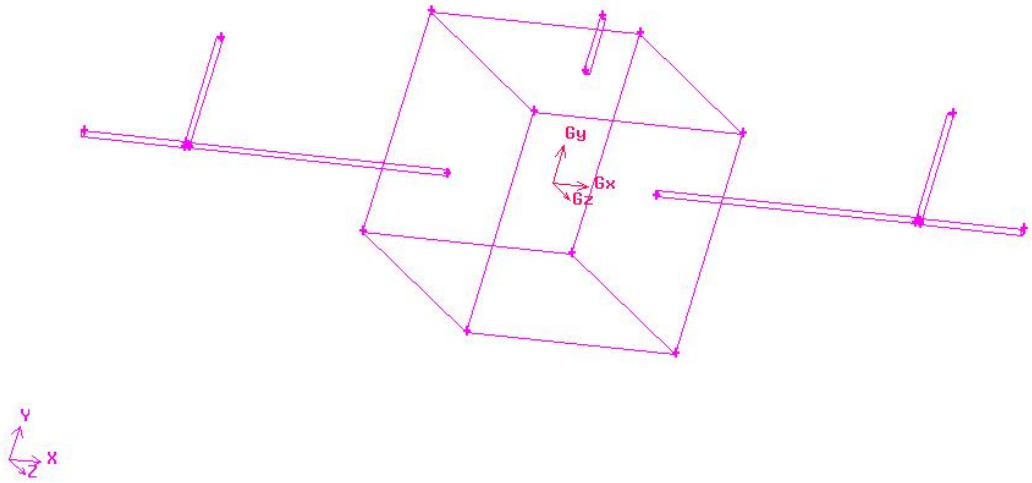

Fig. 4.6 Cavity geometry

In order to mesh the geometry and prepare it to export to FLUENT ®, one must follow:

1. Mesh the injectors and the outlet pipe with the desired mesh size.
2. Use a *sizing function* to mesh the cavity. The volume will be meshed from the meshed faces. The growth rate of the mesh and its maximum size will have values of 20 % and 3, respectively.

Fig. 4.7 shows the view of XY plane. It is possible to observe the mesh growing gradually,

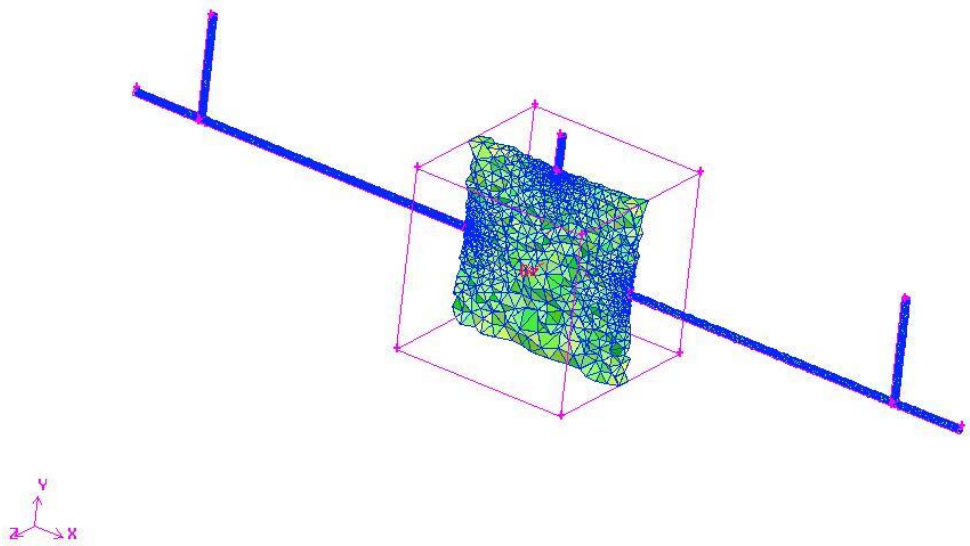

Fig. 4.7 Cavity mesh

In order to configure the cavity, we followed the next steps:

1. Design the inlets as *VELOCITY_INLET*.
2. Design the outlet placed in the upper face of the cavity as *PRESSURE OUTLET*.
3. Define the volumes as *FLUID*.
4. Save the file and export the mesh.

Then, after loading the mesh in FLUENT ® the programme must be configured:

1. Load the generated mesh, check it and tune if necessary.
2. Configure the solver following the steps explained in tutorial number 18 of FLUENT ®, introducing some variations (air velocity: 50 m/s, water velocity: 25 m/s, 100 % of water in the water pipe and 100 % of air in the air pipe).

Fig. 4.8 shows the residuals obtained in the simulation.

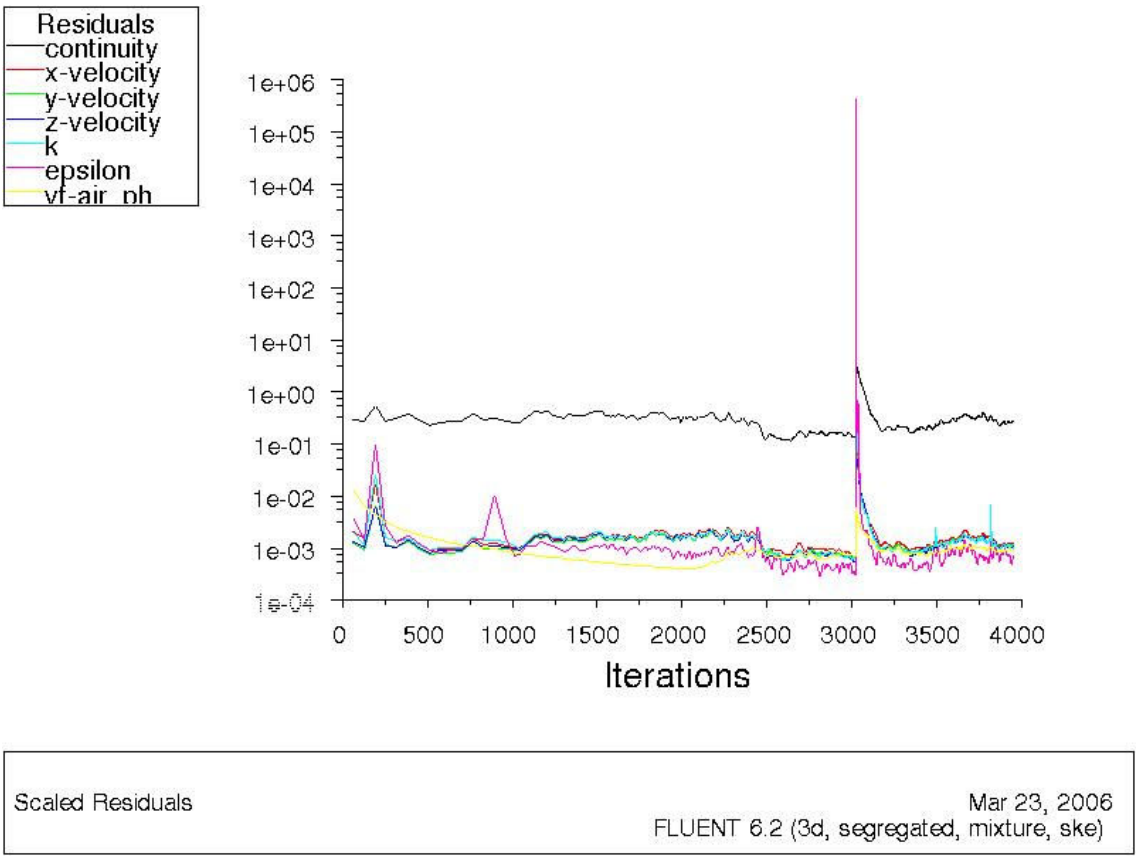

Fig. 4.8 Residuals

As it is shown, it tends to converge, excluding the discontinuity appeared at 3000 iterations. Probably the reason is the arrival of the flow to the cavity.
In Fig. 4.9 a velocity field can be observed.

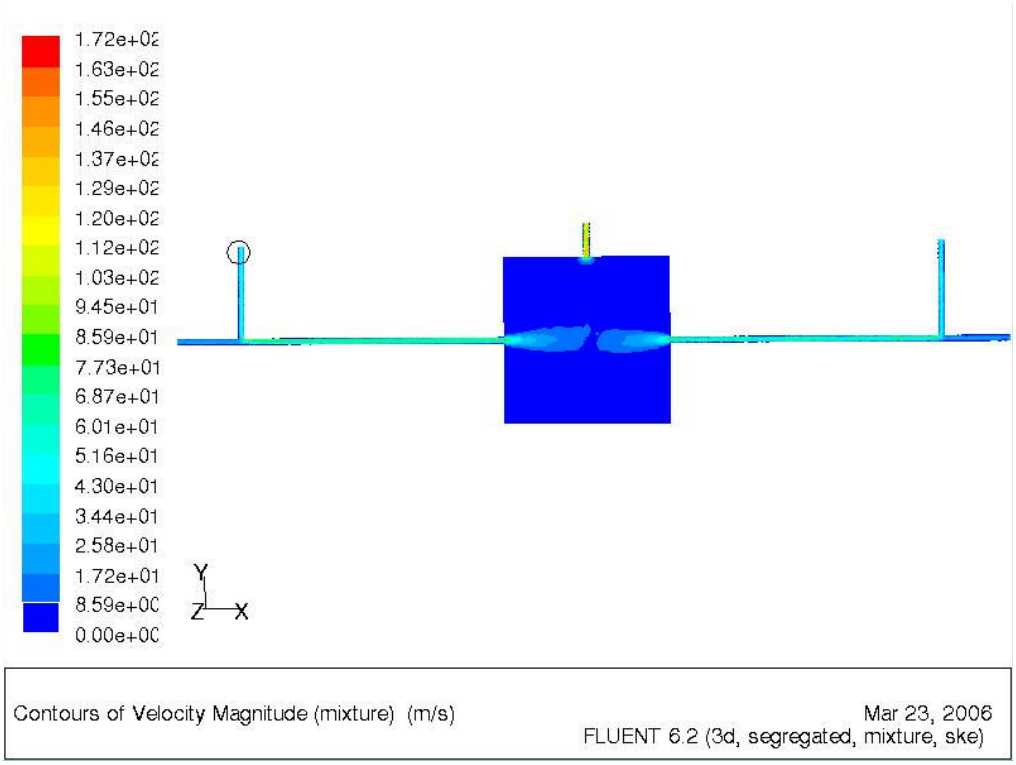

Fig. 4.9 Velocity field

Fig. 4.10 shows the pressure distribution in the system.

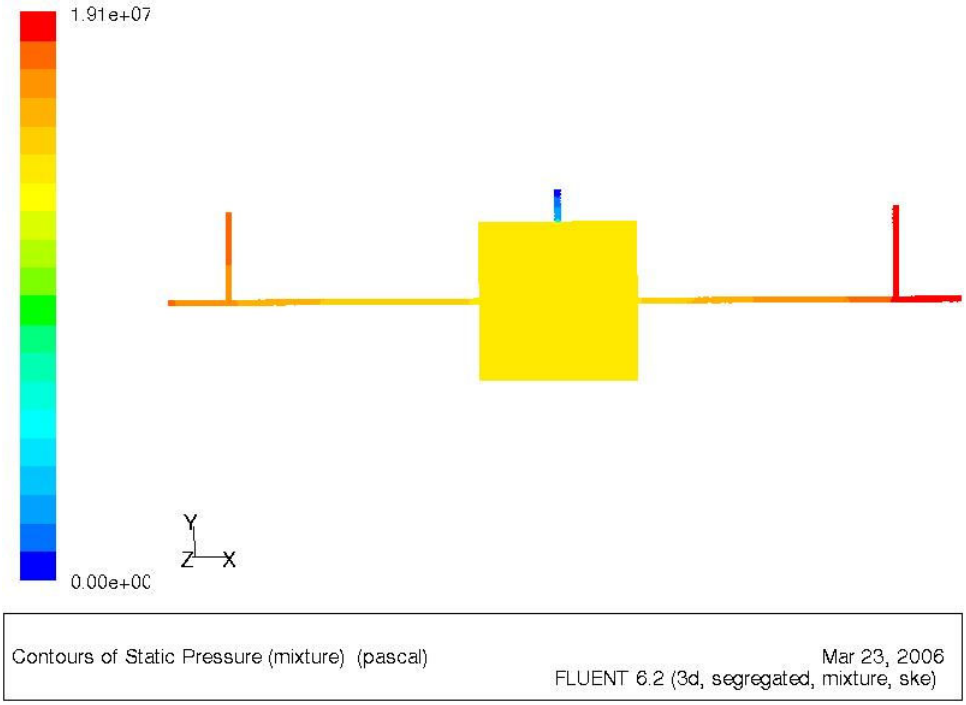

Fig. 4.10 Pressure field

Fig. 4.11 shows the velocities distribution in two different projection plans.

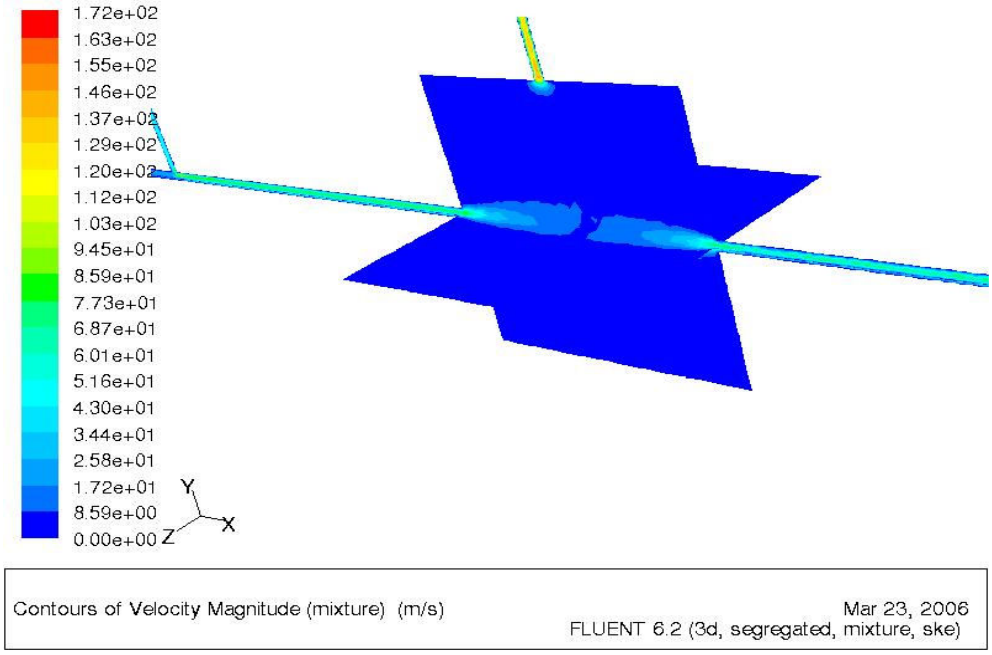

Fig. 4.11 Two plane velocity field

In Fig. 4.12 phases distribution can be observed. Gravity effect is appreciated.

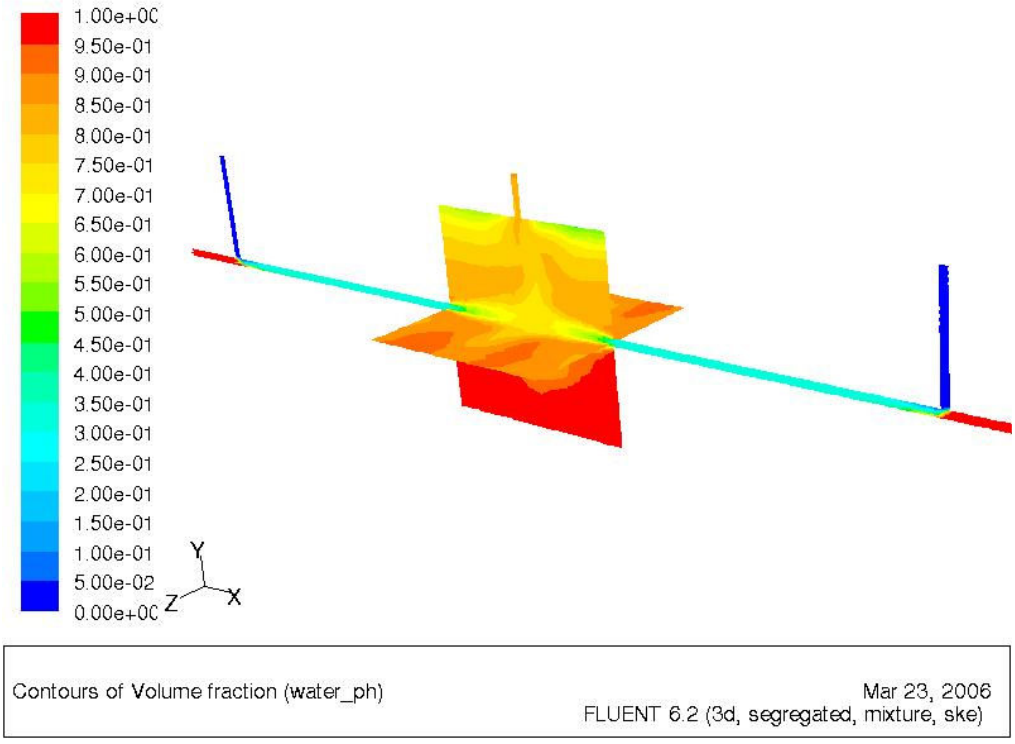

Fig. 4.12 Phase distribution field

Fig 4.13 shows the moment of the detachment of bubbles in the T section of the injector, when a mixture of phases appear. Velocity and phases concentration are represented, respectively, by vectors and colours. It compares the CFD simulation with the result obtained in the lab and some similarities can be observed. On the other hand, Fig. 4.14 represents velocity and phases concentration in two plans.

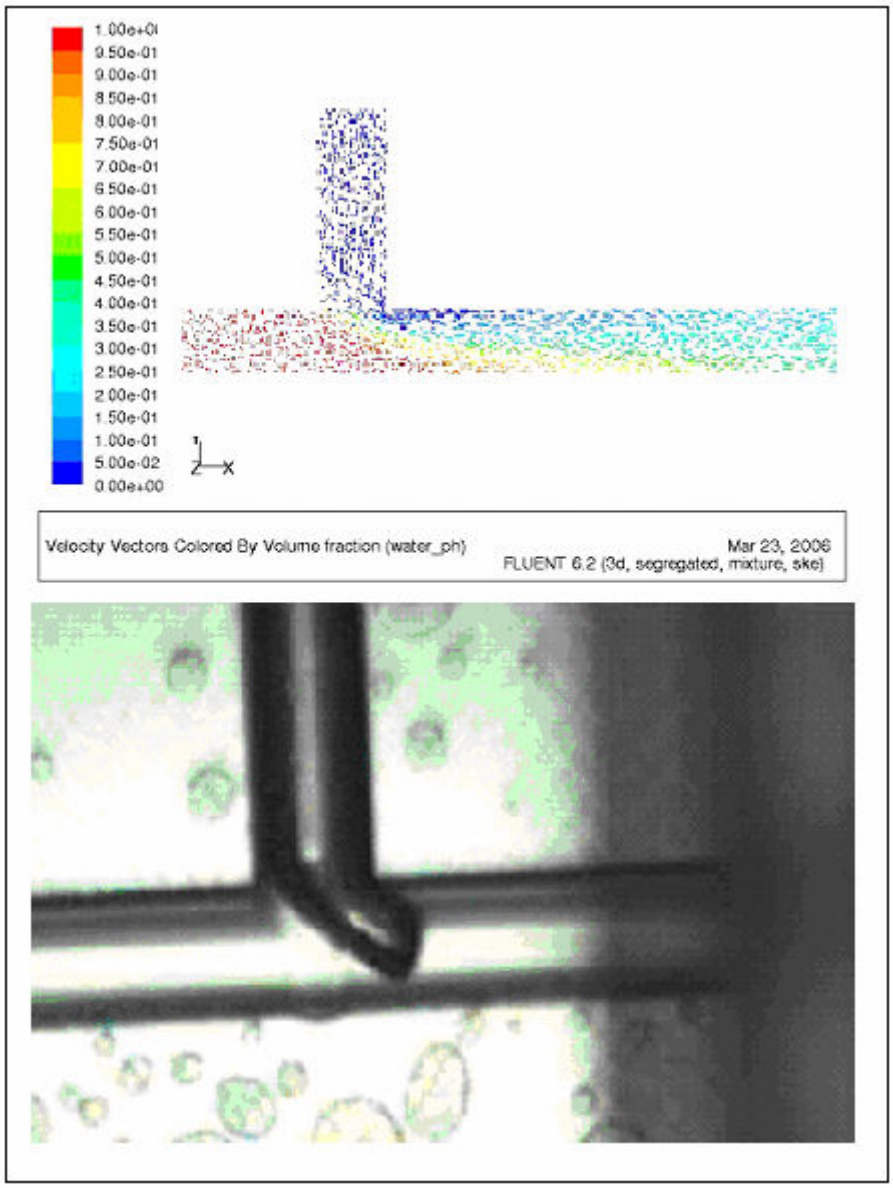

Fig. 4.13 Simulated and experimental T-junction comparison

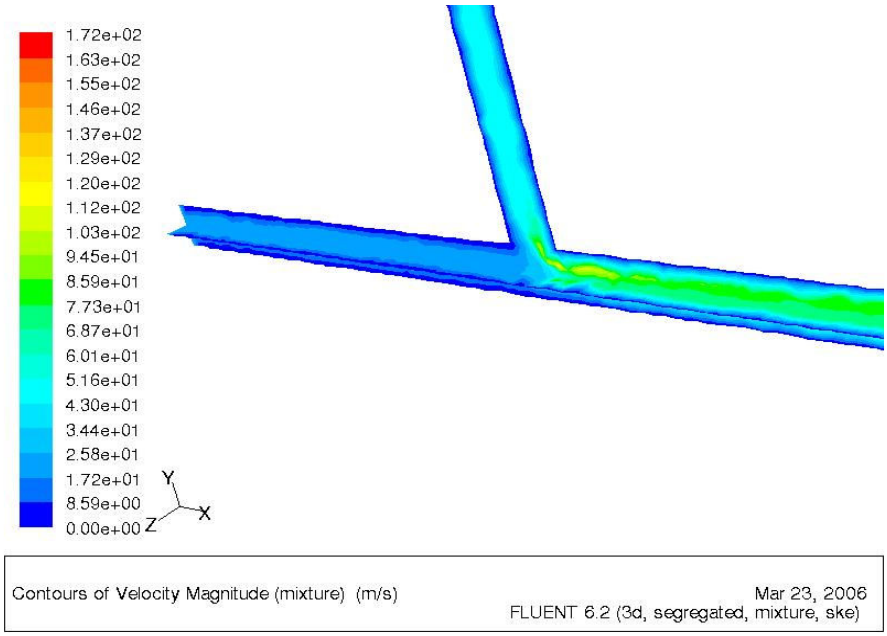

Fig. 4.14 Two plane velocity

Fig. 4.15 shows a detailed view of velocity field, including the fluid injection and outlet.

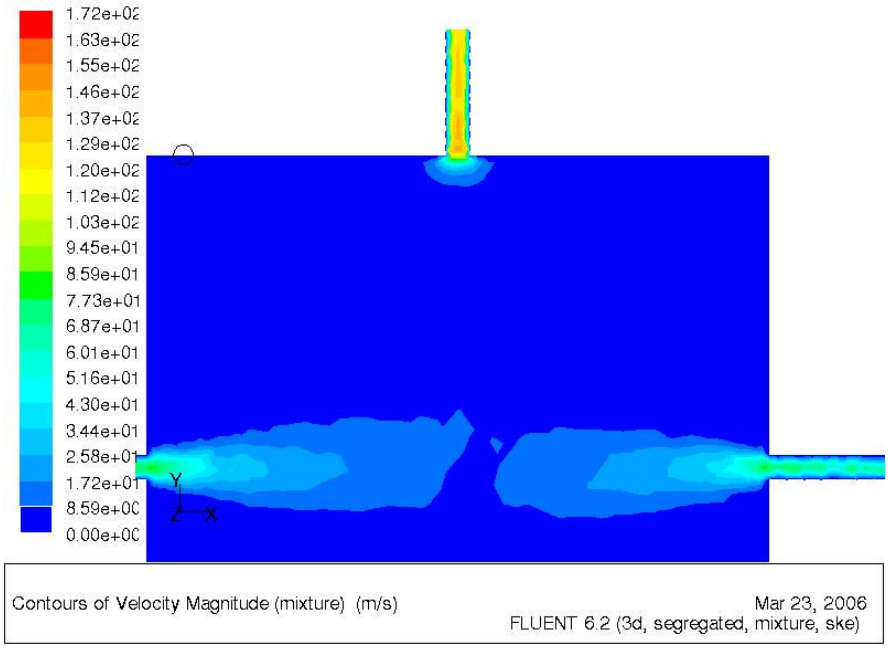

Fig. 4.15 Velocity magnitude

Although we haven't reproduced a "slug-flow", the mixture and the substances concentration can be represented.

CHAPTER 5. CONCLUSIONS

Bubbles in microgravity is a very little studied field. Information about this subject (and coalescence in particular) is not so settled as other physical phenomena are. Thus, most of the bibliography is extracted from articles. Our objective is not developing a theory but carrying out an experiment and then contributing with data and results for later analyses. These studies may help to verify current theories and developing new ones.

It is not easy for researchers to access to microgravity facilities. Student Parabolic Flight Campaign has been our chance to do it. It has not only been a way to accede to microgravity but also an opportunity to visit ESA facilities, meet experts on physics and technology and exchange knowledge with other European students. We have also become aware of ESA and Novespace rigour when delivering the *Experimental Form* and being constantly asked to hand in certificates and datasheets of the products used and to modify some details of the experiment in order to ensure its safety. We have gotten experience in different disciplines such as working on team or getting in touch with scientifics and experts at different fields in order to learn from them.

By now, the main experiment objectives have been achieved. After the tests made at the lab, we can state that *BubCoa* is able to generate bubbles and coalescence can be observed. Next step will be running the experiment under microgravity conditions in the Parabolic Flight at Bordeaux; the results obtained for the time being point to the achievement of good results in this environment.

Regarding to the experiment design, we can define it as the process to turn theory into practice. The starting point was a reference to T injector and we have arrived to the design and construction of a microbubble generation system. It has been a constant daily work. Despite it has been planned as much as possible, we have been subject to external factors all the time because we have been dependent on the work of other people such as manufacturers and suppliers. We have learnt that it is very important to have a clear idea of what you want, study and compare all the available options, not depend too much on others and have alternatives in case of fails.

In many cases, we have applied knowledge that does not belong to our field (aeronautics) and we have had to learn it from its basis.
Material and manufacturers selection has been one of the most difficult points. It is not easy to find the person that can build exactly what you want and find the shops and enterprises that sell what we need since our materials are not really common.

New necessities have come up during the experiment construction and many parts of the systems have been corrected or repeated again.

One of the most ambitious challenges in the development of this experiment has been the automation with Labview. When we set it we were not aware of its

complexity which lies in the fact that we have had to design and build many of the components instead of buying them and it is a really hard work. As we are not electronic engineers and we have some gaps in this field, we have tried to learn by contacting experts on the subject.

Another complex point in the experiment has been the image capture system. We have needed to attend courses of photographic control software. As far as we are concerned, we think that this software is quite rudimentary and it would have been convenient to use software specialized in image processing.

To finish, we will focus on the results of the experiment. With respect to the CFD simulation, we have not been able to obtain accurate results with Fluent ®. They have shown us the fluid dynamics in general, but not that of bubbles. A more detailed study is required to achieve it, but it was not really our objective. These results have been useful for designing the cavity, the injectors, etc.

We obtained the expected results when we run the first experiments in the lab: coalescence is not very likely to occur because of external forces. We expect them to change under microgravity conditions.

BIBLIOGRAPHY

[1] http://www.slb.com/

[2] http://www.isso.uh.edu/publications/A9798/bala.htm

[3] Colin, C., J. Fabre, and A. E. Dukler, “Gas-Liquid Flow at Microgravity Conditions: I. Dispersed Bubble and Slug Flow,” Int. J.Multiphase Flow, 17, 4 (1991).

[4] J. Carrera, X. Ruiz, L. Ramirez-Piscina, J.Casademunt, “Generation of a Monodisperse Microbubble Jet in Microgravity” (in preparation).

[5] L. Hagesaether Coalescence and breakup of droplets and bubbles. Ph.D, 2002 in norweigan university of science and technology.

[6] http://resources.highett.cmit.csiro.au/rmanasseh/a915/node2.html

[7] CHESTERS, A. K. & HOFMAN, G., Bubble coalescence in pure liquids. Applied Science Research 38 (1982), 353-361.

[7] Enrico Ceglia (ESA), *European Users Guide to Low Gravity Platforms*, William Carey, pagines, Noordwijk, 2005.

[8] http://www.esa.int/esaED/SEMFSU1A6BD_index_0.html

[9] http://epsc.upc.edu/projectes/microgravitylab/SPFC/index.html

[10] R. Shankar Subramanian, R. Balasubramanian, Günter Wozniak “Fluid mechanics of bubble drops” Chapter 6 of “Physics of Fluids in microgravity” Edited by R.Monti 2001.

[11] Marcello Lappa “Fluids, Materials, and Microgravity” Edited by Elsevier, 2004

[12] A.M. Kamp, A.K. Chesters, C.Colin, J.Fabre “Bubble Coalescence in turbulent flows: A mechanistic model for turbulence induced coalescence applied to microgravity bubbly pipe flow” International Journal of Multiphase Flow 27 (2001) 1363-1396.

[13] S. Marcelja “Short-range forces in surface and bubble interaction” Current Opinion in Colloid and Interface Science 9 (2004) 165-167.

[14] G. Duhar, C. Colin “A predictive model for the detachment of bubbles injected in a viscous shear flow with small inertial effects” Physics of Fluids 16, L31 (2004).

[15] www.hoke.com/products/gyrolok_feat.htm

[16] The facts about interchangeability and intermixability Hoke incorporated.

[17] RS Amidata Website, www.amidata.es

[18] Texas Instruments INA114P Datasheet, www.ti.com

[19] MCLENNAN Servo suppies HSX 23 Hybrid Stepper Motor DataSheet, www.amidata.es

[20] Adquisición y distribución de señales. Ramón Pallás Areny. Marcombo Boixareu editores, Barcelona, 1993.

[21] Bükert 6011 Miniature Solenoid Valve Datasheet.

[22] CCD vs CMOS Maturing Technologies, Maturing Markets, Dave Litwiller, Dalsa.

[23] Infaimon, Análisis de imagen y visión artificial.

[24] Guidelines for Designing and Building an Experiment for the A300 ZERO-G, Novespace, Rev. January 2006-06-25.

Complementary bibliography

Herold. K. E.. and K. R. Kolos. “Bubbles Aboard the Shuttle,” Mech. Eng., 119, 10 (1997).

Jayawardena, S. S., V. Balakotaiah, and L. C. Witte, “Flow Pattern Transition Maps for Microgravity Two-Phase Flows,” AIChE J., 43, 6 (1997).

Mecánica de Fluidos, Frank M White, Ed McGraw-Hill1988 SPAIN.

http://space.epfl.ch/page57218.html

ANNEX A. A300 ZERO G

This appendix includes different views and details of the Airbus A300 ZERO G that will perform the maneouvres of the Parabolic Flight.

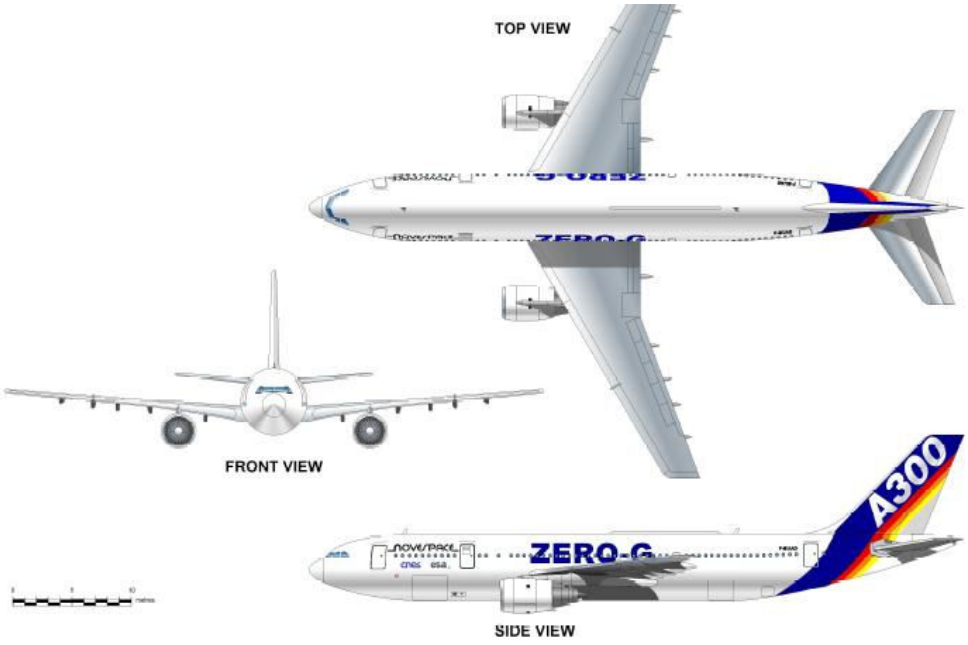

Fig. A.1 Airbus A300 Zero-G

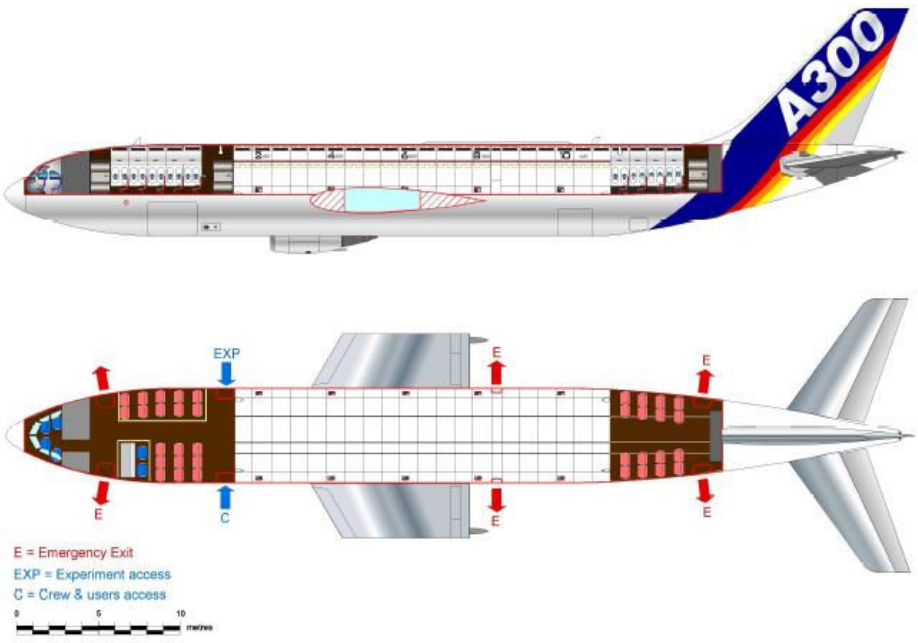

Fig. A.2 Side and upper views of the interior of Airbus A300

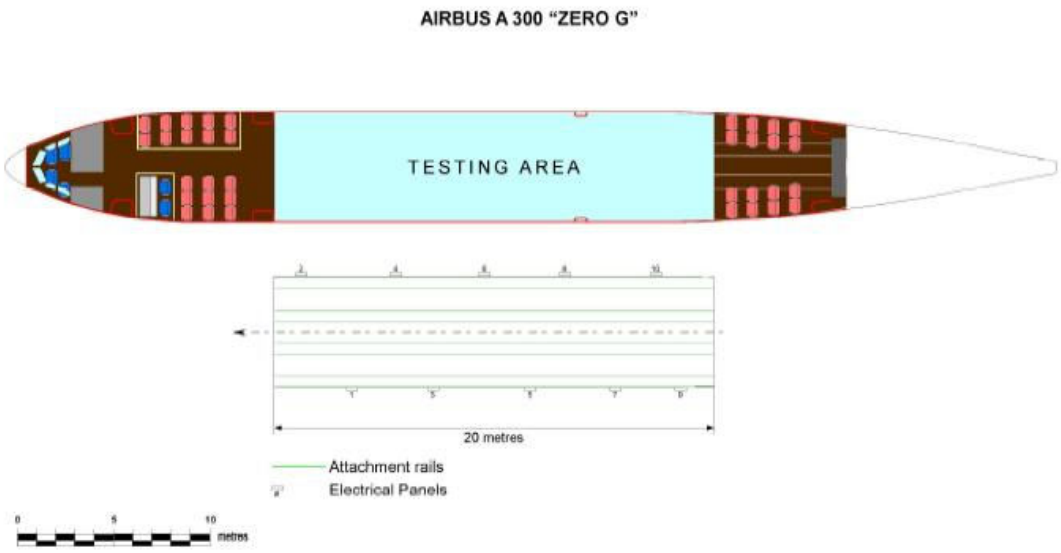

Fig. A.3 Upper view of the testing area

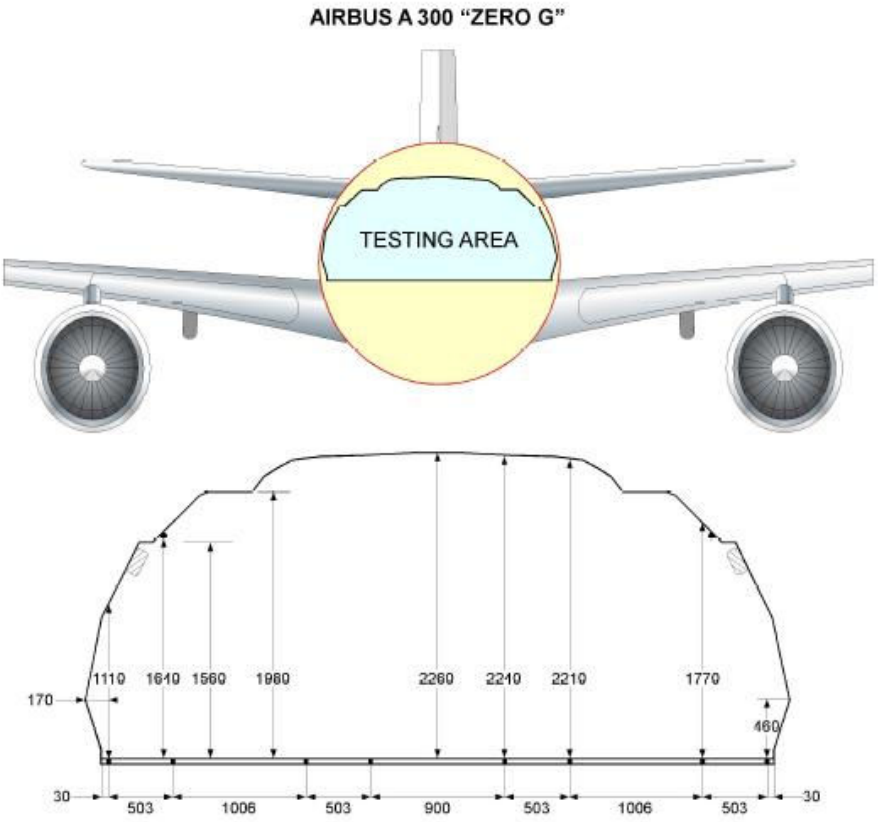

Fig. A.4 Front view of the testing area

ANNEX B. TECHNICAL DESCRIPTION OF THE EQUIPMENT

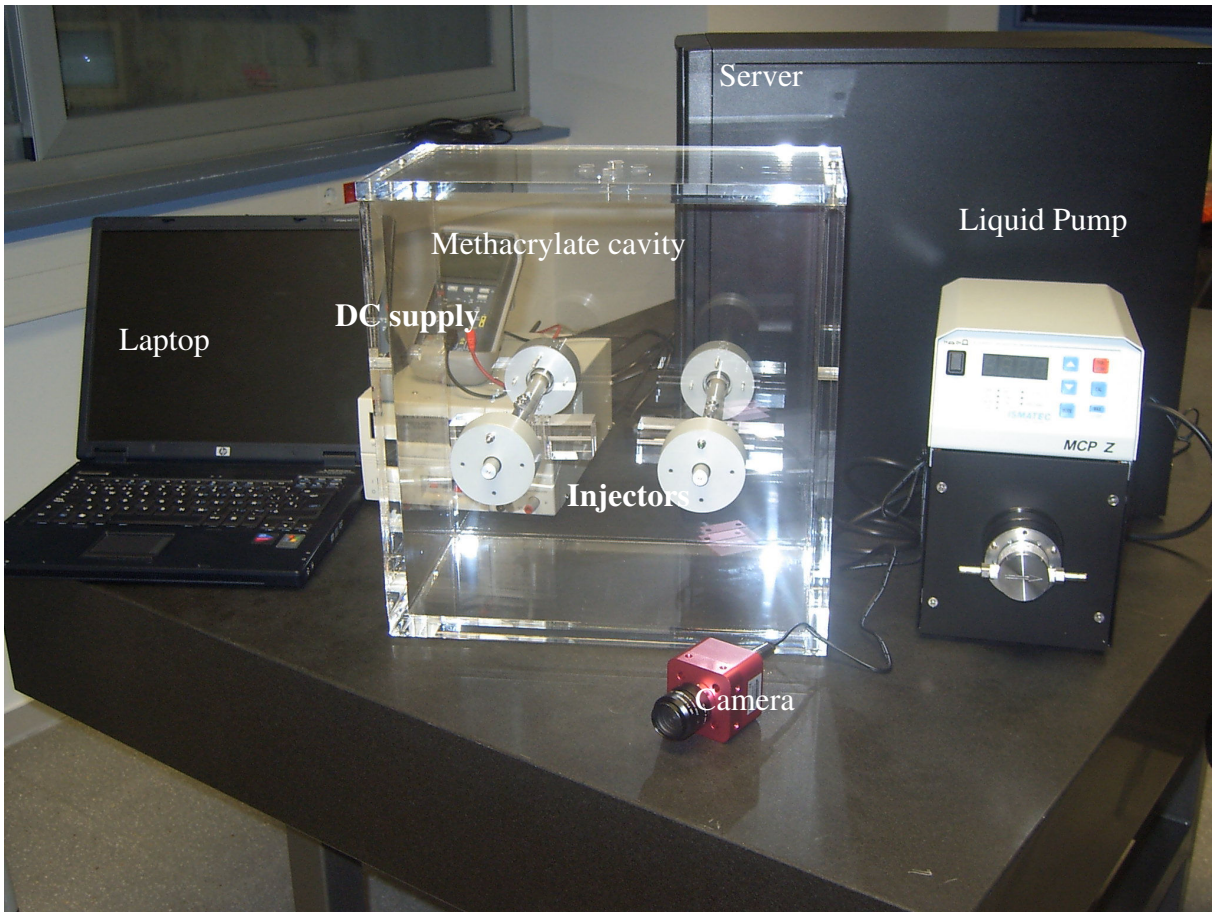

Fig. B.1 Experimental Equipment

All the devices and components needed in this experiment have been tested in the Microgravity Lab of EPSC. The fact of having tested the components that will be used in the flight (numbered afterwards) minimize any possible difficulties during its preparation and installation in the aircraft.

To carry out our experiment some electronic and hydraulic components are needed. Their technical characteristics are the following:

Methacrylate cavity:

Depth, Width, Height: 360x200x360 mm (26 litres).

Its function is containing the liquid where the experiment is performed and constitutes the basic body of the project. It is made of a transparent material (methacrylate) which allows the visualization of the interior and assists in

preventing risks or anomalies during the experiment development. Both injectors are placed inside this cavity.

Liquid Pump:

Ismatec MCP-Z Standard
Flow Rates: 1-7241 ml/min.
Motor Speed: 60-6000 rpm (DC motor).
Power consumption: 150 W
Power supply: 115-230 VAC, 50-60 Hz.
Depth, Width, Height: 220x155x260 mm.
Weight: 6.4 Kg (14 lb).
Differential Pressure: max. 5.4 bar

It allows injecting the liquid into the cavity by means of the injectors. We work with two different liquids (water and silicone oil).

Air Pressure Bottle:

Air Liquide
5 litres of laboratory synthetic air
Inside pressure: 200 atm
Outlet pressure: 1.5 bars

The air pump is directly connected to a pressure gauge, to regulate the air outlet pressure to the injectors in which the bubbles are formed. These bubbles are expulsed in a controlled way towards the cavity.

Camera:

Photon Focus MV-D1024
Power supply: 5 VDC.
Power consumption: 2 W.
Depth, Width, Height: 55x55x46 mm.
Weight: 200 g.

This high velocity camera can obtain more than 500 images per second with a resolution of 500x500 pixels which is the main element for data storage. It is connected to a computer where data are stored for further analyses.

Computer:

Power supply: 230 Vac.
Power consumption: 600 W
Depth, Width, Height: 520x240x450 mm
Weight: 7 kg.

Laptop:

Power supply: 240 V
Power consumption: 65 W
Weight: 3 kg
Depth, Width, Height: 275x350x320 mm

Liquid Tank:

Weight: 9kg;
Depth, Width, Height: 200x200x200 mm

Illumination system:

280 LEDs
Power supply: 30 V
Intensity: 1.2 A

DC Supply:

Weight: 3 kg
Power supply: 0-30 V / 5 V / 12 V
Intensity: 0-5 A

ANNEX C. CAMERA CONFIGURATION

The current annex includes an explanation of the way to configure the high velocity camera used to record our experiment. It helps to understand how an image acquisition system works. Some images have been attached in order to show the key points of the camera configuration.

C.1. PC connection

Once the frame grabber is installed and all the wires are connected, the next step consists on determining which the camera connection port is. The frame grabber creates some virtual COMs. Fig. C.1 shows the PFRemote program which is necessary to indicate the port for camera connection.

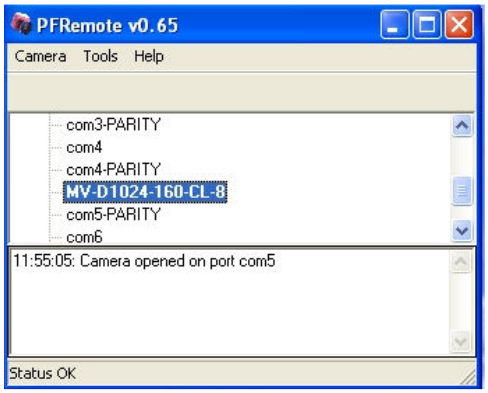

Fig. C.1 PFRemote

C.2. Camera configuration

Once the port is selected, the camera configuration program will appear. It is essential to optimize the camera and get proper images. Let's briefly list and explain each flap which appears in the program:

C.2.1. Exposure / Trigger

Here it is possible to configure the number of fps at which the camera works, as well as select the option *extern triggering* (Fig. C.2). Configuring the number of fps by varying the exposure time and the frame time is the most interesting possibility.

Let's focus on this point and explain the theoretical proportion between fps, pixels and illumination. A maximum number of fps can be achieved for a given resolution. If the number of fps is increased, more illumination is required. If the

resolution is reduced, the number of fps will increase and, consequently, a higher illumination will be needed. To sum up, we can say that resolution and fps are inversely proportional while illumination and fps are directly proportional. It is also important to take into account that for a given velocity, if we want more resolution we must increase illumination. It will be clarified with some examples explained afterwards.

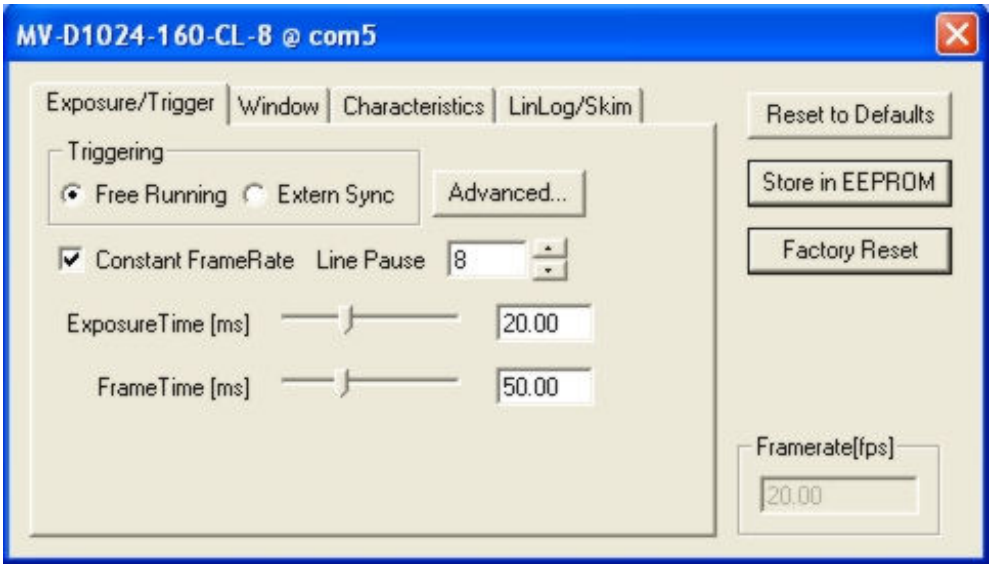

Fig. C.2 PFRemote - Exposure/Trigger

C.2.2. Window

At this flap, the resolution can be varied and it is possible to create masks (Fig. C.3). As we have said before, the number of fps can be increased by varying the resolution. Masks creation is a very interesting option provided by this software. They allow creating different recording areas on the condition that they must take up the two parts by which the CMOS sensor is divided. The fact of recording just two areas of interest is an advantage because the resolution used is lower and it is possible to increase the fps number.

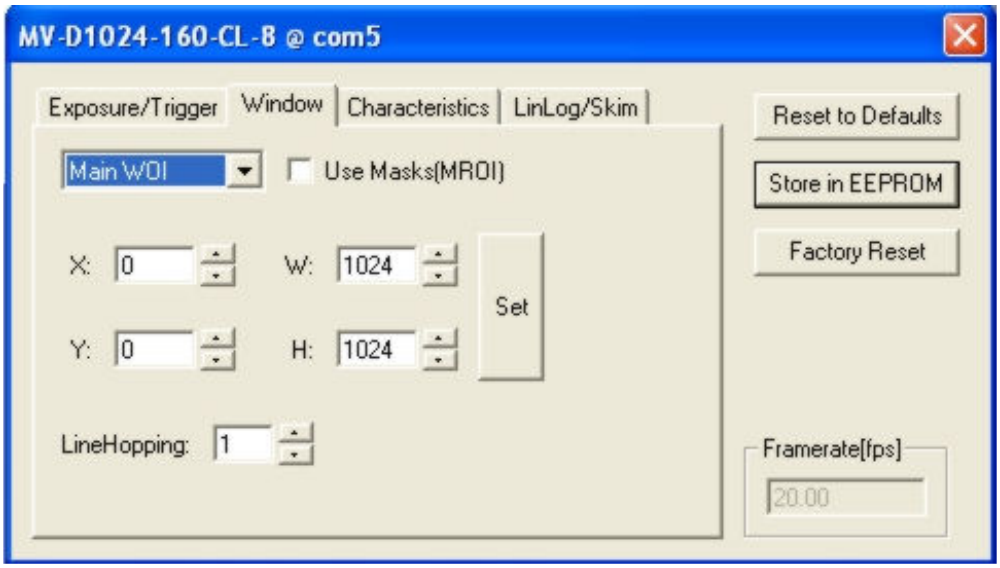

Fig. C.2 PFRemote - Window

C.2.3. Characteristics:

This section allows increasing the gain and the resolution (Fig. C.3). The problem is that any variation on the parameters of this section will increase the noise which will be difficult to characterize and eliminate.

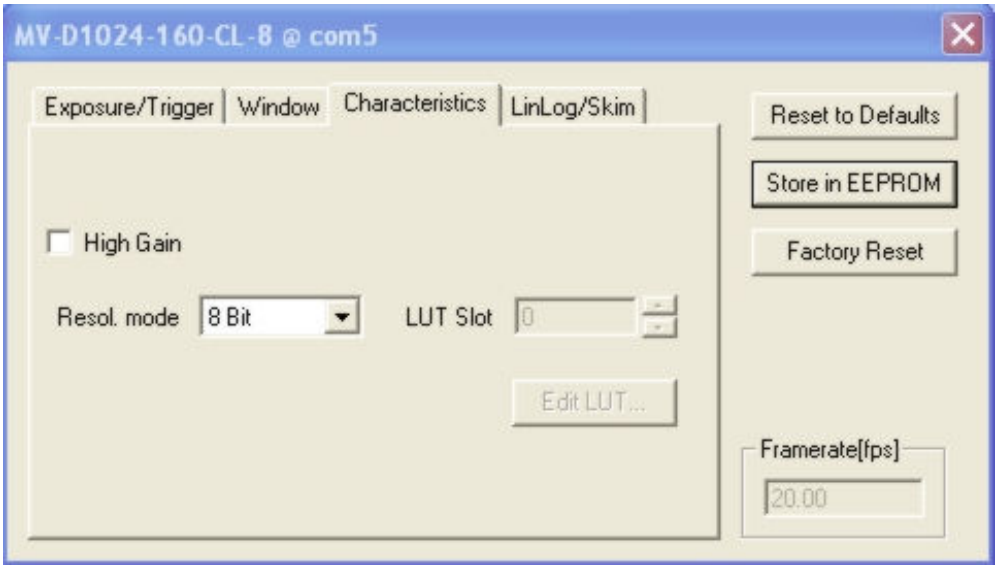

Fig. C.3 PFRemote - Characteristics

C.2.4. LinLog / Skim

This section allows using the LinLog system (Fig. C.4) which is a CMOS sensors technology created and patented by Photonfocus. It has been created to capture images with high and low luminosity areas. Its operation can be summed up as a linear response at low luminosity areas and a logarithmic compression at high intensities.

Once the different options are explained and the camera is configured, changes must be saved at the camera memory by selecting the option *Store in EEPROM.* We can retrieve the original configuration with the option *Factory Reset.*

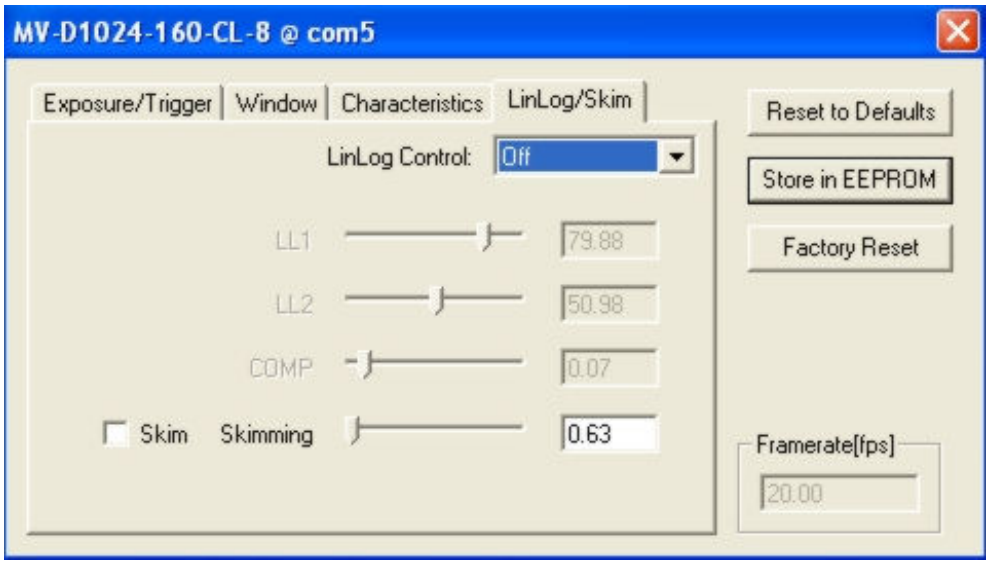

Fig. C.4 PFRemote – LinLog/Skim

C.3. Options file creation

The next step consists on creating a file with the camera profile to load in the recording programs. This process can be done while configuring the camera options which is even advisable because you can see how the new configuration influences on the capture.

Sapera CamExpert, from Coreco Imaging is the programme used to create this file. It includes the frame grabber, the recording programs and its code for possible modifications.
We can modify the image size, related to the PFRemote resolution, and eliminate the noise.
Once we have the file, we can start capturing images with the existing programs or create a new one.

Fig. C.5 shows an image of the software environment.

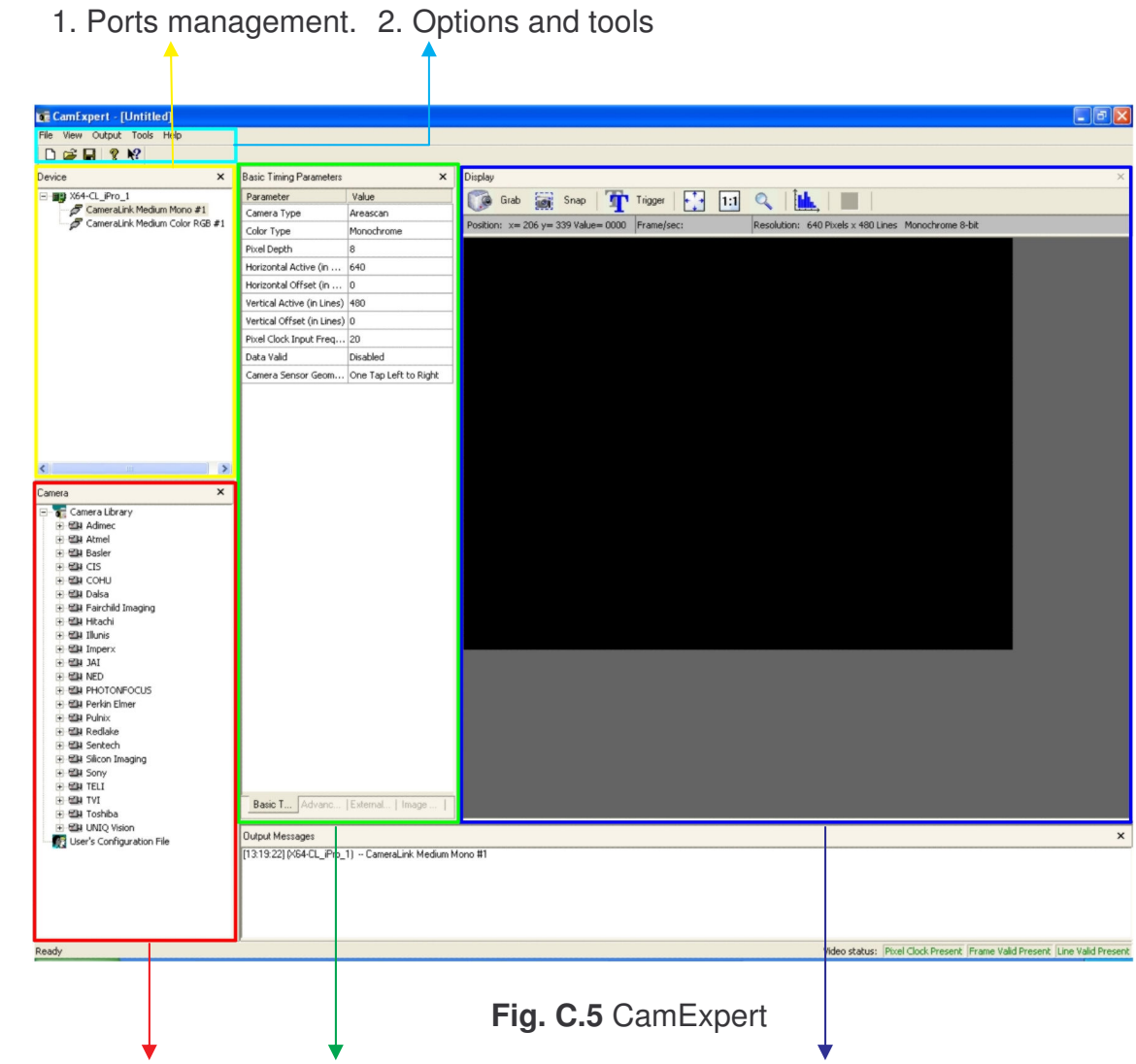

Fig. C.5 CamExpert

As shown in the previous image, this software has the following frames:

1. Ports management: In this section we can observe the available ports to connect the camera. In our case, there are two of them.

2. Options and tools: It contains the instructions which appear in all the programs. *Eliminate noise* stands out among the *tools* options, which will be commented on afterwards.

3. Camera model: It is used to select our camera model or a profile saved before.

4. Configuration options: In this section we will only settle the image size, which must correspond with the size indicated in the PFRemote. There is no need to modify the rest of options.

5. Image management: Here it can be observed the way to obtain images with our configuration. We can use the *zoom*, see the coordinates needed to create a mask or center the camera and the fps.

The recording software that we use is Sapera Sequential Grab. The created file is selected in the first window that appears when running the software (Fig C.6).

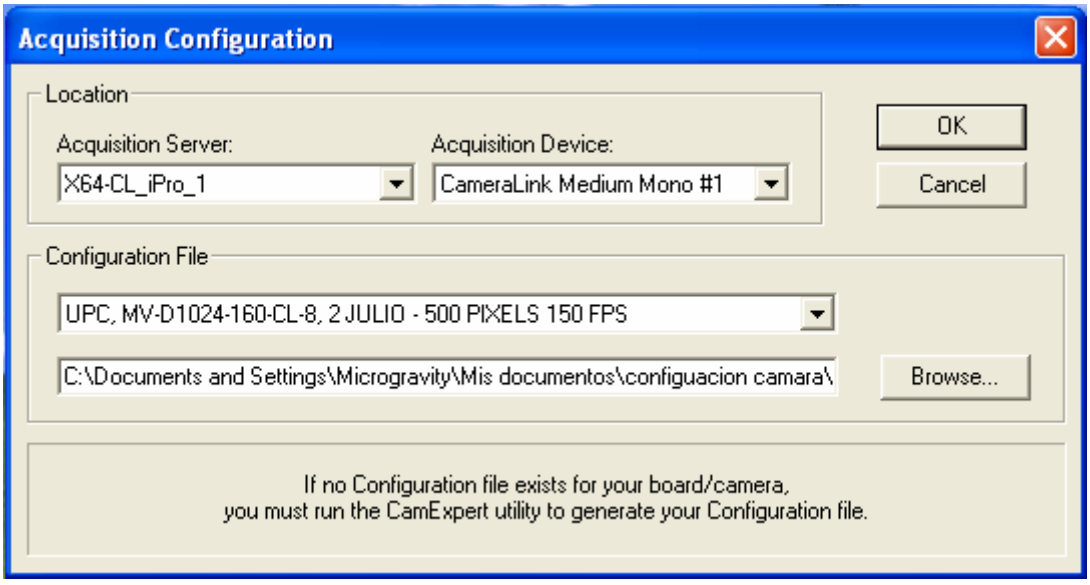

Fig. C.6 Acquisition Configuration

The main window of the software is shown in Fig. C.7 It contains the recording options.

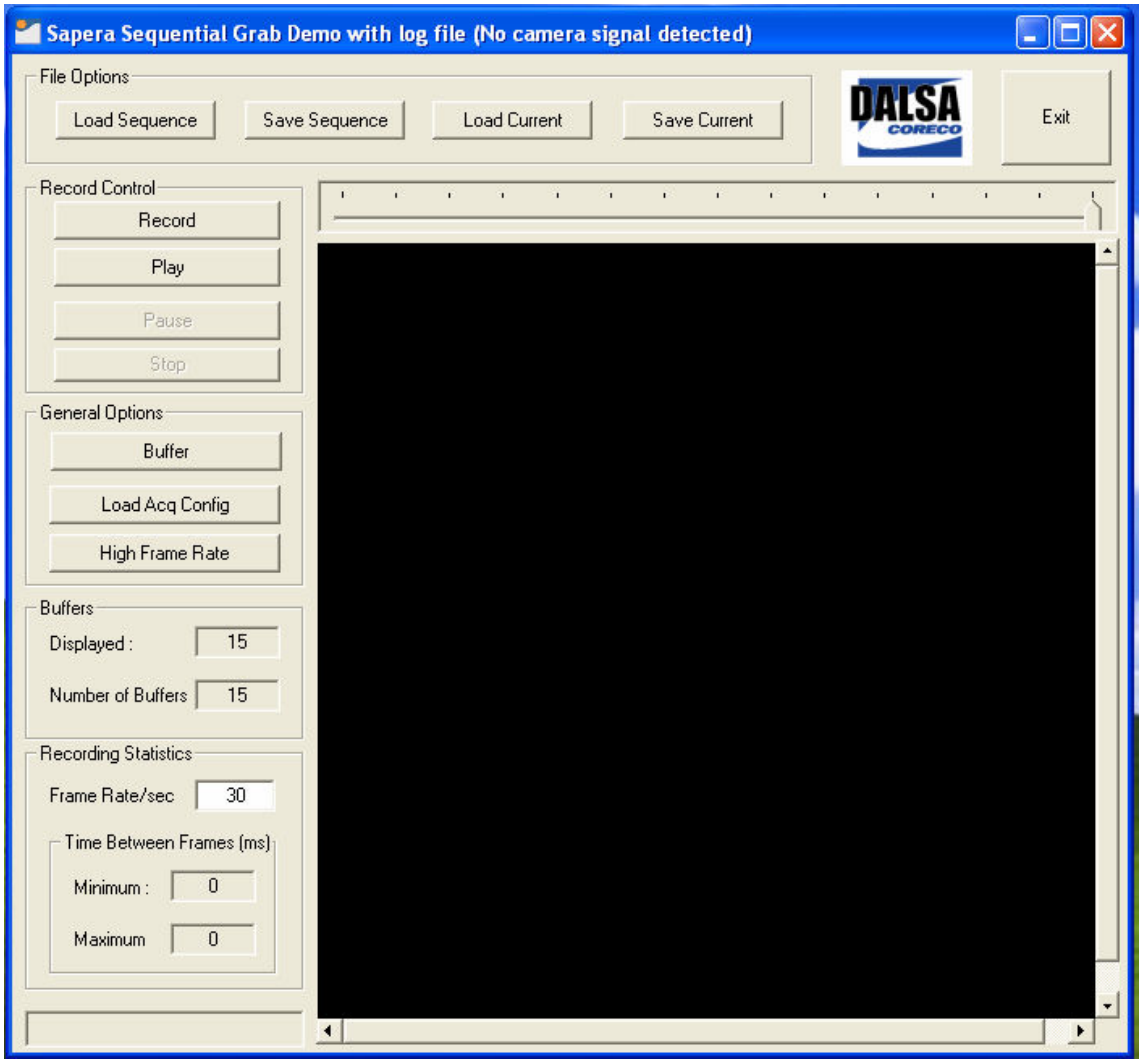

Fig. C.7 Sapera Sequential Grab

ANNEX D. SAFETY FACTOR CALCULATION

Safety factor is the parameter that Novespace uses to ensure the correct distribution of the components in the rack and compute the stress and forces that the fixation elements supports

.

D.1. Previous calculations

- **Strut profiles:**

-The total length of strut profiles is:

4x1008 mm+4x500 mm+4x866 mm+2x926 mm=11348 mm

-The total mass of strut profiles:

1.5x11.348=17 kg

- **Aluminium plates:**

-Volume: 1270x1036x10 mm^3+ 1016x956x3 mm^3

-Aluminium density: 2700 $kg \cdot m^3$

-Total mass:

(1270x1036x10x2700x10^{-9}) + (1016x956x3x2700x10^{-9}) = 43.39 kg

-**Test Equipment**:

-Mass: Cavity=30 kg

Liquid Pump=6.4 kg
Liquid Tank=9 kg
Air bottle=8 kg
Server=7 kg
Laptop=3 kg
Camera + Illumination + Supports = 1 kg
DC Supply=3 kg.

-Total mass=67.4 kg

-**Mass of the Total equipment (Test Equipment + Aluminium plates + Strut profiles)**:

- M = 17 kg + 43.39 kg + 67.4 kg = 127.8 kg.

-**Height of the center of gravity**:

(7.87x545 + 35.52x5+ 67.4x 252)/127.8=167.8 mm.

-**Rail linear loading**:

$$M_{attach} = \frac{M}{4} = 31.95 \text{ kg.}$$

-**Shear Force**:

- $F_s = \frac{9gM}{N_{attch}} = \frac{9x9.81x127.8}{4} = 2820.8$ N

- Safety Factor= $\frac{F_{s\max}}{F_s}$ = 12.3

-**Traction Force**:

- $F_t = \frac{9gMH}{N_{\substack{rear \\ attact}} D} = \frac{9x9.81x127.8x167.8}{4x1006} = 470.64$ N

Taking into account the load induced by the torque of the screw to the floor (F_t=28300 N), the total traction force on a rear floor attachment is in case of a 9g forward load:

$$F_t = 470 + 28300 = 28770.64 \text{ N}$$

The safety factor for the traction force on each rear floor attachment is:

-Safety Factor = $\frac{58000}{28770.64} = 2$

- **Bending moment**:

- $M_b = \frac{9gMH}{N_{uprights}} = \frac{9x9.81x127.82x167.82}{4} = 473471.7$ Nmm

- The maximum allowable bending moment of the upright is:

$$M_{b\max} = R_{p0.2} x W = 200(4.89 x 10^3) = 978000 \text{ Nmm}$$

- Safety Factor: SF = $\frac{M_{b\max}}{M_b} = 2.06$

A summary with all the results obtained before is attached below.

D.2. Determination of shear stress on the attachment screws

The screws to be considered in this section are the ones provided by Novespace and fixing the experiment to the aircraft rails. Screws are assessed with consideration of 9g acceleration due to crash.

$$Fc = \frac{9Wg}{n}$$

W-experiment weight (kg)	n-number of screws	Fc (N) (1)	Fc max(N) (2)	S.F. (3)
127.8	4	2820.8	34800	12.3

(1) Shearing load : Fc = 9Wg/n with g=9.81 m/s^2 (2) Max. allowable shearing load on Novespace screws (3) Safety factor : SF= FC max/Fc to be >1

D.3. Determination of traction force on the attachment screws

The screws to be considered in this section are the ones provided by Novespace and fixing the experiment to the aircraft rails. Screws are assessed with consideration of 9 g acceleration.

$$Ft = \frac{9Wgh}{nd}$$

W-experiment weight (kg)	h- height of centre of gravity (mm)	n [1]	d (mm) [2]	Ft (N)[3]
127.8	167.8	4	1006	470.64

[1] n: number of Novespace screws at the back of the experiment on X-axis
[2] d: distance between front and back Novespace screws on X-axis
[3] traction force: Ft=9Wgh/nd with g=9.81 m/s^2

Ft (N)	Fcs (N) [1]	F (=Ft+Fcs)	Fmax (N) [2]	SF[3]
470.64	28300	28770.64	58000	2

[1] load applied on the screws by torquing
[2] Max. allowable traction load on Novespace screws
[3] Safety factor: SF= Fmax/F to be >1

D.4. Determination of bending strength on uprights

This part defines the ability of each upright to undergo the bending strength under 9g load (crash conditions)

$$Mf = \frac{9Wgh}{n}$$

W-experiment weight (kg)	h- height of centre of gravity (mm)	n[1]	Mf (Nmm) [2]	Mf max (Nmm) [3]	S.F. [4]
127.8	127.8	4	473471.7	978000	2.06

[1] n: number of uprights in the rack
[2] Bending strength applied on each upright under 9 g: Mf=9WgH/n with g=9.81 m/s^2
[3] Max allowable bending strength on X-axis : defined by upright manufacturer
[4] Safety factor : SF= MFmax/ Mf to be >1.1